University of Southampton

Testing the No-lose and More-to-gain Theorems of the NMSSM at the LHC

by

Mosleh Maeedh Almarashi

A thesis submitted in partial fulfillment for the degree of Doctor of Philosophy in the
Faculty of Physical and Applied Sciences
School of Physics and Astronomy

November, 2011

To

MY PARENTS,

WIFE & CHILDREN

UNIVERSITY OF SOUTHAMPTON

ABSTRACT

FACULTY OF PHYSICAL AND APPLIED SCIENCES
SCHOOL OF PHYSICS AND ASTRONOMY

Doctor of Philosophy

TESTING THE NO-LOSE AND MORE-TO-GAIN THEOREMS OF THE NMSSM AT THE LHC

by Mosleh Maeedh Almarashi

The Higgs sector of the Next-to-Minimal Supersymmetric Standard Model (NMSSM) consists of seven physical Higgs states, two more than the MSSM, due to the existence of a Higgs singlet field in addition to the usual two Higgs doublets of the MSSM. This thesis is devoted to investigate the potential of the Large Hadron Collider (LHC) for discovering at least one of the NMSSM Higgs bosons. In addition, we study whether there exist regions in the NMSSM parameter space in which more and/or different Higgs states can be discovered at the LHC compared to those available in the MSSM. We prove that, at large tanβ, a very light CP-odd Higgs boson produced in association with a $b\bar{b}$ pair can be discovered at the LHC through the $\tau^+\tau^-$ and $\mu^+\mu^-$ decay modes. Further, we investigate the LHC discovery potential of the two lightest CP-even Higgs states, decaying into two lighter Higgs states or into the lightest CP-odd Higgs state and the Z gauge boson. We show that the LHC has the potential to discover two and also three neutral Higgs states at the same time.

Contents

List of Figures

List of Tables

Declaration of Authorship

I, Mosleh Maeedh Almarashi, declare that this thesis titled, "Testing the No-lose and More-to-gain Theorems of the NMSSM at the LHC" and the work presented in it are my own. I confirm that:

■ This work was done wholly or mainly while in candidature for a research degree at this University.

■ Where any part of this thesis has previously been submitted for a degree or any other qualification at this University or any other institution, this has been clearly stated.

■ Where I have consulted the published work of others, this is always clearly attributed.

■ Where I have quoted from the work of others, the source is always given. With the exception of such quotations, this thesis is entirely my own work.

■ I have acknowledged all main sources of help.

■ Where the thesis is based on work done by myself jointly with others, I have made clear exactly what was done by others and what I have contributed myself.

■ Parts of this work have been published as:

M. M. Almarashi and S. Moretti, Eur. Phys. J. C **71** (2011) 1618.

M. M. Almarashi and S. Moretti, Phys. Rev. D **83** (2011) 035023.

M. M. Almarashi and S. Moretti, Phys. Rev. D **84** (2011) 015014.

M. M. Almarashi and S. Moretti, Phys. Rev. D **84** (2011) 035009.

M. M. Almarashi and S. Moretti, arXiv:1109.1735 [hep-ph] (Accepted for publication in Phys. Rev. D).

Signed:

Date:

Acknowledgements

I would like to express my sincere appreciation to my supervisor Prof. S. Moretti who suggested my research project. His guidance, helpful comments and comprehensive knowledge of particle physics helped me a lot at all stages of this research.

I am grateful to A. Belyaev, C. Hugonie, U. Ellwanger, M. Won, L. Basso and all the staff of the theory group at the University of Southampton for their help and assistance.

I am also greatly thankful to Taibah University, Saudi Arabia, for the scholarship which enabled me to study for my PhD at the University of Southampton. Without their support and financial help it would not have been possible for me to pursue and to complete my PhD study.

Further, I am most grateful to my parents for their continuous encouragement and infinite support during my whole life.

Last but not at all least, I express my thank and love to my wife and children for their patience and loving support.

Chapter 1

Introduction

The Standard Model (SM) of particle physics [1] is one of the greatest achievements of human kind in the last century. In general, almost all its predictions are accurately tested in high energy physics experiments. Despite its outstanding successes, it can not be considered as an ultimate theory of particle physics because it leaves some problems unsolved. One of its major flaws is the so-called 'hierarchy problem': i.e., why the unification scale is much larger than the electroweak (EW) scale? Other problems in the context of the SM are: gravity is not incorporated, there is no good candidate for Dark Matter (DM) in the universe, there is no explanation for why matter is more numerous than antimatter, neutrinos are massless and there are a lot of free parameters which can only be extracted from experiments.

Because of these problems, particle physicists are not satisfied with the SM. So, they are looking for new physics beyond it. One of the most elegant scenarios that may solve most of the problems existing in the SM is Supersymmetry (SUSY) [2], for instance, its minimal realisation the so-called Minimal Supersymmetric Standard Model (MSSM) [3, 4]. The MSSM extends the SM by introducing two Higgs doublets instead of the one of the SM and hence (more than) doubling the particle spectrum by introducing the SUSY version of the SM particle states, the 'sparticles', which have 1/2 unit less of spin. In fact, this model has the positive points of the SM and solves the main negative ones. So, a huge effort has been devoted to study its phenomenology by both particle theorists and experimentalists. However, the MSSM suffers from two serious flaws. The first one is the so-called μ-problem in the Superpotential and the second one is the little hierarchy problem[1].

[1] We will give more details about these two aspects in Chapter 4.

An elegant solution to the above two flaws of the MSSM is expanding the latter by introducing a Higgs singlet Superfield in addition to the usual Higgs doublet ones, so to obtain the Next-to-MSSM (NMSSM) [5]. This additional singlet Superfield results in richer phenomenology in the NMSSM Higgs and neutralino sectors compared to those of the MSSM. The particle spectrum of the NMSSM compared to MSSM contains: one more CP-even Higgs boson, one more CP-odd Higgs state and one more neutralino. As for the neutralino sector of the NMSSM, there is a potential that the singlino-like neutralino is a DM candidate.

In the context of the NMSSM, we will test the applicability of the so-called 'No-lose' and 'More-to-gain' theorems of the NMSSM Higgs sector at the Large Hadron Collider (LHC). Assuming CP conservation, there are seven Higgs bosons in this model: three CP-even Higgses, two CP-odd Higgses and a pair of charged Higgses. Hence, we expect a wider phenomenological variety at colliders. In this thesis, we will test whether the discovery of at least one of the NMSSM Higgs bosons is possible at the LHC ('No-lose theorem') – just like that for the MSSM. In addition, we will investigate whether there exist regions in the NMSSM parameter space where more and/or different Higgs states can be discovered at the LHC compared to those available within the MSSM scenario ('More-to-gain theorem').

The thesis is organised as follows. In chapter 2, the particle content of the MSSM and also its Superpotential and Supersymmetric breaking sector are presented. Furthermore, we introduce in some detail the Higgs sector of the MSSM.

In chapter 3, the basic information about the LHC is reviewed. We also give a brief description of the four major experiments at the LHC. In addition, the LHC discovery potential for the MSSM Higgs boson is described.

In Chapter 4, we overview the NMSSM from the point of view of its phenomenology at colliders. In particular, Higgs sector phenomenology in the context of the NMSSM is presented in this chapter.

In Chapter 5, we explore the detectability of the lightest CP-odd Higgs boson, a_1, of the NMSSM at the LHC in the $\tau^+\tau^-$ and $\gamma\gamma$ decay modes through its production in association with a $b\bar{b}$ pair. The first results that support establishing both the 'No-lose' and 'More-to-gain' theorems for the NMSSM are presented.

In chapter 6, we study the viability of discovering a_1 in the $\mu^+\mu^-$ and $b\bar{b}$ decay channels again through its production in association with a $b\bar{b}$ pair. In this chapter, after making some realistic signal and dominant background analysis, we show the

detectability of this state at the LHC though these two channels.

In chapter 7, the LHC discovery potential for a CP-even Higgs boson of the NMSSM, h_1 or h_2, decaying into two lighter Higgs bosons and into a light CP-odd Higgs and a gauge boson through Higgs production in association with a $b\bar{b}$ pair is described. We discuss the importance of such decays in establishing the 'No-lose' and 'More-to-gain' theorems in the context of the NMSSM.

Finally, in chapter 8, we summarise the main ingredients of our thesis, highlighting the results of our work.

Chapter 2

The Minimal Supersymmetric Standard Model

The SM gives a good description of three forces in nature, electromagnetic, weak and strong forces, but the fourth force called gravity is not incorporated in the SM context. Furthermore, it is well-known that the running coupling constants of the three forces described by the SM do not unify at a would-be Grand Unification Theory (GUT) scale, $M_{\rm GUT} \sim 10^{16}$ GeV. So, the need to go beyond the SM is urgent.

One of the most appealing candidates for physics Beyond the SM (BSM) is, as intimated, SUSY, the symmetry between fermions and bosons. Even though there is no experimental evidence for SUSY right now, its theoretical arguments have attracted the majority of particle physicists. Among these arguments we count: the running coupling constants for the electroweak and strong forces meet at $M_{\rm GUT}$, already in the simplest version of SUSY, the MSSM, for example. Furthermore, a local SUSY can incorporate gravity, giving the possibility of unifying all the four forces in nature. In addition, the hierarchy problem can also be solved by SUSY, and we will give more explanations of this in Sec. 2.2.

2.1 Supersymmetry

SUSY is a symmetry that relates matter particles (fermions) with force-mediating particles (bosons), for reviews see: e.g., [3, 6, 7]. For every particle in the SM there is a Superpartner, which has the same properties of the SM particle except for the spin which differs by one half unit. The particles and their Superpartners of differing spins

are combined into Superfields. In fact, there are two types of Superfields:

• Chiral Superfield which consists of a complex scalar field, S, and a Majorana fermion field, ζ, with two components.

• Vector Superfield which contains a massless gauge field, A^a_μ, and two Majorana fermion fields called gauginos, λ_a.

If SUSY were an exact symmetry, then all particles and their Superpartners would share the same characteristics such as masses and quantum numbers, except spin. Unfortunately, no Superpartner has been discovered yet, which means SUSY must be broken. To maintain the exciting properties of SUSY, such as the elegant solution of the hierarchy problem and the unification of running coupling constants of $SU(3)_C \times SU(2)_L \times U(1)_Y$, SUSY breaking should occur at low energies, i.e., the Supersymmetric particle masses should be $\lesssim \mathcal{O}(1 \text{ TeV})$. Moreover, to preserve the SUSY solution to the hierarchy problem, SUSY should be broken 'softly', in the sense that they do not produce any quadratic divergences to the Higgs mass corrections.

2.2 Hierarchy problem

The main motivation for introducing SUSY is that it can offer a natural solution to the hierarchy problem of the SM. We know from EW observable measurements that the Vacuum Expectation Value (VEV) of the Higgs field is of the order of the EW scale, $\mathcal{O}(100 \text{ GeV})$, so one expects the Higgs boson mass to be around such a value. However, the SM Higgs mass receives quadratically divergent corrections, resulting from its coupling to virtual SM particles. The largest correction comes from the top quark, which is the heaviest particle in the SM. In general, the observable Higgs mass m^2_H can be written as the sum of the bare Higgs mass $m^2_{H_0}$ and its radiative corrections $\triangle m^2_H$ as follows:

$$m^2_H = m^2_{H_0} + \triangle m^2_H. \tag{2.1}$$

For instance, the one loop correction to m^2_H coming from a SM fermion with mass m_f is

$$\triangle m^2_H \sim -\frac{|\lambda_f|^2}{8\pi}\Lambda^2_{UV}, \tag{2.2}$$

where λ_f is the Yukawa coupling between the fermion and Higgs boson and Λ_{UV} is the ultraviolet cutoff scale at which the theory is no longer valid and BSM physics should be introduced to explain the dynamics at this scale. Therefore, if we assume that the

SM is an effective theory valid up to the Plank mass, $\Lambda_{UV} = m_{\rm Pl}$, then m_H will be close to $m_{\rm Pl}$. But for phenomenological reasons we know that m_H should be around the EW scale. This instability of the Higgs mass under the quadratic divergence is known as the hierarchy problem of the SM. Even in order to be consistent with unitarity and perturbativity bounds which necessitate $m_H \lesssim \mathcal{O}(1\text{ TeV})$, a huge cancellation between $m^2_{H_0}$ and $\triangle m^2_H$ has to take place at all orders in perturbation theory. So, one needs to add a counterterm and adjust it with a very high precision of $\mathcal{O}(10^{-30})$, which seems very unnatural. This whole problem is therefore also called the naturalness or fine-tunning problem [8].

To solve the hierarchy problem and make the cancellation hold through all orders, a new type of symmetry could be introduced. For example, SUSY can give an elegant solution to this problem. Due to Bose and Fermi statistics, the radiative corrections to the Higgs mass resulting from fermions come with different signs to those coming from bosons.

The one loop correction to the Higgs mass coming from a scalar with mass m_s and with a coupling to the Higgs boson λ_s is given by:

$$\triangle m^2_H \sim \frac{\lambda_s}{8\pi}\Lambda^2_{UV}. \tag{2.3}$$

From Eqs. (2.2) and (2.3), one can see that if the Higgs coupling to the fermion, λ_f, and to the scalar, λ_s, are related in such a way that $\lambda^2_f{=}\lambda_s$, the dangerous quadratic divergences will disappear. In fact, we need two complex scalars per each fermion in the SM to achieve this. Indeed, if SM particles and their Superpartners have the same mass but different spin, their quadratic contributions will cancel each other out exactly. Representative one loop Feynman diagrams which contribute to the Higgs boson mass corrections due to both SM particles and their Superpartners are shown in figure 2.1.

As intimated though, we know that SUSY must be broken and the masses of the Supersymmetric particles must generally be heavier than those of the SM particles[1]. These differences in the partner masses give finite contributions to the Higgs mass. For example, if we have a boson with mass m_b and the boson has a fermionic partner with mass m_f, their contribution to the Higgs mass is proportional to their mass-squared difference as follows:

$$\triangle m^2_H \propto |m^2_b - m^2_f|, \tag{2.4}$$

[1]The lightest SUSY Particle (LSP) could be light but has not been observed experimentally yet.

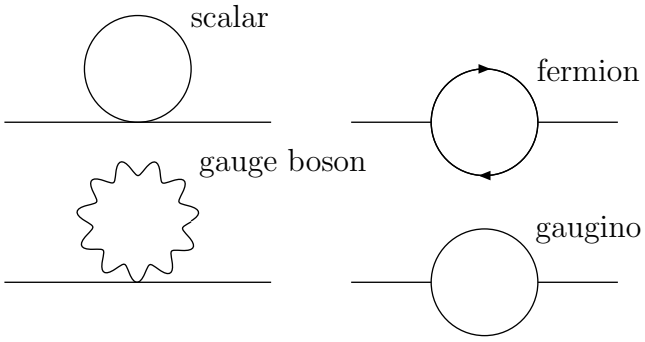

Figure 2.1: Representative one loop corrections to the Higgs boson mass from SM and SUSY (s)particle loops.

in addition to a logarithmic dependence on the cut-off scale. So, in order not to re-introduce the hierarchy problem, the Supersymmetric particles should have masses of $\mathcal{O}(1$ TeV) or less.

2.3 The MSSM particle content

The MSSM has the same gauge group as the SM, i.e., $SU(3)_C \times SU(2)_L \times U(1)_Y$. In this model, the particle spectrum is more than doubled compared with the number of SM particles. For a start, there is a Superpartner for each fermion and gauge boson in the SM. Likewise, any Higgs boson should have a Superpartner too, termed a higgsino. However, this Superpartner would contribute to the triangle $SU(2)_L$ and $U(1)_Y$ gauge anomalies. Therefore, two Higgs doublets, with opposite hypercharge ± 1, are required in the MSSM to cancel these anomalies since the contributions of the two fermionic partners of these two Higgs doublets cancel each other, making the model anomaly free. Moreover, these two Higgs doublets are necessary to give masses to both up- and down-type quarks and leptons as well.

The particle content of the MSSM is shown in table 2.1. In this table only the first generation of the quark and lepton Superfields is shown, the second and third generations are on the same footing as the first one.

The left- and right-handed quarks and leptons and their bosonic Superpartners belong to chiral Superfields. These Superpartners are named by adding an "s", which stands for scalar, in the beginning of the names of the corresponding SM particles, e.g., the Superpartner of the electron is called selectron or scalar electron and so on. More-

Chiral Superfield $\hat{\Phi}$	spin $\frac{1}{2}$	spin 0	$SU(3)_C$	$SU(2)_L$	$U(1)_Y$
$\hat{Q}$	(u_L, d_L)	$(\tilde{u}_L, \tilde{d}_L)$	3	2	$\frac{1}{3}$
$\hat{U}^c$	$\bar{u}_R$	$\tilde{u}_R^*$	$\bar{3}$	1	$-\frac{4}{3}$
$\hat{D}^c$	$\bar{d}_R$	$\tilde{d}_R^*$	$\bar{3}$	1	$\frac{2}{3}$
$\hat{L}$	(ν_L, e_L)	$(\tilde{\nu}_L, \tilde{e}_L)$	1	2	-1
$\hat{E}^c$	$\bar{e}_R$	$\tilde{e}_R^*$	1	1	2
$\hat{H}_d$	$\tilde{h}_d$	H_d	1	2	-1
$\hat{H}_u$	$\tilde{h}_u$	H_u	1	2	1
Vector Superfield $\hat{A}$	spin 1	spin $\frac{1}{2}$	$SU(3)_C$	$SU(2)_L$	$U(1)_Y$
$\hat{G}^a$	G^μ	$\tilde{g}$	8	1	0
$\hat{W}^i$	W_i^μ	$\tilde{w}_i$	1	3	0
$\hat{B}$	B^μ	$\tilde{b}$	1	1	0

Table 2.1: MSSM particle content.

over, the SM bosons have fermionic Superpartners with the same name except adding the suffix "*ino*" for the fermionic Superpartners, e.g., the Superparner of the Higgs is higgsino. The scalar Higgses and their Superpartners, higgsinos, belong also to chiral Superfields. In contrast, the gauge bosons of the SM and their Superpartners, gauginos, belong to vector Superfields. The Superpartners of the gauge bosons are gluinos $\tilde{g}$, winos $\tilde{w}_i$ and bino $\tilde{b}$ corresponding to G^μ, W_i^μ and B^μ, respectively. After EW Symmetry Breaking (EWSB), all neutral gauginos mix with each other to form four neutralinos χ_i^0 for $i = 1, 2, 3, 4$ and all charged gauginos mix to form two charginos $\chi_i^\pm$ for $i = 1, 2$.

2.4 The MSSM Superpotential

In order to determine the MSSM scalar potential, one needs to define a function called Superpotential. In fact, this function should be invariant under gauge transformations and SUSY. The general form of this function should obey the following conditions [4]:

• It must be a function of the Superfields ϕ_i and not their conjugate ϕ_i^*.

• It should at maximum be cubic in the Superfields.

• It should be an analytical function so no derivative interactions are allowed.

The form of the MSSM Superpotential, which satisfies those conditions, can be written

as:

$$W = \mathbf{h_u}\hat{Q}\hat{H}_u\hat{U}^c - \mathbf{h_d}\hat{Q}\hat{H}_d\hat{D}^c - \mathbf{h_e}\hat{L}\hat{H}_d\hat{E}^c + \mu\hat{H}_u\hat{H}_d, \tag{2.5}$$

where hatted variables $\hat{Q}$, $\hat{L}$ and $\hat{H}_d$ ($\hat{H}_u$) are $SU(2)$-doublet quark, lepton and Higgs Superfields while $\hat{U}^c$ ($\hat{D}^c$) and $\hat{E}^c$ are $SU(2)$-singlet quark and lepton Superfields. In addition, $\mathbf{h_u}$, $\mathbf{h_d}$ and $\mathbf{h_e}$ are Yukawa coupling constants, which form a 3×3-matrix in family space. In fact, there are other terms that can be added to the Superpotential. These terms can take the following form:

$$W^{NR} = \mathbf{h_L}\hat{L}\hat{L}\hat{E}^c + \mathbf{h'_L}\hat{L}\hat{Q}\hat{D}^c + \mu'\hat{L}\hat{H}, + \mathbf{h_B}\hat{U}^c\hat{D}^c\hat{D}^c \tag{2.6}$$

but they either violate lepton number conservation, the first three terms, or the baryon one, the last term. These violations have not been seen in nature and could result in rapid proton decay. To solve this problem, a new discrete symmetry called R-parity has to be introduced [9]. This symmetry is defined by

$$P_R = (-1)^{3(B-L)+2S}, \tag{2.7}$$

where B is the baryon number, L the lepton number and S the spin of the particle. All SM particles and Higgs bosons have $P_R = +1$ while their Supersymmetric partners have $P_R = -1$. If R-parity is conserved, this will lead to the following phenomenological consequences:

• There should be no mixing between SM particles and their Supersymmetric partners.

• Supersymmetric particles must be produced in pairs in collider experiments.

• Any one of the SUSY particles decays into an odd number of SUSY particles until the LSP is produced. This particle is absolutely stable and can not decay into other particles. If the LSP is electrically neutral and interacts weakly with other particles, it can be a good candidate for (cold) DM.

2.5 SUSY breaking sector

The MSSM Lagrangian can be divided into two parts, so that it can be written as:

$$\mathcal{L} = \mathcal{L}_{SUSY} + \mathcal{L}_{\text{soft}}. \tag{2.8}$$

The first part, $\mathcal{L}_{SUSY}$, preserves SUSY while the second one, $\mathcal{L}_{\text{soft}}$, breaks it. We know that SUSY, if existing, must be broken due to the fact that no Supersymmetric particles have been discovered yet and so their masses should generally be larger than those of

the corresponding SM ones. The Lagrangian $\mathcal{L}_{\rm soft}$ should not spoil the elegant solution to the hierarchy problem and should also preserve R-parity. Therefore, the general form for $\mathcal{L}_{\rm soft}$ consists of the following terms [4]:

• Gaugino mass terms M_3, M_2 and M_1, corresponding to the $SU(3)_C$, $SU(2)_L$ and $U(1)_Y$ subgroups, respectively:

$$\mathcal{L}_{\rm gaugino} = \frac{1}{2}\Bigg[M_1\tilde{B}\tilde{B} + M_2\sum_{a=1}^{3}\tilde{W}^a\tilde{W}_a + M_3\sum_{a=1}^{8}\tilde{G}^a\tilde{G}_a + h.c.\Bigg]. \tag{2.9}$$

• Scalar fermion mass terms:

$$\mathcal{L}_{\rm sfermions} = \sum_{i=gen} m^2_{\tilde{Q}_i}\tilde{Q}^\dagger_i\tilde{Q}_i + m^2_{\tilde{L}_i}\tilde{L}^\dagger_i\tilde{L}_i + m^2_{\tilde{u}_i}|\tilde{u}_{R_i}|^2 + m^2_{\tilde{d}_i}|\tilde{d}_{R_i}|^2 + m^2_{\tilde{l}_i}|\tilde{l}_{R_i}|^2. \tag{2.10}$$

• Mass and bilinear terms for the Higgs boson:

$$\mathcal{L}_{\rm Higgs} = m^2_{H_d}H^\dagger_d H_d + m^2_{H_u}H^\dagger_u H_u + B\mu(H_u.H_d + h.c.). \tag{2.11}$$

• Trilinear interaction terms of scalar fermions and Higgs bosons:

$$\mathcal{L}_{\rm trilinear} = \Bigg[A_u\mathbf{h_u}\hat{Q}\hat{H}_u\hat{U}^c - A_d\mathbf{h_d}\hat{Q}\hat{H}_d\hat{D}^c - A_l\mathbf{h_e}\hat{L}\hat{H}_d\hat{E}^c + h.c\Bigg]. \tag{2.12}$$

The SUSY breaking sector of the MSSM introduces a huge number of parameters, over 100, leading to phenomenological problems in the general form of the MSSM. In fact, these parameters can be reduced by introducing three assumptions [4]:

(i) All parameters of the soft SUSY breaking Lagrangian are real to prevent any new source of CP-violation.

(ii) The trilinear coupling and sfermion mass matrices are diagonal to insure the absence of Flavour Changing Neutral Currents (FCNCs) at tree level.

(iii) Universality of the first and second scalar fermion generations to pass the severe constraints from K^0–$\bar{K}^0$ mixing, see, e.g., Ref. [10] (and references therein).

These assumptions allow one to reduce the input parameters to only 22 defined as follows:

• The ratio of the VEVs of the two Higgs doublets: tanβ.

• The Higgs mass parameters squared: $m^2_{H_d}$ and $m^2_{H_u}$.

• The gluino, wino and bino mass parameters: M_3, M_2, and M_1.

• The quark and lepton mass parameters of the first and second generations: $m_{\tilde{q}}$, $m_{\tilde{u}_R}$, $m_{\tilde{d}_R}$, $m_{\tilde{l}}$, $m_{\tilde{e}_R}$.

• The quark and lepton mass parameters of the third generation: $m_{\tilde{Q}}$, $m_{\tilde{t}_R}$, $m_{\tilde{b}_R}$, $m_{\tilde{L}}$,

$m_{\tilde{\tau}_R}$.

• The trilinear couplings of the first and second generations: A_u, A_d, A_e.

• The trilinear couplings of the third generation: A_t, A_b, A_τ.

The dynamics of SUSY breaking is still unknown. The most common scenario imposes that SUSY breaking occurs in a hidden sector which interacts with the visible sector through exchanging some fields, called messengers. In fact, there are several different models that can explain how SUSY breaking can be transmitted from the hidden to the visible sector. Here we give three examples of these models:

(1) Gravity mediated models [11]: in which gravity is the messenger of SUSY breaking. One example of these models is minimal Supergravity (mSUGRA). mSUGRA imposes the following conditions at $M_{\rm GUT}$:

• Gaugino unification: $M_3{=}M_2{=}M_1{=}m_{\frac{1}{2}}$.

• Scalar mass unification: $m_{H_d}{=}m_{H_u}{=}m_{\tilde{L}}{=}m_{\tilde{l}_R}{=}m_{\tilde{u}_R}{=}m_{\tilde{d}_R}{=}m_0$.

• Trilinear coupling unification: $A_l{=}A_u{=}A_d{=}A_0$.

As a result, the model parameters can be reduced to only 5 parameters:

$$m_{\frac{1}{2}},\ m_0,\ A_0,\ \tan\beta,\ \mathrm{sign}(\mu).$$

In order to determine the soft SUSY breaking parameters at the low energy scale, Renormalization Group Equations (RGEs) are used.

(2) Gauge Mediated Supersymmetry Breaking (GMSM) models [12]: in which the interaction between the hidden and visible sectors occur through messenger fields which have gauge interactions.

(3) Anomaly Mediated Supersymmetry Breaking (AMSB) models [13]: in which SUSY breaking occurs due to loop effects because of a Superconformal anomaly that breaks scale invariance, i.e., this breaking is transmitted to the visible sector by the Super-Weyl anomaly.

2.6 The MSSM Higgs sector

As previously mentioned, the MSSM requires the existence of two complex Higgs doublets

$$H_d = \begin{pmatrix} H_d^0 \\ H_d^- \end{pmatrix}, \qquad H_u = \begin{pmatrix} H_u^+ \\ H_u^0 \end{pmatrix}. \tag{2.13}$$

The scalar potential for the Higgs scalar fields can be written as:

$$V_H = V_F + V_D + V_{\rm soft}, \tag{2.14}$$

where the F-term of the Higgs potential, V_F, [14] is derived from the Superpotential through its derivatives with respect to all scalar fields and it is given by

$$V_F = \sum_i \left| \frac{\partial W(\phi_j)}{\partial \phi_i} \right|^2 = \mu^2(|H_d|^2 + |H_u|^2). \tag{2.15}$$

The so-called D-term, V_D, [15] contains the quartic Higgs interactions and takes the following form:

$$\begin{aligned} V_D &= \frac{1}{2}\sum_{a=1}^{3}\left(\sum_i g_a \phi_i^* T^a \phi_i\right)^2 && (2.16)\\ &= \frac{g_2^2}{8}\left[4|H_d^\dagger.H_u|^2 - 2|H_d|^2|H_u|^2 + (|H_d|^2)^2 + (|H_u|^2)^2\right] && (2.17)\\ &\quad + \frac{g_1^2}{8}(|H_u|^2 - |H_d|^2)^2, && (2.18) \end{aligned}$$

where g_a are the coupling constants of the gauge groups (g_1 for the group $U(1)_Y$ and g_2 for the group $SU(2)_L$) and T^a the corresponding generators.
Finally, the soft breaking terms corresponding to the MSSM Superpotential are

$$V_{\rm soft} = m_{H_d}^2 H_d^\dagger H_d + m_{H_u}^2 H_u^\dagger H_u + B\mu(H_u.H_d + h.c.). \tag{2.19}$$

Therefore, the full scalar potential can be written as [4]:

$$\begin{aligned} V_H = (|\mu|^2 + m_{H_d}^2)|H_d|^2 + (|\mu|^2 + m_{H_u}^2)|H_u|^2 - B\mu(H_u.H_d + h.c.)\\ + \frac{g_2^2 + g_1^2}{8}(|H_d|^2 - |H_u|^2)^2 + \frac{1}{2}g_2^2|H_d^\dagger H_u|^2. \end{aligned} \tag{2.20}$$

In order to obtain the physical Higgs states, the minimum of V_H must break the EW symmetry, $SU(2)_L \times U(1)_Y$, and preserve the electromagnetic one, $U(1)$. So, the VEVs of the charged Higgs fields must be zero, i.e., $< H_d^+ >=< H_u^- >=0$ while the neutral components of the Higgs doublets must acquire VEVs such that

$$< H_d^0 >= \upsilon_d = \upsilon\cos\beta \quad \text{and} \quad < H_u^0 >= \upsilon_u = \upsilon\sin\beta, \tag{2.21}$$

where $\tan\beta = \frac{\upsilon_u}{\upsilon_d}$. Here, υ_u and υ_d are the VEVs of the two Higgs doublets.

In the end, EWSB results in five physical Higgs states: two CP-even Higgses, h and H ($m_h < m_H$), one CP-odd Higgs, A, and a pair of charged Higgses, $H^{\pm}$. The masses of these physical states at tree level are given by [3]:

$$m^2_{h,H} = \frac{1}{2}\big[m^2_A + M^2_Z \mp \sqrt{(m^2_A + M^2_Z)^2 - 4m^2_A M^2_Z \cos^2 2\beta}\big], \tag{2.22}$$

$$m^2_A = m^2_{H_d} + m^2_{H_u} + 2|\mu|^2, \tag{2.23}$$

$$m^2_{H^{\pm}} = m^2_A + M^2_W. \tag{2.24}$$

The mixing angle α, $-\frac{\pi}{2} \leq \alpha \leq 0$, between weak and mass eigenstates of the neutral Higgs bosons is given by:

$$\tan 2\alpha = \tan 2\beta \frac{m^2_A + M^2_Z}{m^2_A - M^2_Z}. \tag{2.25}$$

Therefore, one can deduce some relations between physical Higgs masses and those of the massive gauge bosons [4]:

$$m_h \leq \min(m_A, m_Z) \mid \cos 2\beta \mid, \tag{2.26}$$

$$m_H > \max(m_A, M_Z), \tag{2.27}$$

$$m^{\pm}_H \geq M_W. \tag{2.28}$$

Please, notice that these limits are lifted by radiative corrections.

It is clear that at tree level the MSSM Higgs sector can be described by only two parameters: $\tan\beta$ and (conventionally) m_A. In fact, LEP experiments searched for Higgs bosons and put the following limits: $m_h > 91$ GeV, $m_A > 91.9$ GeV, $m_{H^{\pm}} > 78.6$ GeV and the range $0.5 < \tan\beta < 2.4$ is excluded in maximal stop mixing scenario. In this scenario m_h reaches its maximal value when the stop mixing parameter X_t is maximal, assuming that the top quark mass is $m_t \leq 174.3$ GeV and $X_t = 2M_S$, with M_S (SUSY scale) $= 1$ TeV [16].

The couplings of the MSSM CP-even Higgs states to SM fermions and gauge bosons, which affect strongly the production cross sections and the decay widths, depend on both $\tan\beta$ and the mixing angle α. Further, the couplings of the CP-odd Higgs state to SM fermions depend on $\tan\beta$ and this state does not couple to gauge bosons at tree level because of CP-invariance. Table 2.2 summarises these couplings normalised to the SM Higgs couplings [4].

In the MSSM, the lightest CP-even Higgs boson, h, is a SM-like Higgs in the decoupling limit where $m_A \gg M_Z$. However, since the lightest scalar Higgs mass, m_h, is

Φ	$g_{\Phi\bar{u}u}$	$g_{\Phi\bar{d}d}$	$g_{\Phi VV}$
h	$\cos\alpha/\sin\beta$	$-\sin\alpha/\cos\beta$	$\sin(\beta-\alpha)$
H	$\sin\alpha/\sin\beta$	$\cos\alpha/\cos\beta$	$\cos(\beta-\alpha)$
A	$1/\tan\beta$	$\tan\beta$	0

Table 2.2: Neutral MSSM Higgs state couplings to SM fermions and gauge bosons normalised to the SM Higgs state couplings.

$\lesssim M_Z$ at tree level, the radiative corrections to this mass, basically from top and stop loops, should be large enough to escape the LEP bound, $m_h \geq 114.4$ GeV at 95% CL [17]. By assuming SUSY particle masses of 1 TeV or below, these radiative corrections can lift m_h up to 130 GeV, see e.g., [18] and references therein.

Chapter 3

The LHC

3.1 Introduction

The LHC at the European Organisation for Nuclear Research (CERN) [19] is currently the biggest and most powerful particle accelerator in the world. It is located between Switzerland and France with a circumference of 26.659 km about 100 m underground. It was approved for construction by the CERN Council in 1994.

The LHC is a proton-proton collider and the two beams of protons are designed to have a Centre-of-Mass (CM) energy of 14 TeV, i.e., 7 TeV per beam, and to have 100 fb^{-1} of integrated luminosity. It started its first attempt in 2008 but a technical fault occurred at that time and it successfully started again in 2009. Currently, in 2011, it works with a CM energy of 7 TeV and it is expected to collect a few fb^{-1} of luminosity during this year. The LHC is expected to run at 14 TeV in 2014.

Particle physicists hope that the LHC can help them to answer many fundamental questions in the context of particle physics, shedding light on mysteries that are still unsolved. Searching for BSM physics and exploring the mechanism responsible for EWSB are among the primary goals of the LHC.

3.2 The LHC: statistics

The LHC resides in the same tunnel where the Large Electron-Positron (LEP) collider was built. LEP operations ended in 2000. However, the CERN accelerator complex is designed, see figure 3.1, such that it is a succession of machines with the next one providing higher energies than the previous one. The last one of this chain is the LHC,

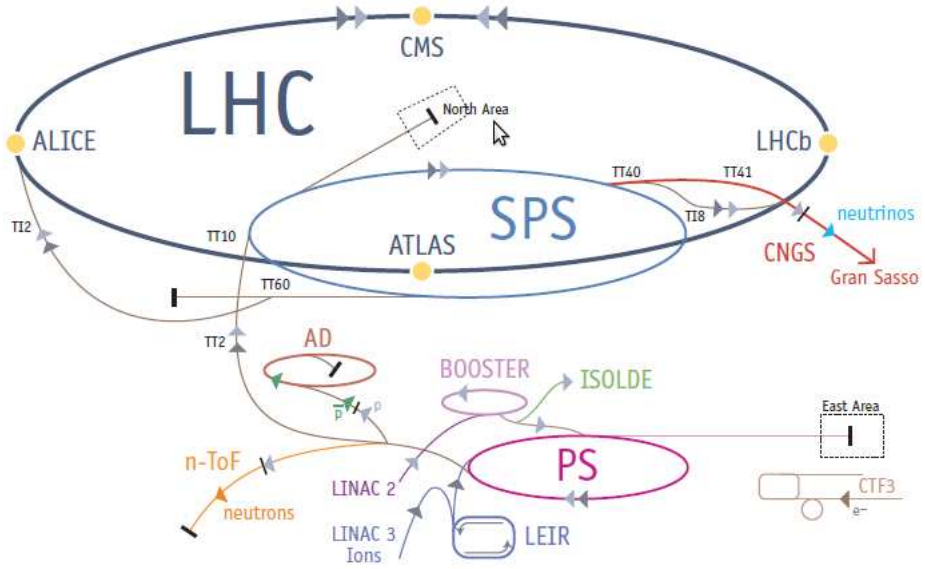

Figure 3.1: The CERN accelerator complex leading up to the LHC [19].

which collides protons and also lead ions in opposite directions.

Protons brought from hydrogen atoms, by stripping electrons off the latter, arrive to the LHC in bunches. Each proton beam contains 2808 bunches and each bunch has roughly 100 billion protons. In contrast, lead ions are obtained by heating up a purified lead sample to approximately 550° C. The LHC will accelerate each lead beam to 2.76 TeV/u (energy per nucleon) [19].

The most effective parameters for studying a physical process are the beam energy and luminosity. In fact, the luminosity depends on the number of bunches, the number of particles in each bunch, the cross section and the frequency of turns around the ring. However, to keep accelerated particles on specific tracks one needs strong electromagnetic devices. For example, dipole magnets keep the particles on circular orbits, quadruple magnets are used to focus the beam at the collision points and cavities to squeeze the bunches in order to obtain high luminosity. It is expected that the strength of the dipole magnets at the LHC will reach 8.33 T over their length. These magnets are important ingredients for the LHC to achieve the maximum energy. Table 3.1 shows some important quantities at the LHC [19].

3.3 The LHC experiments

At the present CERN collider there are six detectors: 4 major ones and 2 smaller ones. The major experiments are: A Large Ion Collider (ALICE) [20], A Toroidal LHC Ap-

Quantity	number
Circumference	26.659 km
Dipole operating temperature	-271.3° C
Number of magnets	9593
Number of main dipoles	1232
Number of main quadrupoles	392
Number of RF cavities	8 per beam
Nominal energy, protons	7 TeV
Nominal energy, ions	2.76 TeV/u
Peak magnetic dipole field	8.33 T
Minimum distance between bunches	7 m
Design integrated luminosity per year	100 fb^{-1}
No. of bunches per proton beam	2808
Number of collisions per second	600 million

Table 3.1: The main quantities for the LHC.

paratuS (ATLAS) [21], a Compact Muon Solenoid (CMS) [22] and the LHC beauty (LHCb) detector [23]. The other two experiments are the LHC forward (LHCf) detector and the TOTal Elastic and diffractive cross section Measurement (TOTEM) experiment. Below, we will give a short description of the main detectors at the LHC.

ALICE (shown in figure 3.2) is a detector specialised in the study of heavy ion collisions. At the very large energies and temperatures reachable by the LHC, partons inside hadrons behave as free particles. The main goal of ALICE is the study of properties of quark-gluon plasma, the state of matter in which quarks and gluons are considered as free particles inside hadrons, e.g., protons. This state of matter is believed to have existed in the first moments of the creation of the universe. The study of quark-gluon plasma and knowing its properties will give a better understanding of Quantum Chromo-Dynamics (QCD).

ATLAS (shown in figure 3.3) is a general purpose detector. It is designed to be used in many aspects of physics at the LHC: e.g., the search for Higgs boson(s), SUSY particles, extra dimensions and DM.

CMS (shown in figure 3.4) is also a multi-purpose detector. This experiment is similar to ATLAS in terms of purposes but with a different technical design. One of the main

differences in strategies used by CMS and ATLAS is that CMS uses one magnet, providing a magnetic field of 4 T, while ATLAS uses four magnets. Also, the electromagnetic calorimeter (ECAL) of CMS is lead tungstate ($PbWO_4$) crystal detector with excellent resolution while ATLAS uses a lead-liquid argon for ECAL. Furthermore, the ATLAS hadronic calorimeter offers a better energy resolution than that of the CMS because it is thicker and has a finer sampling [24].

LHCb (shown in figure 3.5) is an experiment specialised in exploring the origin of CP-violation in B meson decays. The study of such a violation could determine the origin of the asymmetry between matter and antimatter in the universe, i.e, why the former is dominant over the latter.

Particle detectors are used to detect the particles produced in collisions. If a particle is unstable, like a Higgs boson, it will decay shortly into secondary particles and one has to look for these decays to determine the nature of the original particle. Furthermore, the detectors measure the energy and charge of the visible particles. In general, every detector can be divided into subdetectors. If we take ATLAS as an example, we find that it can be divided into the following sections: (i) tracking devices which measure the tracks of charged particles; (ii) calorimeters which measure the energy of particles passing through them[1]; (iii) muon spectrometer which identify the tracks of muons (in practice, the muon is the only charged particle that can pass all calorimeters without being stopped) [19].

3.4 The LHC discovery potential for MSSM Higgs bosons

The search for Higgs bosons, if existing, is one of the primary goals of the LHC. In fact, one of the main tasks of the ATLAS and CMS experiments is searching for such peculiar states. In the SM, there is only one scalar Higgs boson, which is neutral. The direct searches for Higgs bosons carried out at LEP2 in the process $e^+e^- \to HZ$ and with up to $\sqrt{s}$=209 GeV in energy put a lower limit on the mass of the SM Higgs state, i.e., $m_H \geq 114.4$ GeV. However, it is expected that the LHC is capable of discovering

[1]In fact, there are two types of calorimeters: first, the Electromagnetic Calorimeter (ECal) which measures the energy of electrons and photons; second, the Hadronic Calorimeter (HCal) which measures the energy of hadrons.

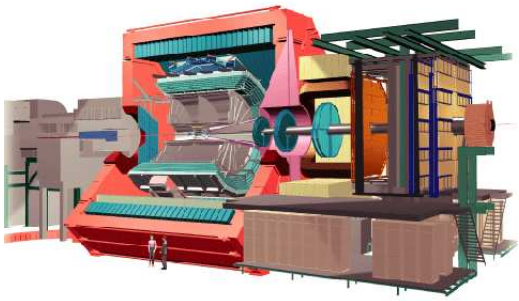

Figure 3.2: The ALICE detector.

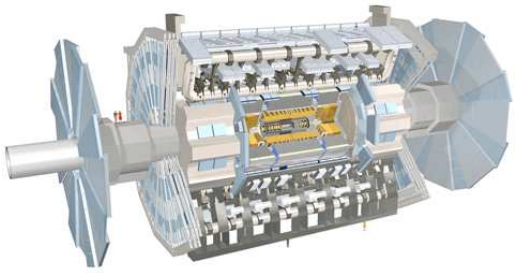

Figure 3.3: The ATLAS detector.

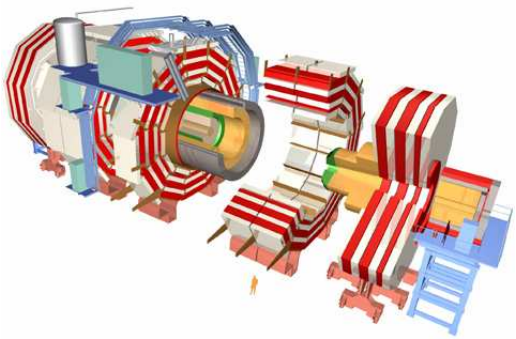

Figure 3.4: The CMS detector.

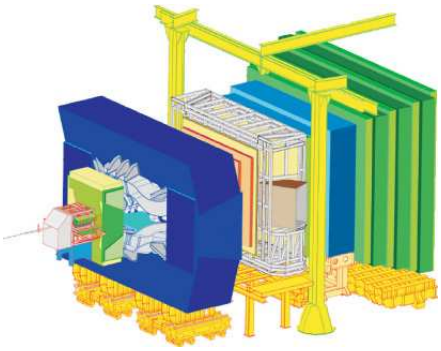

Figure 3.5: The LHCb detector.

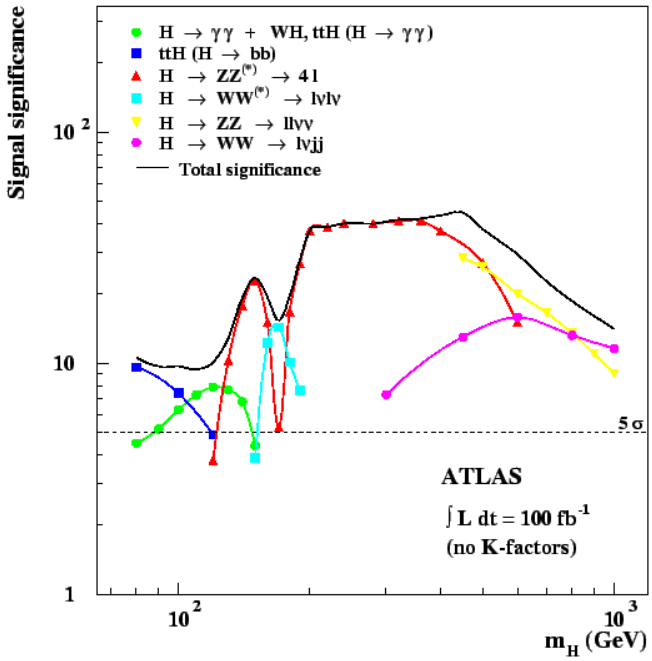

Figure 3.6: The ATLAS discovery potential for a SM Higgs boson with an integrated luminosity of 100 fb^{-1} [25].

the SM Higgs boson with mass range up to 1000 GeV. Figure 3.6 summarises the SM Higgs discovery potential in the ATLAS experiment for an integrated luminosity of 100 fb^{-1}. It is clear that a 5σ discovery can be achieved over the whole Higgs mass range and mostly with two different discovery channels[2].

In the MSSM, the Higgs spectrum contains five Higgs states: h, H, A and $H^{\pm}$ instead of the only one in the SM. The main production mechanisms for the neutral SM and MSSM Higgs bosons at the LHC are [27]:

- gluon-gluon fusion;
- Higgs production in association with b and t pairs;
- vector boson fusion;
- Higgs production in association with W and Z bosons;

Typical Feynman diagrams for these production modes are shown in figure 3.7.

The charged Higgses $H^{\pm}$ can be produced from the top decays $t \to H^{+}b$ and $\bar{t} \to H^{-}\bar{b}$ if $m_{H^{\pm}} \lesssim m_t - m_b$. Conversely, if the charged Higgses are heavier than the top quark, they can be produced through the production modes $gb(g\bar{b}) \to tH^{-}(\bar{t}H^{+})$ and $gg, q\bar{q} \to tH^{-}\bar{b}(gg, q\bar{q} \to \bar{t}H^{+}b)$ [4].

[2]The current experimental searches at the LHC have disfavoured the SM-like Higgs with mass between 141 – 476 GeV while the Tevatron excluded it with mass between 100 – 109 GeV and 156 – 177 GeV [26].

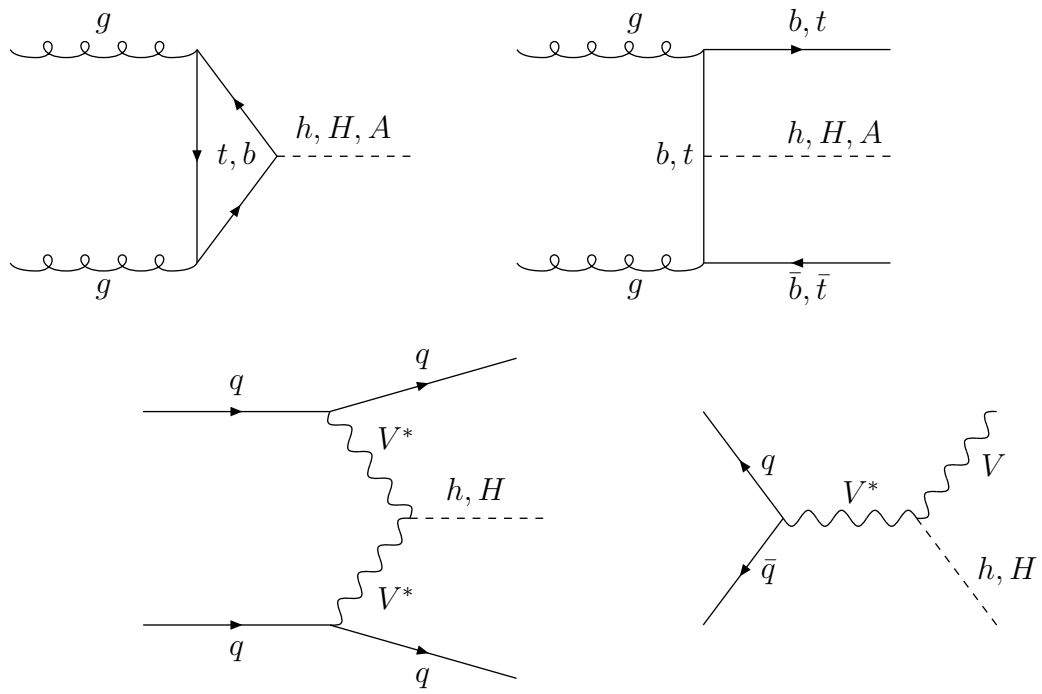

Figure 3.7: Representative Feynman diagrams for MSSM neutral Higgs production at the LHC, where the top ones are gluon-gluon fusion (left) and Higgs production in association with b and t pairs (right) while the bottom ones are vector boson fusion (left) and Higgs production in association with gauge bosons (right).

The main decay channels which could play crucial roles to discover the MSSM Higgs states at the LHC, see figures 3.8 and 3.9, are:

- $h \to \gamma\gamma$;
- $h \to b\bar{b}$;
- A, $H \to \tau^+\tau^-$;
- A, $H \to \mu^+\mu^-$;
- $H^\pm \to \tau\nu$;
- $H^\pm \to tb$;
- A, $H \to \chi_2^0\chi_2^0 \to 4l^\pm + X$;
- h, $H \to ZZ^* \to 4l^\pm$;
- A, $H \to t\bar{t}$;
- $H \to hh \to b\bar{b}\gamma\gamma$;
- $A \to Zh \to l^+l^-b\bar{b}$.

As mentioned, at tree level, the MSSM Higgs masses can be determined by only two parameters: tanβ and (conventionally) the mass of the CP-odd Higgs state, m_A. The summary of the CMS and ATLAS discovery potential for the MSSM Higgs bosons are shown in figures 3.8 and 3.9. In our study, we have chosen the maximal stop mixing scenario as a benchmark scenario. Figure 3.8 summarises the expected 5σ MSSM Higgs discovery reach at the CMS experiment with an integrated luminosity of 30 fb^{-1}. Almost the whole parameter range can be covered except for small values of m_A and tanβ which can be covered with a luminosity of 60 fb^{-1}. In a considerable fraction of parameter space more than one Higgs boson can be discovered, though not everywhere [28]. Figure 3.9 shows the 5σ discovery reach at the ATLAS experiment with an integrated luminosity of 300 fb^{-1}. Over a large region of the MSSM parameter space at least two decay modes are accessible.

Overall, figure 3.10 shows that over the entire tanβ-m_A plane at least one Higgs boson will be discovered at the LHC. Furthermore, two or more Higgs bosons can be discovered over large regions of parameter space, in low and large tanβ regions, allowing to distinguish the MSSM from the SM. However, for intermediate values of tanβ between 3 and 10, only a light CP-even Higgs boson can be discovered, over which the discrimination between the light CP-even Higgs boson of the MSSM and the SM one is difficult unless the SUSY particles have small masses, so that they are separately detectable.

In brief, with full design luminosity, the LHC will discover at least one of the MSSM

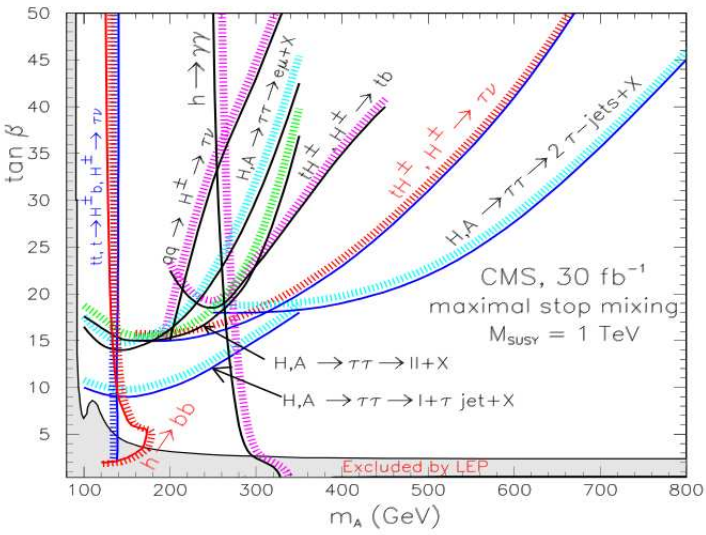

Figure 3.8: The expected 5σ discovery contour plot for the MSSM Higgs bosons with an integrated luminosity of 30 fb^{-1} in the CMS experiment [28].

Higgs bosons over the full parameter space or otherwise exclude this model, see figure 3.10.

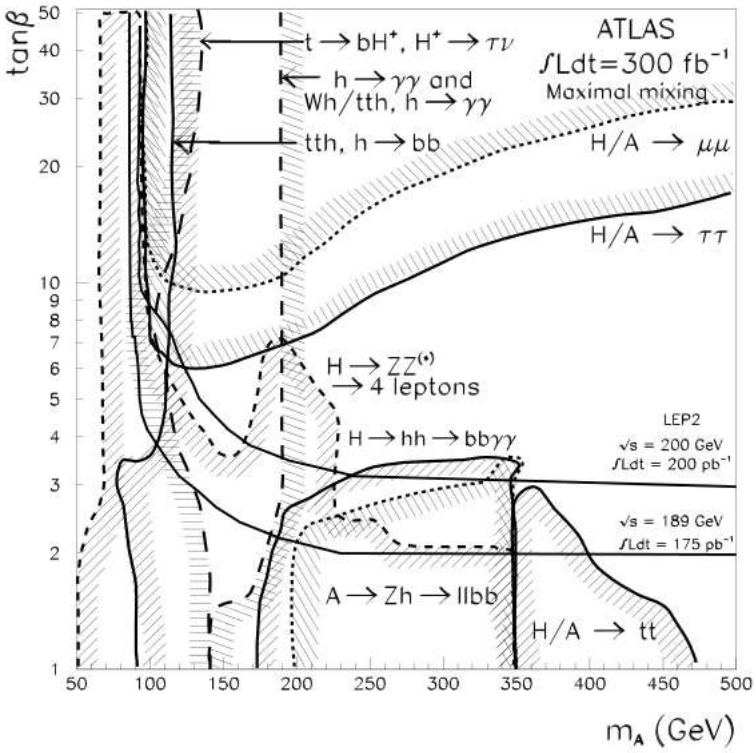

Figure 3.9: The expected 5σ discovery contour plot for the MSSM Higgs bosons with an integrated luminosity of 300 fb^{-1} in the ATLAS experiment [25].

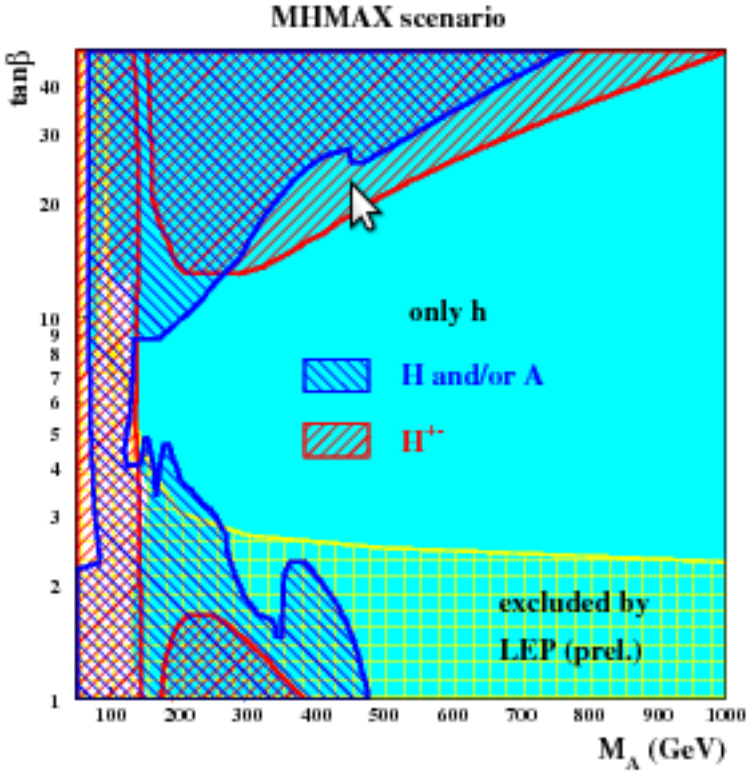

Figure 3.10: Overall discovery potential for the MSSM Higgs bosons in the maximal stop mixing scenario after 300 fb^{-1} of luminosity in the ATLAS experiment [29].

Chapter 4

The NMSSM

4.1 Introduction

The MSSM is probably one of the most studied BSM scenarios. However, this model suffers from two critical flaws: the μ-problem [30] and the little hierarchy problem. The former problem results from the fact that the Superpotential has a dimensional parameter, μ (the so-called 'Higgs(ino) mass parameter'), whose natural value would be either 0 or $m_{\rm Pl}$[1]. However, phenomenologically, in order to achieve EWSB, μ is required to take values of the order of the EW scale or possibly up to the TeV range. The latter problem emerges from LEP, which failed to detect a light CP-even Higgs boson, h, thereby imposing severe constraints on m_h. For this kind of Higgs state to pass the experimental constraints, large higher order corrections from both the SM and SUSY particle spectrum are required. The largest contributions come from the third generation, quarks and squarks. However, these required large corrections seem quite unnatural and cause the so-called 'little hierarchy problem'. Recall the fact that at tree level the lightest CP-even Higgs boson mass of the MSSM is less than M_Z[2].

The simplest SUSY realisation beyond the MSSM that can solve these two problems is the NMSSM (for reviews see [37, 38]). As mentioned already, this scenario includes a Higgs singlet Superfield in addition to the two MSSM-type Higgs doublets, giving rise to seven Higgs states: three CP-even Higgses $h_{1,2,3}$ ($m_{h_1} < m_{h_2} < m_{h_3}$), two CP-odd Higgses $a_{1,2}$ ($m_{a_1} < m_{a_2}$) and a pair of charged Higgses $h^{\pm}$[3]. When the scalar

[1] The μ-problem can be naturally solved by the Giudice-Masiero mechanism [31].

[2] Parts of this chapter have been taken from Refs. [32, 33, 34, 35, 36].

[3] As we used capital letters to denote the MSSM Higgs states, we use small letters to denote the NMSSM ones, to avoid confusion.

component of the singlet Superfield acquires a VEV, an 'effective' μ-term, $\mu_{\rm eff}$, will be automatically generated and can rather naturally have values of order of the EW/TeV scale, as required [39]. In addition, in the NMSSM the little hierarchy problem can be relieved [40, 41], since a SM-like scalar Higgs boson in the NMSSM context requires less quark/squark corrections than those of the MSSM or it can have mass less than the LEP bound due to unconventional decays over some regions of the NMSSM parameter space[4]. In fact, currently, the NMSSM can also explain a possible LEP excess and is definitely preferred by EW global fits, as we shall see later.

4.2 The NMSSM Superpotential

The Superpotential of the NMSSM is given by

$$W = \mathbf{h_u}\hat{Q}\hat{H}_u\hat{U}^c - \mathbf{h_d}\hat{Q}\hat{H}_d\hat{D}^c - \mathbf{h_e}\hat{L}\hat{H}_d\hat{E}^c + \lambda\hat{S}\hat{H}_u\hat{H}_d + \frac{1}{3}\kappa\hat{S}^3, \tag{4.1}$$

where $\mathbf{h_u}$, $\mathbf{h_d}$, $\mathbf{h_e}$, λ and κ are dimensionless couplings. The term $\lambda\hat{S}\hat{H}_u\hat{H}_d$ has been introduced to solve the μ-problem of the MSSM Superpotential. However, the Superpotential in Eq. (4.1) without the term $\frac{1}{3}\kappa\hat{S}^3$ gives rise to an extra global $U(1)$ symmetry, the so-called Peccei-Quinn symmetry $U(1)_{PQ}$ [42, 43]. Once the Higgs bosons take on VEVs, this symmetry will break spontaneously and lead to the appearance of a CP-odd scalar, called a Peccei-Quinn axion. In fact, this axion has not been seen experimentally. In addition, there are severe astrophysical and cosmological constraints on λ, that is $10^{-7} < \lambda < 10^{-10}$ [44]. These constraints necessitate a very large value of $< S >$ in order to solve the μ-problem. So, this is not a satisfactory way to solve the latter.

One elegant way to solve the μ-problem is to break the $U(1)_{PQ}$ by introducing an additional term in the Superpotential. This is the last term in Eq. (4.1) and consequently the axion can be avoided. However, introducing this new term in the Superpotential enables one to break the PQ symmetry but the Superpotential still have a discrete $\mathbb{Z}_3$ symmetry. This discrete symmetry is spontaneously broken when the additional complex scalar field acquires a VEV and that will lead to the domain wall problem. That is, during the EW phase transition of the early universe, this broken symmetry causes a dramatic change of the universe evolution and creates unobserved large anisotropies in the cosmic microwave background [45].

[4]We will give more explanations in Sec. 4.4.

In order to solve the domain wall problem, one needs to break the $\mathbb{Z}_3$ symmetry by introducing higher order operators at the Plank scale. However, these operators generate quadratic tadpoles for the singlet. So, one also needs to impose a new discrete symmetry, called a $\mathbb{Z}_2$ symmetry, on these operators in order to get rid of the dangerous tadpole contributions, see [37] for more details.

4.3 The Higgs sector of the NMSSM

The NMSSM Higgs sector contains two Higgs doublets and one Higgs singlet:

$$H_d = \begin{pmatrix} H_d^0 \\ H_d^- \end{pmatrix}, \qquad H_u = \begin{pmatrix} H_u^+ \\ H_u^0 \end{pmatrix}, \qquad S. \tag{4.2}$$

The scalar potential for the Higgs fields can be written as [46]:

$$V_H = V_F + V_D + V_{\text{soft}}, \tag{4.3}$$

where

$$V_F = |\lambda S|^2(|H_u|^2 + |H_d|^2) + |\lambda H_u H_d + \kappa S^2|^2, \tag{4.4}$$

$$V_D = \frac{g_1^2 + g_2^2}{8}\big(|H_d|^2 - |H_u|^2\big)^2 + \frac{1}{2}g_2^2|H_u^\dagger H_d|^2, \tag{4.5}$$

$$V_{\text{soft}} = m_{H_u}^2 H_u^\dagger H_u + m_{H_d}^2 H_d^\dagger H_d + m_S^2 S^\dagger S + \big(\lambda A_\lambda S H_u H_d + \frac{1}{3}\kappa A_\kappa S^3 + h.c.\big). \tag{4.6}$$

To generate EWSB, the Higgs fields should have VEVs. In fact, if one assumes that the VEVs are real and positive, they can be described by

$$< H_d >= \frac{1}{\sqrt{2}}\begin{pmatrix} \upsilon_d \\ 0 \end{pmatrix}, \qquad < H_u >= \frac{1}{\sqrt{2}}\begin{pmatrix} 0 \\ \upsilon_u \end{pmatrix}, \qquad < S >= \frac{1}{\sqrt{2}}\upsilon_s. \tag{4.7}$$

At the physical minimum of the scalar potential, V_H, the soft mass parameters of the Higgs fields are related to the VEVs through the following relations [46]:

$$m_{H_d}^2 = \frac{g_1^2}{8}(\upsilon_u^2 - \upsilon_d^2) - \frac{1}{2}\lambda^2\upsilon_u^2 + \frac{1}{2}(\sqrt{2}A_\lambda + \kappa\upsilon_s)\lambda\upsilon_s\frac{\upsilon_u}{\upsilon_d} - \frac{1}{2}\lambda^2\upsilon_s^2, \tag{4.8}$$

$$m_{H_u}^2 = \frac{g_1^2}{8}(\upsilon_d^2 - \upsilon_u^2) - \frac{1}{2}\lambda^2\upsilon_d^2 + \frac{1}{2}(\sqrt{2}A_\lambda + \kappa\upsilon_s)\lambda\upsilon_s\frac{\upsilon_d}{\upsilon_u} - \frac{1}{2}\lambda^2\upsilon_s^2, \tag{4.9}$$

$$m_S^2 = -\kappa^2\upsilon_s^2 - \frac{1}{2}\lambda^2\upsilon^2 + \kappa\lambda\upsilon_u\upsilon_d + \frac{1}{\sqrt{2}}\lambda A_\lambda\frac{\upsilon_u\upsilon_d}{\upsilon_s} - \frac{1}{\sqrt{2}}\kappa A_\kappa\upsilon_s. \tag{4.10}$$

The physical Higgs states arise after the Higgs fields acquire VEVs and rotate away the Goldstone modes. As a result, the potential can be written as

$$V_H = m_{h^\pm}^2 h^+ h^- + \frac{1}{2}(P_1 \;\; P_2)\mathcal{M}_P \begin{pmatrix} P_1 \\ P_2 \end{pmatrix} + \frac{1}{2}(S_1 \;\; S_2 \;\; S_3)\mathcal{M}_S \begin{pmatrix} S_1 \\ S_2 \\ S_3 \end{pmatrix}. \tag{4.11}$$

The masses of charged Higgs fields, $h^\pm$, at tree level are

$$m_{h^\pm}^2 = m_A^2 + M_W^2 - \frac{1}{2}(\lambda\upsilon)^2, \tag{4.12}$$

where

$$m_A^2 = \sqrt{2}\frac{\mu_{\rm eff}}{\sin 2\beta}\left(A_\lambda + \frac{\kappa\mu_{\rm eff}}{\lambda}\right). \tag{4.13}$$

Using the minimisation conditions, one can obtain the mass matrices in the scalar and pseudoscalar sectors. First, the mass matrix for CP-even Higgs states at tree level has the following entries [46]:

$$\mathcal{M}_{S11} = m_A^2 + \left(M_Z^2 - \frac{1}{2}(\lambda\upsilon)^2\right)\sin^2 2\beta, \tag{4.14}$$

$$\mathcal{M}_{S12} = -\frac{1}{2}\left(M_Z^2 - \frac{1}{2}(\lambda\upsilon)^2\right)\sin 4\beta, \tag{4.15}$$

$$\mathcal{M}_{S13} = -\frac{1}{2}\left(m_A^2 \sin 2\beta + 2\frac{\kappa\mu_{\rm eff}^2}{\lambda}\right)\left(\frac{\lambda\upsilon}{\sqrt{2}\mu_{eff}}\right)\cos 2\beta, \tag{4.16}$$

$$\mathcal{M}_{S22} = M_Z^2 \cos^2 2\beta + \frac{1}{2}(\lambda\upsilon)^2 \sin^2 2\beta, \tag{4.17}$$

$$\mathcal{M}_{S23} = \frac{1}{2}\left(4\mu_{\rm eff}^2 - m_A^2 \sin^2 2\beta - \frac{2\kappa\mu_{\rm eff}^2 \sin 2\beta}{\lambda}\right)\frac{\lambda\upsilon}{\sqrt{2}\mu_{\rm eff}}, \tag{4.18}$$

$$\mathcal{M}_{S33} = \frac{1}{8}m_A^2 \sin^2 2\beta \frac{\lambda^2\upsilon^2}{\mu_{\rm eff}^2} + 4\frac{\kappa^2\mu_{\rm eff}^2}{\lambda^2}, + \frac{\kappa A_\kappa \mu_{\rm eff}}{\lambda} - \frac{1}{4}\lambda\kappa\upsilon^2 \sin 2\beta. \tag{4.19}$$

Second, the mass matrix for CP-odd Higgs states at tree level has the following entries [46]:

$$\mathcal{M}_{P11} = m_A^2, \tag{4.20}$$

$$\mathcal{M}_{P12} = \frac{1}{2}\left(m_A^2 \sin 2\beta - 6\frac{\kappa\mu_{\rm eff}^2}{\lambda}\right)\frac{\lambda\upsilon}{\sqrt{2}\mu_{\rm eff}}, \tag{4.21}$$

$$\mathcal{M}_{P22} = \frac{1}{8}\left(m_A^2 \sin 2\beta + 6\frac{\kappa\mu_{\rm eff}^2}{\lambda}\right)\frac{\lambda^2\upsilon^2}{\mu_{\rm eff}^2}\sin 2\beta - 3\frac{\kappa\mu_{eff}A_\kappa}{\lambda}. \tag{4.22}$$

To a good approximation, at large tanβ and large m_A, the tree level neutral Higgs boson masses are given by the following expressions [46]:

$$m_{a_1}^2 = -\frac{3\kappa\mu_{\rm eff}A_\kappa}{\lambda}, \tag{4.23}$$

$$m_{a_2}^2 = m_A^2\left(1+\frac{1}{8}(\frac{\lambda^2\upsilon^2}{\mu_{\rm eff}^2})\sin^2 2\beta\right), \tag{4.24}$$

$$\begin{aligned} m_{h_{1/2}}^2 \quad &= \frac{1}{2}\Bigg\{ M_Z^2 + \frac{\kappa\mu_{\rm eff}}{\lambda}\left(\frac{4\kappa\mu_{\rm eff}}{\lambda}+A_\kappa\right) \\ &\mp\sqrt{\left[M_Z^2 - \frac{\kappa\mu_{\rm eff}}{\lambda}\left(\frac{4\kappa\mu_{\rm eff}}{\lambda}+A_\kappa\right)\right]^2 + \frac{\lambda^2\upsilon^2}{2\mu_{\rm eff}^2}\left[4\mu_{\rm eff}^2 - m_A^2\sin^2 2\beta\right]^2}\Bigg\}, \end{aligned} \tag{4.25}$$

$$m_{h_3}^2 = m_A^2\left(1+\frac{1}{8}(\frac{\lambda^2\upsilon^2}{\mu_{\rm eff}^2})\sin^2 2\beta\right). \tag{4.26}$$

4.4 The LHC phenomenology of the NMSSM Higgs sector

Because of the existence of a singlet Superfield in the NMSSM, the latter is phenomenologically richer than the MSSM. In fact, the NMSSM has seven Higgs states and five neutralinos compared to only five Higgs states and four neutralinos in the MSSM. As a consequence, the search for Higgs bosons in the context of the NMSSM at present and future colliders is a big challenge and more complicated than in the MSSM.

It was mentioned before that the mass of the lightest CP-even Higgs boson in the MSSM, m_h, at tree level should be less than M_Z. So, large radiative corrections, mainly from top and stop loops, are required to pass the LEP lower limit on the Higgs mass. In fact, to achieve this we need large stop masses, which only contribute logarithmically in the loop corrections. This large discrepancy between top and stop masses causes essentially a fine tuning problem [37]. This problem is known as the little hierarchy problem.

As for the NMSSM, the situation is quite different. Assuming CP-conservation in the Higgs sector, the upper mass bound for the lightest CP-even Higgs boson at tree level is given by

$$m_{h1}^2 \leq M_Z^2\left(\cos^2(2\beta) + \frac{2\lambda^2\sin^2(2\beta)}{g_1^2+g_2^2}\right). \tag{4.27}$$

The last term in this expression can lift m_{h_1} up to 10 GeV higher than the corresponding mass of the MSSM. So, smaller loop corrections are required to pass the lower bound on the SM-like Higgs mass. However, since the higher order corrections are similar to those in the MSSM, the upper mass bound reaches 135 – 140 GeV for maximal stop

mixing and tanβ = 2 [47, 48], however, this configuration is already excluded in the MSSM by LEP data. Finally, notice that the corrections to the lightest CP-even Higgs boson mass are already calculated at complete one loop level [49, 50, 51] and also at the dominant two loop level [48].

Furthermore, the most interesting property of the NMSSM that can solve the little hierarchy problem of the MSSM comes from the fact that in large areas of the NMSSM parameter space Higgs-to-Higgs decays are kinematically open. For instance, the existence of the lightest CP-odd Higgs boson a_1 with mass less than $\frac{1}{2}m_{h_1}$ is quite natural in the NMSSM, see, e.g., [32]. In fact, the branching ratio for the decay $h_1 \to a_1 a_1$, Br($h_1 \to a_1 a_1$), can be dominant in large regions of parameter space and as a result the Br($h_1 \to b\bar{b}$) is suppressed. This unconventional decay channel is so important as it could explain the 2.3σ excess observed at LEP for a Higgs mass, m_H, around 100 GeV as shown in figure 4.1. The reduced coupling in the figure is defined as follows:

$$\xi^2 = \left(\frac{g_{HZZ}}{g_{HZZ}^{SM}}\right)^2. \tag{4.28}$$

Here, g_{HZZ}^{SM} denotes the SM HZZ coupling while g_{HZZ} the non-standard coupling. As it is clear from the plot the excess occurs when the Br($H_{SM} \to b\bar{b}$) times ξ^2 gives about 20%. In the context of the NMSSM, one can explain this excess in two ways. Firstly, a SM-like Higgs boson, $h_{1,2}$, can decay dominantly into a pair of a_1's and so the Br($H \to b\bar{b}$) is suppressed [52, 53, 54]. This scenario can relieve the little hierarchy problem but requires that $m_{a_1} < 2m_b$. (Notice that this mass region is currently highly constrained by ALEPH [55] and BaBar [56] data.) In fact, there is also another possibility in the NMSSM that can explain the LEP excess due to the fact that the Br($a_1 \to \gamma\gamma$) can be dominant when the a_1 is highly singlet and again, as a result, the Br($a_1 \to b\bar{b}$) is suppressed even with $m_{a_1} > 2m_b$ [32, 34]. Secondly, a CP-even Higgs boson, h_1, has a reduced coupling with $\xi \lesssim 0.4$ [57], due to the mixing between the Higgs singlet and doublets. Notice that neither the SM nor the MSSM can explain such modest excess, as they have a Br($H/h \to b\bar{b}$) which is always dominant, hence yielding an excess much above the experimental limit.

The discovery of one or more Higgs boson at present or future colliders will open a new era in the realm of particle physics. In fact, many efforts have been made to detect such a particle (particles) at colliders. In regard to the Higgs sector of the NMSSM, there has been some work devoted to explore the detectability of at least one Higgs boson at the LHC and the Tevatron. In particular, some efforts have been made to extend the 'No-

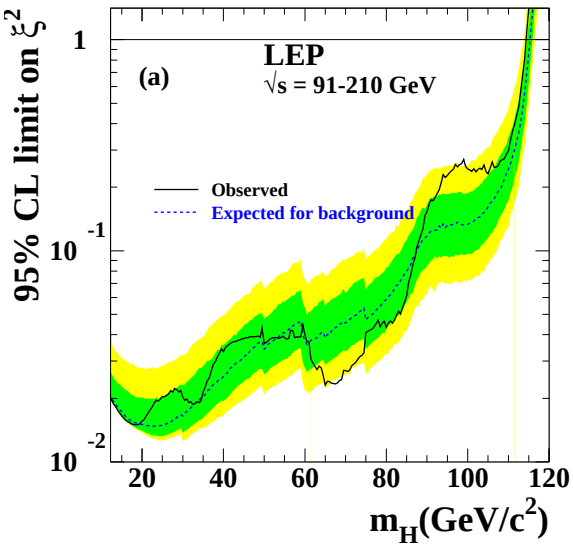

Figure 4.1: Upper limit on the ratio ξ from LEP, where the SM Br($H \to b\bar{b}$) and Br($H \to \tau^+\tau^-$) are assumed. Full line represents the observed limit and dashed line represents the expected limit. The green band and yellow band are within 68% and 95% probability, respectively [38].

lose theorem' of the MSSM (recall that this states that at least one Higgs boson of the MSSM will be found at the LHC via the usual SM-like production and decay channels throughout the entire MSSM parameter space [21, 22, 58]) to the case of the NMSSM [59, 60, 61]. By assuming that Higgs-to-Higgs decays are not allowed, it was realised that at least one Higgs boson of the NMSSM will be discovered at the LHC. However, this theorem could be violated if Higgs-to-SUSY decays are kinematically allowed (e.g., into neutralino or chargino pairs, yielding invisible Higgs signals).

Because of the large number of input parameters of the NMSSM, it is practically very difficult to make a continuous scan over all the NMSSM parameter space. The usual way to do the scan is by resorting to benchmark points in the parameter space. For example, for benchmark points in the NMSSM parameter space see Refs. [59] and [62]. In fact, one can distinguish between two scenarios in which Higgs-to-Higgs decays are either kinematically allowed or not.

So far, there is no conclusive evidence that the 'No-lose theorem' can be confirmed in the context of the NMSSM. In order to establish the theorem for the NMSSM, Higgs-to-Higgs decays should be taken into account, in particular the decay $h_1 \to a_1 a_1$. Such a decay can in fact be dominant in large regions of the NMSSM parameter space, for instance, for small A_k [32], and may not give Higgs signals with sufficient significance at

the LHC. However, a very light CP-odd Higgs boson, a_1, can be produced in association with chargino pairs [63] and in neutralino decays [64] at the LHC.

The importance of Higgs-to-Higgs decays in the context of the NMSSM has been emphasised over the years in much literature in all the above respects, see, e.g., Refs. [41, 65, 66, 67]. Eventually, it was realised that Vector Boson Fusion (VBF)[5] could be a viable production channel to detect $h_{1,2} \to a_1 a_1$ at the LHC, in which the Higgs pair decays into $jj\tau^+\tau^-$ [59, 68]. Some scope could also be afforded by a 4τ signature in both VBF and Higgs-strahlung (off gauge bosons) [69]. The gluon-fusion channel too could be a means of accessing $h_1 \to a_1 a_1$ decays, so long that the two light CP-odd Higgs states decay into four muons [70] or into two muons and two taus [71]. Such results were all supported by simulations based on parton shower Monte Carlo (MC) programs and some level of detector response. For a recent survey of the 'No-lose theorem' in the NMSSM context see Ref. [72].

Besides, there have also been some attempts to distinguish the NMSSM Higgs sector from the MSSM one, by affirming a 'More-to-gain theorem' [73, 74] (that is, to recall, to assess whether there exist some areas of the NMSSM parameter space where more and/or different Higgs bosons can be discovered at the LHC compared with what is expected from the MSSM). Some comparisons between NMSSM and MSSM phenomenology, specifically in the Higgs sectors of the two SUSY realisations, can be found in [75].

4.5 The NMSSM with different scenarios for κ

In this section, we discuss three different scenarios for the NMSSM according to different values for κ. Firstly, the scenario with $\kappa = 0$. In such a case $U(1)_{PQ}$ is unbroken in the Lagrangian. After the Higgs fields acquire VEVs, this symmetry will be broken spontaneously. This breakdown of the symmetry will give rise to the existence of the PQ axion. In this scenario, when $\kappa = 0$ and also $A_\kappa = 0$, the model at tree level is described by only four parameters: λ, A_λ, $\tan\beta$ and $\mu_{\rm eff}$.

In this scenario, the charged Higgs masses are given by Eq. (4.12). However, the two CP-odd Higgs states are given by the following exact expressions [46]:

$$m^2_{a_1} = 0, \tag{4.29}$$

[5]Which is dominated by W^+W^--fusion over ZZ-one.

$$m_{a_2}^2 = m_A^2\left(1+\frac{1}{8}(\frac{\lambda^2\upsilon^2}{\mu_{\rm eff}^2})\sin^2 2\beta\right). \tag{4.30}$$

As for the CP-even Higgs sector, in order to prevent the lightest CP-even Higgs state from having mass less than zero, one needs to improve the approximation given in Eqs. (4.25) and (4.26). In this scenario, the CP-even Higgs bosons can be written as [46]:

$$\begin{aligned} m_{h_1}^2 &= \frac{1}{2}\left[M_Z^2 - \sqrt{\left[M_Z^4 + \frac{\lambda^2\upsilon^2}{2\mu_{\rm eff}^2}\left[4\mu_{\rm eff}^2 - m_A^2\sin^2 2\beta\right]^2\right]}\right. \\ &\quad \left. + \frac{1}{2}\lambda^2\upsilon^2\sin^2 2\beta, \right. \end{aligned} \tag{4.31}$$

$$\begin{aligned} m_{h_2}^2 &= \frac{1}{2}\left[M_Z^2 + \sqrt{\left[M_Z^4 + \frac{\lambda^2\upsilon^2}{2\mu_{\rm eff}^2}\left[4\mu_{\rm eff}^2 - m_A^2\sin^2 2\beta\right]^2\right]}\right. \\ &\quad \left. - (M_Z^2 - \frac{1}{2}\lambda^2\upsilon^2)\sin^2 2\beta, \right. \end{aligned} \tag{4.32}$$

$$m_{h_3}^2 = m_A^2\left(1+\frac{1}{8}(\frac{\lambda^2\upsilon^2}{\mu_{\rm eff}^2})\cos^2 2\beta\sin^2 2\beta\right) + (M_Z^2 - \lambda^2\upsilon^2)\sin^2 2\beta. \tag{4.33}$$

In this scenario and when $\lambda \to 0$, the NMSSM is largely similar to the MSSM since the mass of a_1 and the mass of one of the CP-even Higgses are zero. However, very small values of λ are not favoured since there are stringent astrophysical and cosmological constraints in this regime that require very large VEV for the singlet. In fact, such large values of the VEV are not a good solution to the μ-problem.

Secondly, the scenario with $\kappa << 1$. In this case, the NMSSM has a slightly broken PQ symmetry. This scenario provides a very small mass to the lightest CP-odd Higgs state, a_1. This scenario is favoured by the RGE of the couplings from the GUT scale down to the EW scale [46]. The NMSSM at tree level is in this case described by six parameters: κ, A_κ, λ, A_λ, tanβ and $\mu_{\rm eff}$. In this scenario, the h_1 and h_2 in addition to a_1 have masses below the EW scale while h_3, a_2 and $h^\pm$ are heavy and degenerate in mass similarly to the case of the MSSM. The main advantage of this scenario is the prediction of the existence of three light Higgs states and so the discovery of these states at experimental colliders would enable one to distinguish the NMSSM from the MSSM [46].

Thirdly, the scenario with large values of κ. In this case, the PQ symmetry in the NMSSM potential is strongly broken. Although this scenario is disfavoured by the renormalisation group flow, it is not ruled out. The extra CP-odd and CP-even Higgs states coming from the singlet field have quite large masses in this scenario and so they

no longer are the lightest CP-odd and CP-even Higges in the NMSSM Higgs sector. This scenario of the NMSSM is similar to the MSSM for the states that have predominantly Higgs doublet fields with h_1 below the EW scale and one of the CP-even Higgses, one of the CP-odd Higgses and $h^{\pm}$ being degenerate at the scale m_A [46].

In the next chapters, we will study the LHC discovery potential for the NMSSM Higgs states. Generally, the heaviest CP-even Higgs, h_3, the heaviest CP-odd Higgs, a_2, and the $h^{\pm}$ states have very large masses, above the TeV scale, in particular at large values of tanβ, making their discovery at the LHC very difficult. So, we will focus on the LHC discovery potential of the lightest CP-odd Higgs boson, a_1, and of the lightest two CP-even Higgs states, h_1 and h_2.

Chapter 5

Low mass a_1 signals at the LHC in the NMSSM in photonic and tauonic final states

5.1 Introduction

In the beginning, we would like to mention that our study is motivated by two facts. Firstly, there is no conclusive evidence on whether the 'No-lose theorem' can be proved for the NMSSM. Secondly, there is only one dedicated study in the context of the 'More-to-gain theorem' [73].

In our attempt to test the two theorems, we consider in this chapter the case of the $\gamma\gamma$ and $\tau^+\tau^-$ decay channels of a very light CP-odd Higgs boson. The first mode is the most important one to detect a CP-even Higgs boson below 130 GeV in the SM and MSSM despite the smallness of its branching ratio, of $\mathcal{O}(0.001)$. In addition, this decay mode gives a clean signature and can be resolved efficiently at the LHC. The second one is used in the MSSM as a search channel of rather heavy CP-even and CP-odd states, in particular at large tanβ, and its exploitation has not been proved at very low masses, say, below M_Z.

In the NMSSM, because of the introduction of a complex singlet Superfield, the lightest CP-odd Higgs boson, a_1, can be a singlet-like state with a tiny doublet component in large regions of parameter space. In this chapter (and also in the next one) we are looking for direct production of the a_1 rather than looking for its traditional production through $h_{1,2}$ decay. We examine the discovery potential of the a_1 produced

in association with a bottom-antibottom pair at the LHC through the $\gamma\gamma$ and $\tau^+\tau^-$ decay modes.

We will show that in the NMSSM there exist regions of its parameter space where one can potentially have a dominant di-photon branching ratio of $\mathcal{O}(1)$ for the lightest CP-odd Higgs boson with small mass. This possibility emerges in the NMSSM because of the fact that such a CP-odd Higgs state has a predominant singlet component and a very weak doublet one. As a consequence, all partial decay widths are heavily suppressed as they employ only the doublet component, except one: the $\gamma\gamma$ partial decay width. This comes from the fact that the $a_1\tilde{\chi}^+\tilde{\chi}^-$ coupling is not suppressed, as it is generated through the $\lambda H_1 H_2 S$ Lagrangian term and therefore implies no small mixing. Although the direct decay $a_1 \to \tilde{\chi}^+\tilde{\chi}^-$ is kinematically not allowed, the aforementioned coupling participates in the $a_1\gamma\gamma$ effective coupling [76].

Furthermore, we will show that the τ-pair decay can be a promising decay mode for detecting the a_1 state of the NMSSM with very low mass. The detection of such a very low Higgs state would then unmistakably signal the existence of a non-minimal SUSY Higgs sector.

We build on the results presented in [73], where several such signals (for rather heavy Higgs states) were studied in some (complementary) regions of the NMSSM parameter space. The work in this chapter has been published in [32].

5.2 Parameter space scan

Due to the large number of parameters in the NMSSM, it is practically not feasible to do a comprehensive scan over all of them. These parameters can however be reduced significantly by assuming certain conditions of unification. Since the mechanism of SUSY breaking is still unknown, to explore the NMSSM Higgs sector, we have performed a general scan in parameter space by fixing the soft SUSY breaking terms at high scale to reduce their contributions to the outputs of the parameter scans. Consequently, we are left with six independent inputs. Our parameter space is in particular defined through the Yukawa couplings λ and κ, the soft trilinear terms A_λ and A_κ plus $\tan\beta$ (the ratio of the VEVs of the two Higgs doublets) and $\mu_{\rm eff} = \lambda\langle S\rangle$ (where $\langle S\rangle$ is the VEV of the Higgs singlet). In our numerical analyses we have taken $m_b(m_b) = 4.214$ GeV and $m_t^{\rm pole} = 171.4$ GeV for the running bottom-quark mass and pole top-quark mass, respectively.

We have used here the fortran package NMSSMTools, developed in Refs. [77, 78][1]. This package computes the masses, couplings and decay widths of all the Higgs bosons of the NMSSM, including radiative corrections, in terms of its parameters at the EW scale. NMSSMTools also takes into account theoretical as well as experimental constraints from negative Higgs searches at LEP [79] and the Tevatron, including the unconventional channels relevant for the NMSSM.

We have used the NMHDECAY code to scan over the six tree level parameters of the NMSSM Higgs sector in the following intervals:

$$\lambda : 0.0001 - 0.7, \quad \kappa : 0 - 0.65, \quad \tan\beta : 1.6 - 54,$$
$$\mu_{\rm eff} : 100 - 1000 \text{ GeV}, \quad A_\lambda : -1000 - +1000 \text{ GeV}, \quad A_\kappa : -10 - 0 \text{ GeV}.$$

(Notice that our aim is exploring the parameter space which has very low m_{a_1} and one way to do that is by choosing A_κ small, in which case its negative values are preferred [46]. Also, notice that small A_κ is preferred to have small fine-tuning [54].)

Remaining soft terms, contributing at higher order level, which are fixed in the scan include:

- $m_{\tilde{Q}} = m_{\tilde{t}_R} = m_{\tilde{b}_R} = m_{\tilde{L}} = m_{\tilde{\tau}_R} = 1$ TeV,
- $A_t = A_b = A_\tau = 1.2$ TeV,
- $m_{\tilde{q}} = m_{\tilde{u}_R} = m_{\tilde{d}_R} = m_{\tilde{l}} = m_{\tilde{e}_R} = 1$ TeV,
- $M_1 = M_2 = M_3 = 1.5$ TeV.

As intimated, we have fixed soft term parameters at the TeV scale to minimise their contributions to parameter space outputs but changing values of some of those parameters such as A_t could decrease or increase the number of successful points emerging from the NMSSMTools scans but without a significant impact on the m_{a_1} distribution. Also, notice that the sfermion mass parameters and the $SU(2)$ gaugino mass parameter, M_2, play crucial roles in constraining $\tan\beta$. Decreasing values of those parameters allow smaller values of $\tan\beta$ to pass experimental and theoretical constraints, however, this is a less interesting region of the NMSSM parameter space for our analysis, as our Higgs production mode is only relevant at large values of $\tan\beta$. The effect of heavy gaugino mass parameters on the outputs, in particular m_{a_1}, would be small except for M_2 through its effect on $\tan\beta$. In fact, when $\tan\beta$ is large, the sfermion masses should be large to avoid the constraints coming from the muon anomalous magnetic moment [80]. The dominant Supersymmetric contribution at large $\tan\beta$ is due to a chargino-sneutrino

[1] We have used NMSSMTools_2.3.1.

loop diagram [81]. Also, notice that the chargino masses depend strongly on M_2.

Guided by the assumptions made in the reference [59], the possible decay channels for neutral NMSSM CP-even Higgs boson h, where $h = h_{1,2,3}$, and neutral CP-odd Higgs boson a, where $a = a_{1,2}$, are:

$$h, a \to gg, \quad h, a \to \mu^+\mu^-, \quad h, a \to \tau^+\tau^-, \quad h, a \to b\bar{b}, \quad h, a \to t\bar{t},$$
$$h, a \to s\bar{s}, \quad h, a \to c\bar{c}, \quad h \to W^+W^-, \quad h \to ZZ,$$
$$h, a \to \gamma\gamma, \quad h, a \to Z\gamma, \quad h, a \to \text{Higgses}, \quad h, a \to \text{sparticles}.$$

(Notice that the CP-odd Higgses are not allowed to decay into vector boson pairs due to CP-conservation.) Also, notice that here 'Higgses' denotes any possible final state involving two neutral or two charged Higgs bosons or one Higgs boson and one gauge boson.

We have performed a random scan over 10 million points in the specified parameter space. The output of the scan, as mentioned above, contains masses, Br's and couplings of the NMSSM Higgses for all the successful points which have passed the various experimental and theoretical constraints.

5.3 Inclusive event rates

For the successful data points, we used CalcHEP [82] to calculate the cross sections for NMSSM Higgs production[2]. Some new modules have been implemented for this purpose.

We focus here on the process

$$gg \to b\bar{b}\ a_1 \tag{5.1}$$

i.e., Higgs production in association with a b-quark pair. (The production mode $q\bar{q} \to b\bar{b}\ a_1$ is negligible at the LHC with $\sqrt{s} = 14$ TeV.) We chose the production mode $gg \to b\bar{b}a_1$ because this production is dominant at large tanβ. The gluon fusion channel is instead burdened by huge SM backgrounds and a_1 does not couple to gauge bosons in Higgs-strahlung and Vector Boson Fusion (VBF) processes due to CP-conservation, see [84]. In addition, Higgs production in other modes has been studied before, see for example [61]. In fact, the Higgs production in association with a $b\bar{b}$ pair has an

[2]We adopt herein CTEQ6L [83] as parton distribution functions, with scale $Q = \sqrt{\hat{s}}$, the centre-of-mass energy at parton level, for all processes computed.

extra advantage where the associated $b\bar{b}$ pair can be tagged, allowing a useful handle for background rejection.

In the NMSSM, the a_1 state is a composition of the usual doublet component of the CP-odd MSSM Higgs boson, $a_{\rm MSSM}$, and the new singlet component, $a_{\rm S}$, coming from the singlet Superfield of the NMSSM. This can be written as [54]:

$$a_1 = a_{\rm MSSM} \cos\theta_A + a_{\rm S} \sin\theta_A. \tag{5.2}$$

For very small values of A_k, the lightest CP-odd Higgs, a_1, is mostly singlet-like with a tiny doublet component, i.e., the mixing angle $\cos\theta_A$ is small, see the top-pane of figure 5.1 which shows the relation between m_{a_1} and $\cos\theta_A$. The bottom-pane of the figure shows that the Br($a_1 \to \gamma\gamma$) can be dominant in some regions of the NMSSM parameter space with the possibility of reaching unity when $\cos\theta_A \sim 0$.

To a good approximation, m_{a_1} can be written in the NMSSM as [54]:

$$m^2_{a_1} = -3\frac{\kappa A_\kappa \mu_{\rm eff}}{\lambda} \sin^2\theta_A + \frac{9 A_\lambda \mu_{\rm eff}}{2\sin 2\beta} \cos^2\theta_A. \tag{5.3}$$

The first term of this expression is dominant at large tanβ. Furthermore, it is clear that a combination of all the tree level Higgs sector parameters affects m_{a_1} in general.

In the second step, in analysing the data, we have computed m_{a_1} against each of the six tree level Higgs sector parameters of the NMSSM. Figure 5.2 presents some results of our scan, these series of plots illustrating the distribution of m_{a_1} over the six parameters and as a function of the Br($a_1 \to \gamma\gamma$) and of the Br($a_1 \to \tau^+\tau^-$). In the parameter space adopted for this analysis, we have noticed that the large tanβ and small $\mu_{\rm eff}$ (and, to some extent, also small λ) region is the one most compatible with current theoretical and experimental constraints, though this conclusion should not be generalised to the entire parameter space. Herein, it is also obvious that m_{a_1} increases by increasing κ and $-A_\kappa$, whereas it decreases by increasing A_λ. Moreover, from a closer look at figure 5.2, it is clear that the Br($a_1 \to \gamma\gamma$) can be very large, indeed dominant, in some regions of the NMSSM parameter space and m_{a_1} values in the region 50 to 100 GeV maximise that rate. Also, notice that the Br($a_1 \to \tau^+\tau^-$) reaches about 10% in most of the parameter space that has $m_{a_1} \gtrsim 10$ GeV, in which case the a_1 decay into $b\bar{b}$ is open and dominant. Further, notice that there is a small region with low values of m_{a_1}, $m_{a_1} < 10$ GeV, that yields Br($a_1 \to \tau^+\tau^-$) $\gtrsim 90\%$, (the bottom-right corner of the bottom-right pane of the figure). The latter region occurs when the decay $a_1 \to b\bar{b}$ is closed, in which case the

$\mathrm{Br}(a_1 \to \tau^+\tau^-)$ is dominant compared to $c\bar{c}$, $\mu^+\mu^-$, etc.[3]

Figure 5.3 shows the distribution of the event rates $\sigma(gg \to b\bar{b}a_1)\ \mathrm{Br}(a_1 \to \gamma\gamma)$ and $\sigma(gg \to b\bar{b}a_1)\ \mathrm{Br}(a_1 \to \tau^+\tau^-)$ as functions of m_{a_1}, Br's of the corresponding channel and of $\tan\beta$. As expected, the inclusive cross section decreases with increasing m_{a_1}, see the top panes of the figure. It is worth mentioning that the $\mathrm{Br}(a_1 \to \gamma\gamma)$ can be dominant over a sizable expanse of the NMSSM parameter space, which originates from tiny widths into all other channels due to the dominant singlet nature of a_1 as mentioned in Sec. 5.1. However, the dominance of $\mathrm{Br}(a_1 \to \gamma\gamma)$ does not correspond to the region that maximises the yield of $\sigma(gg \to b\bar{b}a_1)\ \mathrm{Br}(a_1 \to \gamma\gamma)$, as the maximum of the latter occurs for Br's in the region of some 10^{-5} to 10^{-4}, see the middle-left pane of the figure. Therefore, one cannot take full advantage of the phenomenon described in the introduction of this chapter with respect to the singlet nature of the a_1 state, at the LHC, which couples to $\gamma\gamma$ through charginos. Thus, if a_1 were highly singlet, it would be difficult for the LHC to discover this particle as the doublet component (necessary to enable a large $a_1 b\bar{b}$ coupling at production level) would be suppressed. The tension between the two components is such that the cross section times Br rates are less than 100 fb.

The outlook for the $\tau^+\tau^-$ decay mode is much brighter where the corresponding signal rates are at nb level for $\mathrm{Br}(a_1 \to \tau^+\tau^-) \approx 0.1$ or even 10 nb for $\mathrm{Br}(a_1 \to \tau^+\tau^-) \approx 1$, see the middle-right pane of figure 5.3. Also, notice that such large rates naturally hold for different values of m_{a_1}, in the allowed interval, but they decrease with increasing m_{a_1} (see the top-right pane of this figure).

Incidentally, notice in the case of both decay channels that not only the density of NMSSM parameter configurations is larger as $\tan\beta$ grows[4] but also the event rates are maximal at large values of this parameter (see the bottom-left and the bottom-right panes of figure 5.3). This confirms what we intimated at the beginning of this section about the relevance of the $pp \to b\bar{b}a_1$ production mode (whose cross section is essentially proportional to $\tan^2\beta$).

In the NMSSM, there is a large area of parameter space where one Higgs state can

[3]Recall that the mass region below the $b\bar{b}$ threshold is severely constrained, see, e.g., Ref. [85] (and references therein). Very light CP-odd Higgs bosons of the NMSSM could also be produced in some rare hadron decays [86].

[4]Again, notice that for a more general choice of the range of A_κ and values of the soft SUSY breaking parameters this would not necessarily hold.

decay into two, e.g., $h_1 \to a_1 a_1$: see figure 5.4. As it is clear from the top-pane of this figure, the majority of points generated here have $m_{h_1} > 110$ GeV and $m_{a_1} < 55$ GeV, thereby allowing the possibility of $h_1 \to a_1 a_1$ decays. Moreover, this decay can be dominant and can reach unity as shown in the bottom-pane of the figure. Despite this, such a decay may not give Higgs signals with sufficient statistical significance at the LHC (as discussed in previous literature). Therefore, we are here well motivated to look further at the scope of direct production of a_1 state in single mode at the LHC, through $gg \to b\bar{b}a_1$, over overlapping regions of NMSSM parameter space, which we are going to do next.

5.4 Signal-to-background analysis

In our calculations, we have performed a partonic signal-to-background (S/B) analysis based on CalcHEP for the signal and irreducible background while the reducible background has been calculated by S. Moretti using MadGraph [87]. We have studied the LHC discovery potential of a_1 through the two channels $\gamma\gamma$ and $\tau^+\tau^-$ shown in the two forthcoming subsections. We have assumed a CM energy of $\sqrt{s} = 14$ TeV throughout for the LHC energy and we have benchmarked event rates on the basis of 300 inverse femtobarn of integrated luminosity.

From the output of NMSSMTools, we have chosen some points as illustrative examples to test the detectability of a_1 with various masses at the LHC. These illustrative points are as follows:

- For m_{a_1}=9.76 GeV:
  $\lambda = 0.22341068$, $\kappa = 0.4184933$, $\tan\beta = 53.819484$,
  $\mu_{\rm eff} = 228.94259$ GeV, A_λ = -415.57365 GeV and A_κ = -6.1773643 GeV.

- For m_{a_1}=19.98 GeV:
  $\lambda = 0.075946278$, $\kappa = 0.11543578$, $\tan\beta = 51.507125$,
  $\mu_{\rm eff} = 377.4387$ GeV, A_λ = -579.63592 GeV and A_κ = -3.5282881 GeV.

- For m_{a_1}=30.67 GeV:
  $\lambda = 0.10861169$, $\kappa = 0.4654168$, $\tan\beta = 48.063727$,
  $\mu_{\rm eff} = 222.99377$ GeV, A_λ = -952.59787 GeV and A_κ = -7.2147327 GeV.

- For m_{a_1}=46.35 GeV:

$\lambda = 0.14088263$, $\kappa = 0.25219468$, $\tan\beta = 50.558484$,
$\mu_{\text{eff}} = 317.07532$ GeV, $A_\lambda =$ -569.60665 GeV and $A_\kappa =$ -8.6099538 GeV.

- For m_{a_1}=60.51 GeV:
  $\lambda = 0.17410656$, $\kappa = 0.47848034$, $\tan\beta = 52.385408$,
  $\mu_{\text{eff}} = 169.83139$ GeV, $A_\lambda =$ -455.85097 GeV and $A_\kappa =$ -9.0278415 GeV.

- For m_{a_1}=80.91 GeV:
  $\lambda = 0.10713292$, $\kappa = 0.13395171$, $\tan\beta = 44.721569$,
  $\mu_{\text{eff}} = 331.43456$ GeV, $A_\lambda =$ -418.13018 GeV and $A_\kappa =$ -9.7077267 GeV.

5.4.1 The $\gamma\gamma$ channel

The fact that the production cross section $\sigma(gg \to b\bar{b}a_1)$ and the $\gamma\gamma$ branching ratio $\text{Br}(a_1 \to \gamma\gamma)$ are not maximised in the same regions of the NMSSM parameter space makes it extremely difficult to obtain detectable event rates in this channel. In fact, the signal yields for this channel are generally small and also overwhelmed by the irreducible background. This is made explicit in figures 5.5–5.6, which show how the signals are completely spoilt by the irreducible background. As it is shown in the figures the signals have sizable peaks in the di-photon invariant mass, $m_{\gamma\gamma}$, but the event rates are quite small, some $\mathcal{O}(10)$ events for 300 fb^{-1} of integrated luminosity. The m_{a_1} masses considered are roughly 10 and 46 GeV. The cuts used in this analysis are as follows[5]:

$$\Delta R(b,\bar{b}), \Delta R(b,\gamma), \Delta R(\bar{b},\gamma), \Delta R(\gamma,\gamma) > 0.4,$$

$$0 < \eta(b), \eta(\bar{b}), \eta(\gamma) < 2.5,$$

$$P_T(b), P_T(\bar{b}) > 20 \text{ GeV}, P_T(\gamma) > 2 \text{ GeV}. \tag{5.4}$$

In practice, for triggering purposes, at least one of the two photon transverse momenta ought to be increased to some 10 GeV or so but that does not help to improve S/B. For a_1 masses above 50 GeV or so the signal rates are (in general) too poor to even pass the observability threshold of 1 event for 300 fb^{-1} of integrated luminosity.

In brief, despite the uniqueness of an a_1 signal with the possibility of having large $\text{Br}(a_1 \to \gamma\gamma)$, this channel is not feasible to detect a_1 at the LHC in the NMSSM.

[5]Hereafter, η refers to the pseudorapidity and ΔR to the cone distance expressed in differences of pseudorapidity and azimuthal angle ϕ: i.e., $\Delta R = \sqrt{(\Delta\eta)^2 + (\Delta\phi)^2}$. Further, the notation P_T refers to the transverse momentum.

5.4.2 The $\tau^+\tau^-$ channel

The $\tau^+\tau^-$ decay mode is a promising channel to discover the lightest CP-odd Higgs a_1 with very small masses at large tanβ. We have implemented the following cuts[6]:

$$\Delta R(b,\bar{b}), \Delta R(b,\tau^+), \Delta R(\bar{b},\tau^+), \Delta R(b,\tau^-), \Delta R(\bar{b},\tau^-), \Delta R(\tau^+,\tau^-) > 0.4,$$

$$0 < \eta(b), \eta(\bar{b}), \eta(\tau^+), \eta(\tau^-) < 2.5,$$

$$P_T(b), P_T(\bar{b}) > 20 \text{ GeV}, P_T(\tau^+), P_T(\tau^-) > 10 \text{ GeV}. \tag{5.5}$$

In the top-panes of figures 5.7–5.12, we have shown the invariant masses of the $\tau^+\tau^-$ system, where the signal clearly appears over the irreducible background coming from $pp \to b\bar{b}\gamma, Z \to b\bar{b}\tau^+\tau^-$. Recall that for very low Higgs masses, say below M_Z, in the $b\bar{b}\tau^+\tau^-$ channel, the dominant background is indeed the irreducible one, see, e.g., Ref. [88]. Assuming that at least one tau decays leptonically to suppress QCD background, it is clear that there exist substantial discovery potential of a very light CP-odd Higgs boson of the NMSSM at the LHC.

We have also shown in figures 5.7–5.12 the top-antitop reducible background, i.e., $pp \to t\bar{t} \to b\bar{b}W^+W^- \to b\bar{b}\tau^+\tau^- P_T^{\rm miss}$, where $P_T^{\rm miss}$ is the missing transverse momentum produced by the neutrinos, with no cuts on $P_T^{\rm miss}$. The case of fully hadronic decays of the signal is further burdened by pure QCD backgrounds, the more so, the smaller the m_{a_1} values, so that we have not taken it into account in our analysis. Finally, we have shown in the bottom-panes of figures 5.7–5.12 the differential cross sections as functions of transverse momenta. We believe that an increase of even a factor of 2 in transverse momentum out of the leptonic/hadronic τ decay products should not dramatically spoil the signal significances in the low a_1 mass region.

Overall, the $\tau^+\tau^-$ signal yield in the very low a_1 mass region is quite large, of order 3000 signal events for m_{a_1} reaching 80 GeV or so to 30000 events for m_{a_1} starting at 10 GeV or so, over a much smaller background. Notice that the width of each histogram in the figures is 1 GeV and the plots are in log scale but even if we assume that $\tau^+\tau^-$ resolutions are 10 GeV or so, the signal significance will be large enough to discover a very light a_1 at the LHC.

[6]Here, for the sake of illustration, we take the τ's to be on shell.

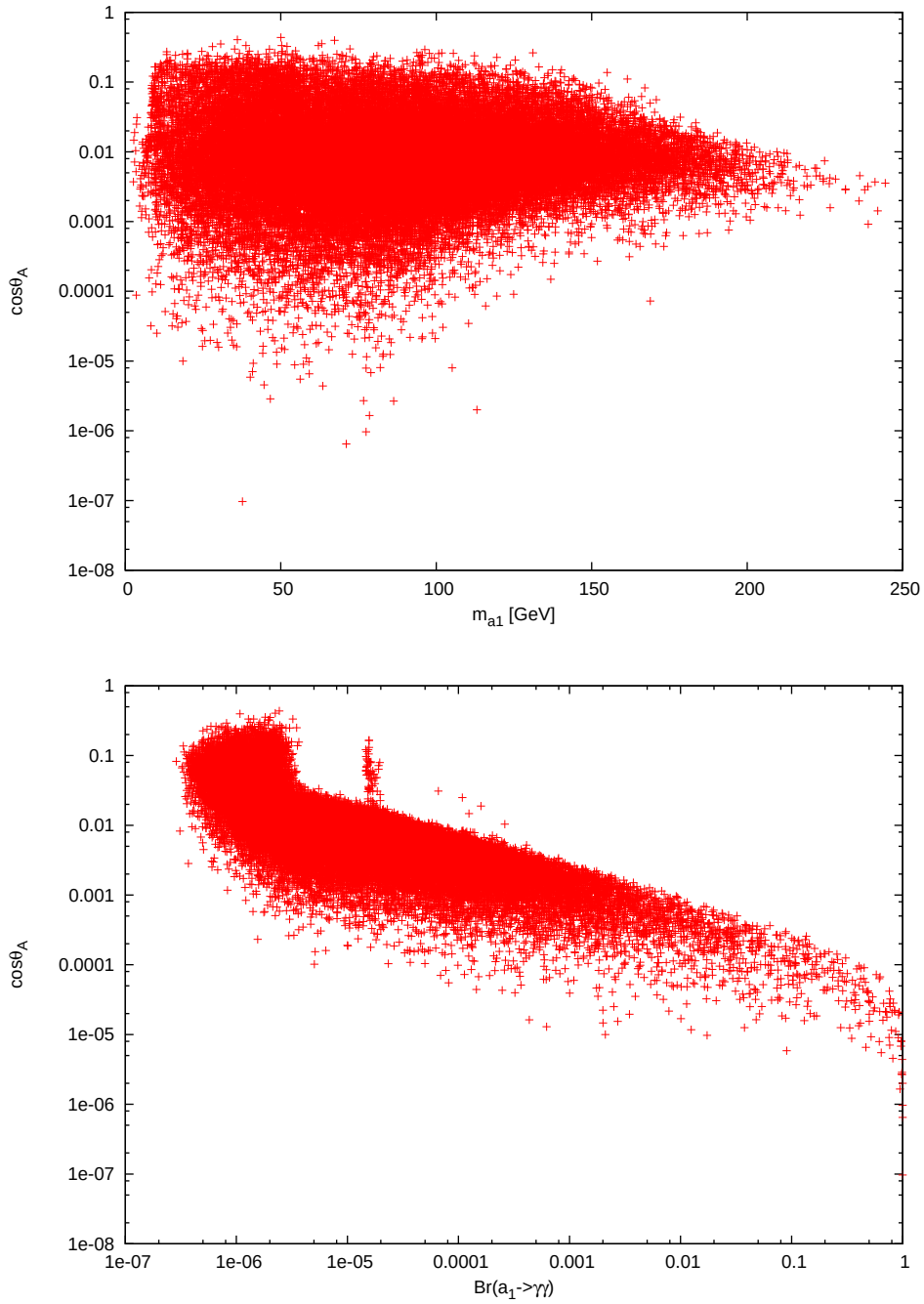

Figure 5.1: The lightest CP-odd Higgs mass m_{a_1} and the $\mathrm{Br}(a_1 \to \gamma\gamma)$ plotted against the mixing angle in the CP-odd Higgs sector $\cos\theta_A$.

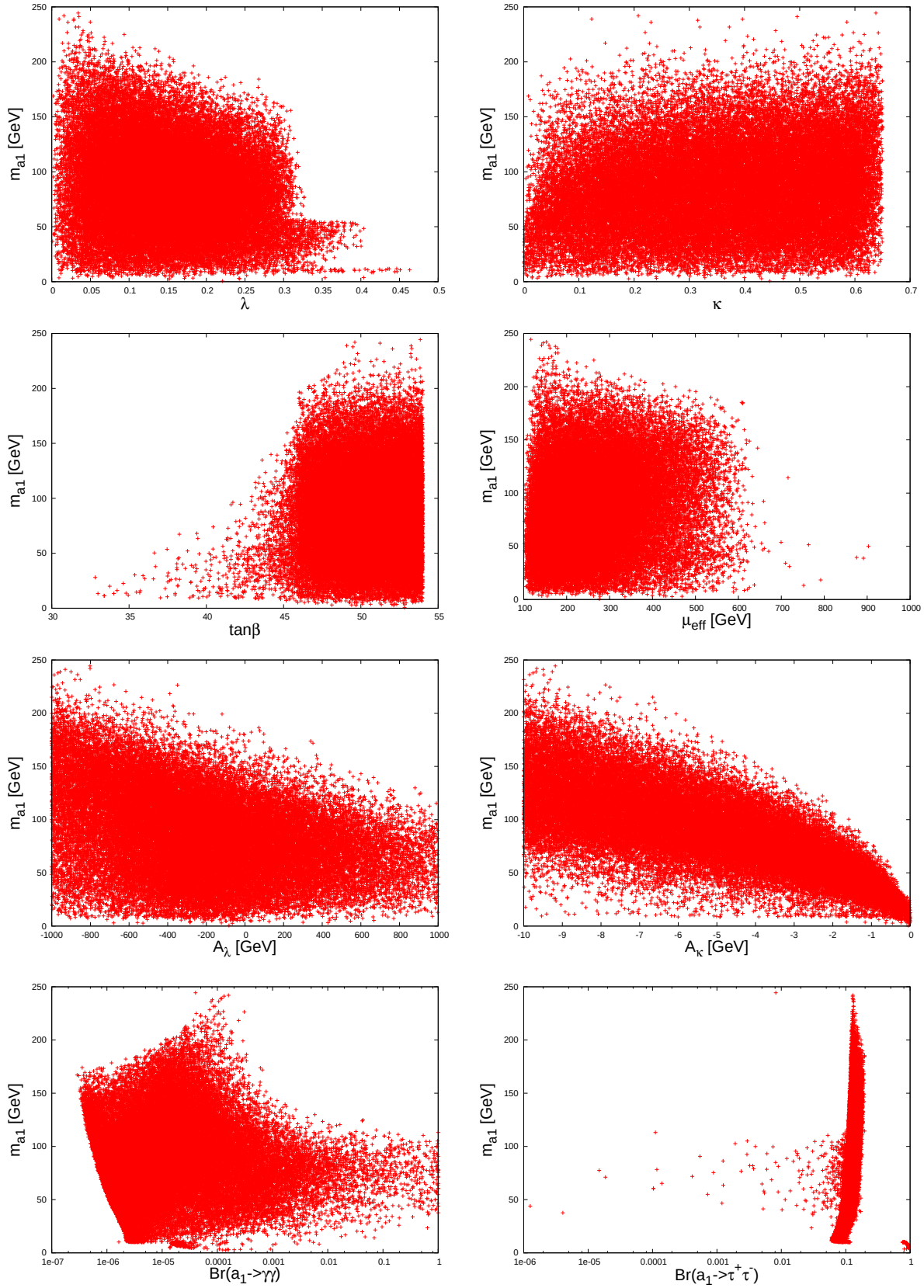

Figure 5.2: The CP-odd Higgs mass m_{a_1} as a function of λ, κ, $\tan\beta$, $\mu_{\rm eff}$, A_λ, A_κ, $\mathrm{Br}(a_1 \to \gamma\gamma)$ and of $\mathrm{Br}(a_1 \to \tau^+\tau^-)$.

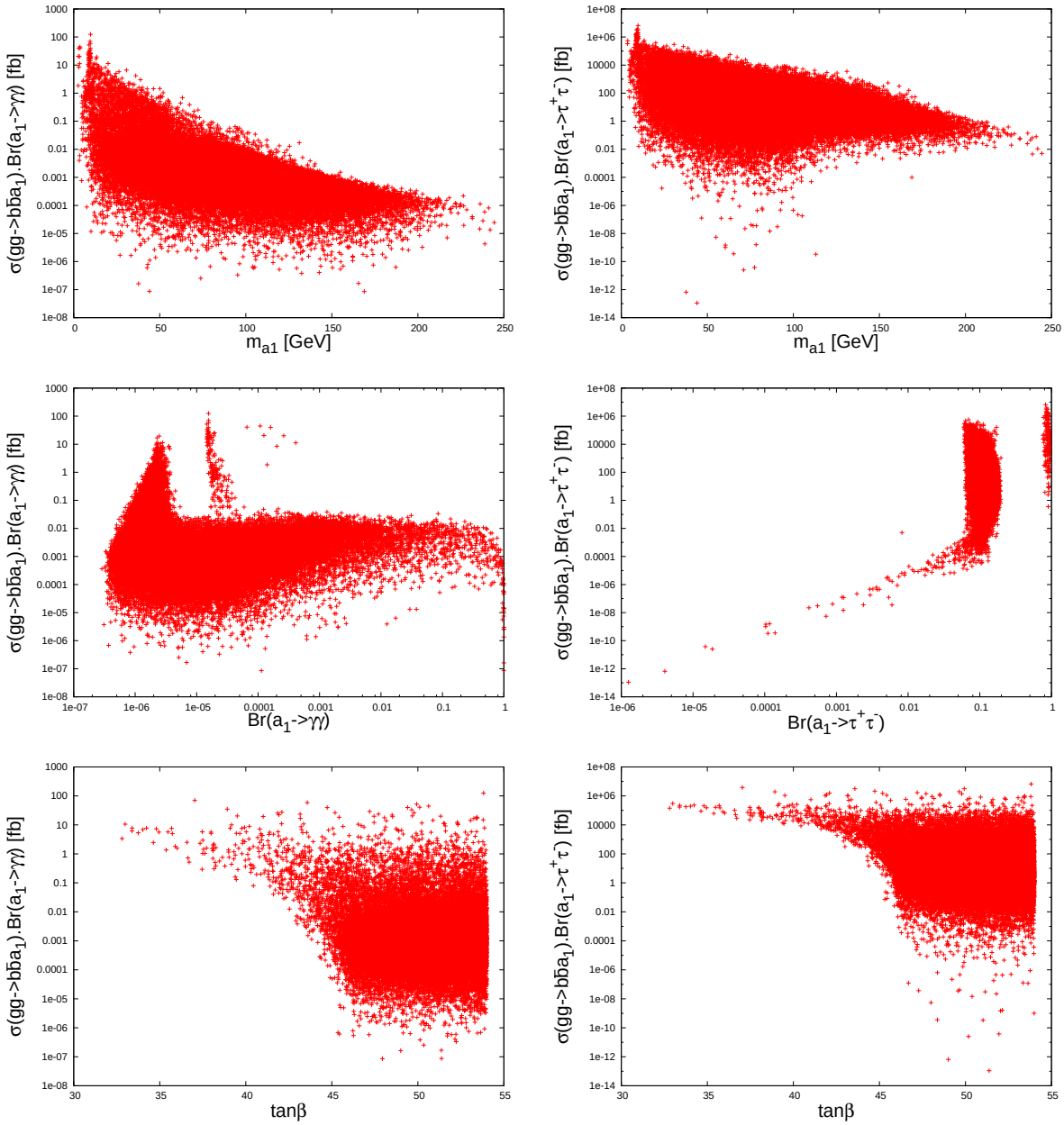

Figure 5.3: The rates for $\sigma(gg \to b\bar{b}a_1)\,\mathrm{Br}(a_1 \to \gamma\gamma)$ (left) and for $\sigma(gg \to b\bar{b}a_1)\,\mathrm{Br}(a_1 \to \tau^+\tau^-)$ (right) as functions of m_{a_1}, the Br of the corresponding channel and of $\tan\beta$.

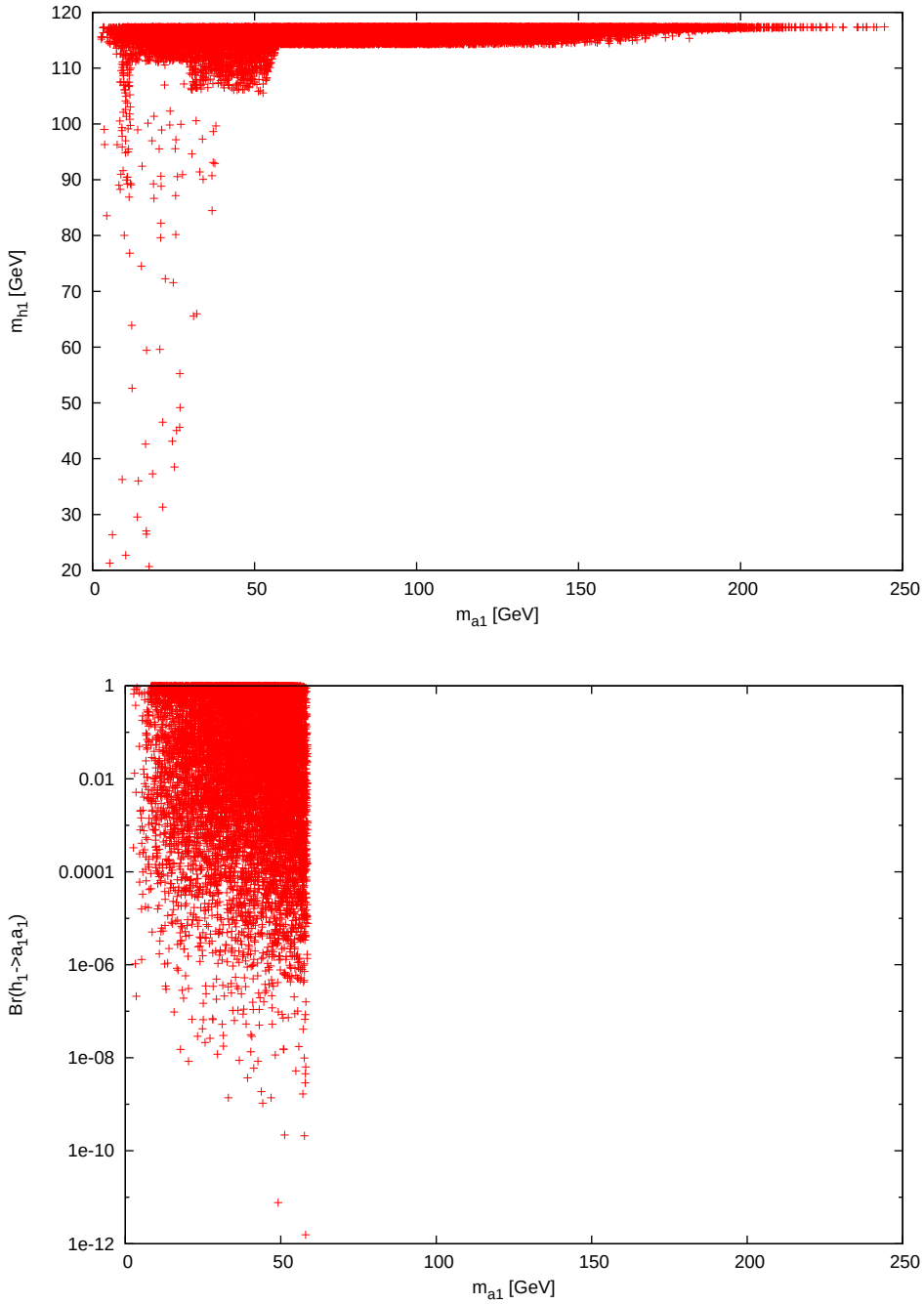

Figure 5.4: The lightest CP-odd Higgs mass m_{a_1} plotted against the lightest CP-even Higgs mass m_{h_1} and against $\mathrm{Br}(h_1 \to a_1 a_1)$.

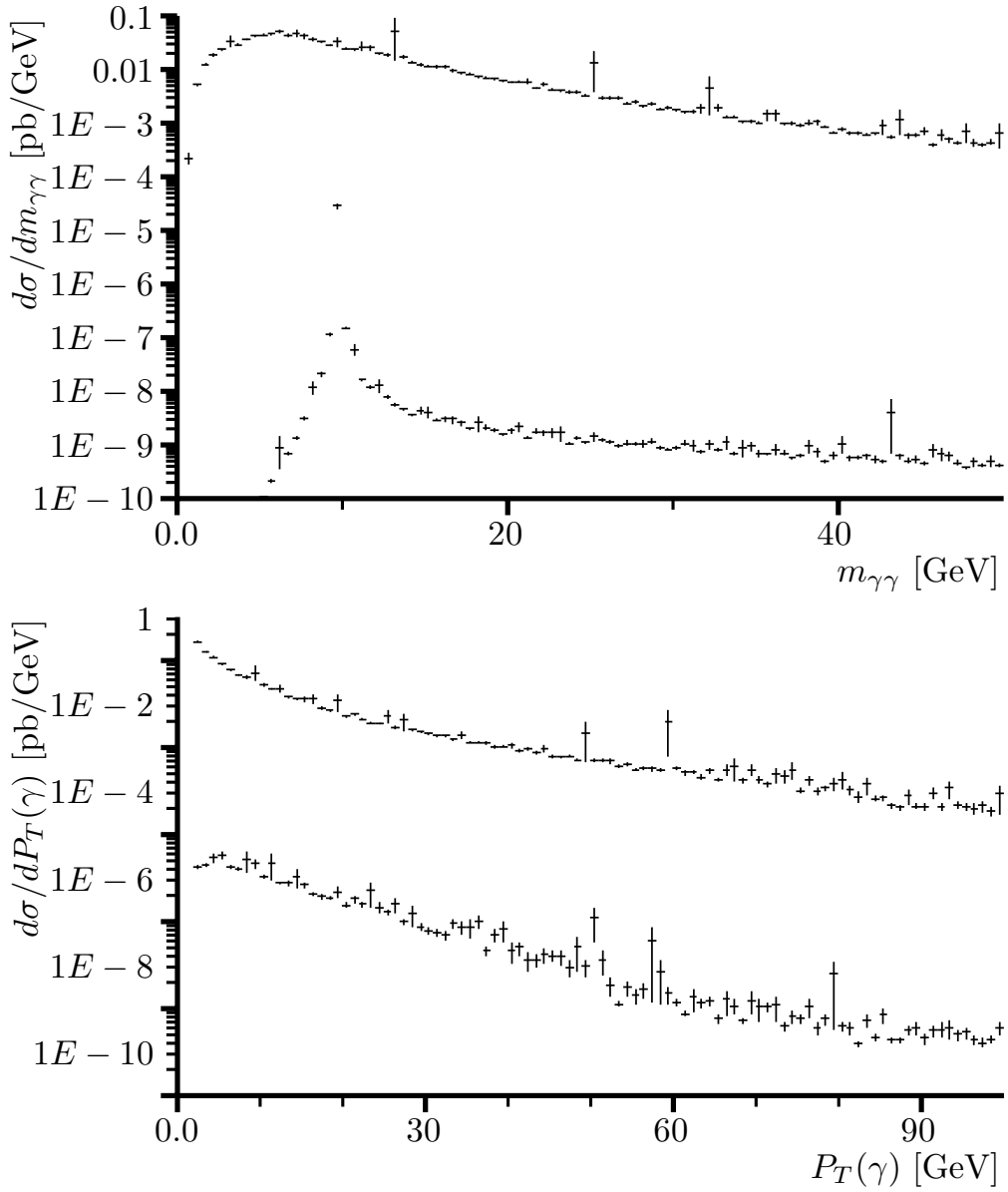

Figure 5.5: The differential cross section in the $\gamma\gamma$ channel for $m_{a_1} = 9.76$ GeV as a function of the invariant mass $m_{\gamma\gamma}$ (top) and of $P_T(\gamma)$ (bottom) for the signal (bottom distribution) only and for the signal and background together (top distribution) after applying the cuts in (5.4).

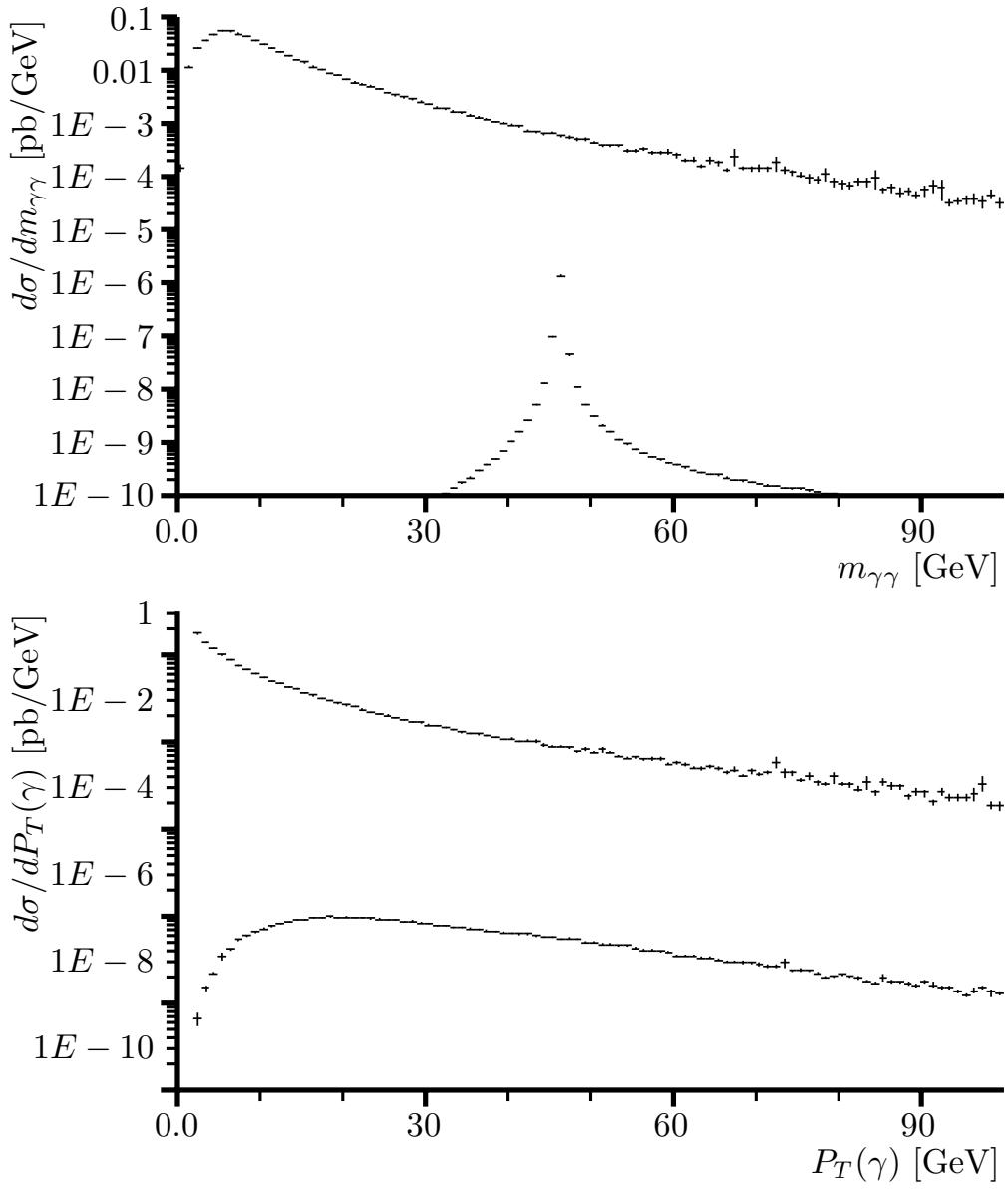

Figure 5.6: The differential cross section in the $\gamma\gamma$ channel for $m_{a_1} = 46.35$ GeV as a function of the invariant mass $m_{\gamma\gamma}$ (top-pane) and of $P_T(\gamma)$ (bottom-pane) for the signal (bottom distribution) only and for the signal and background together (top distribution) after applying the cuts in (5.4).

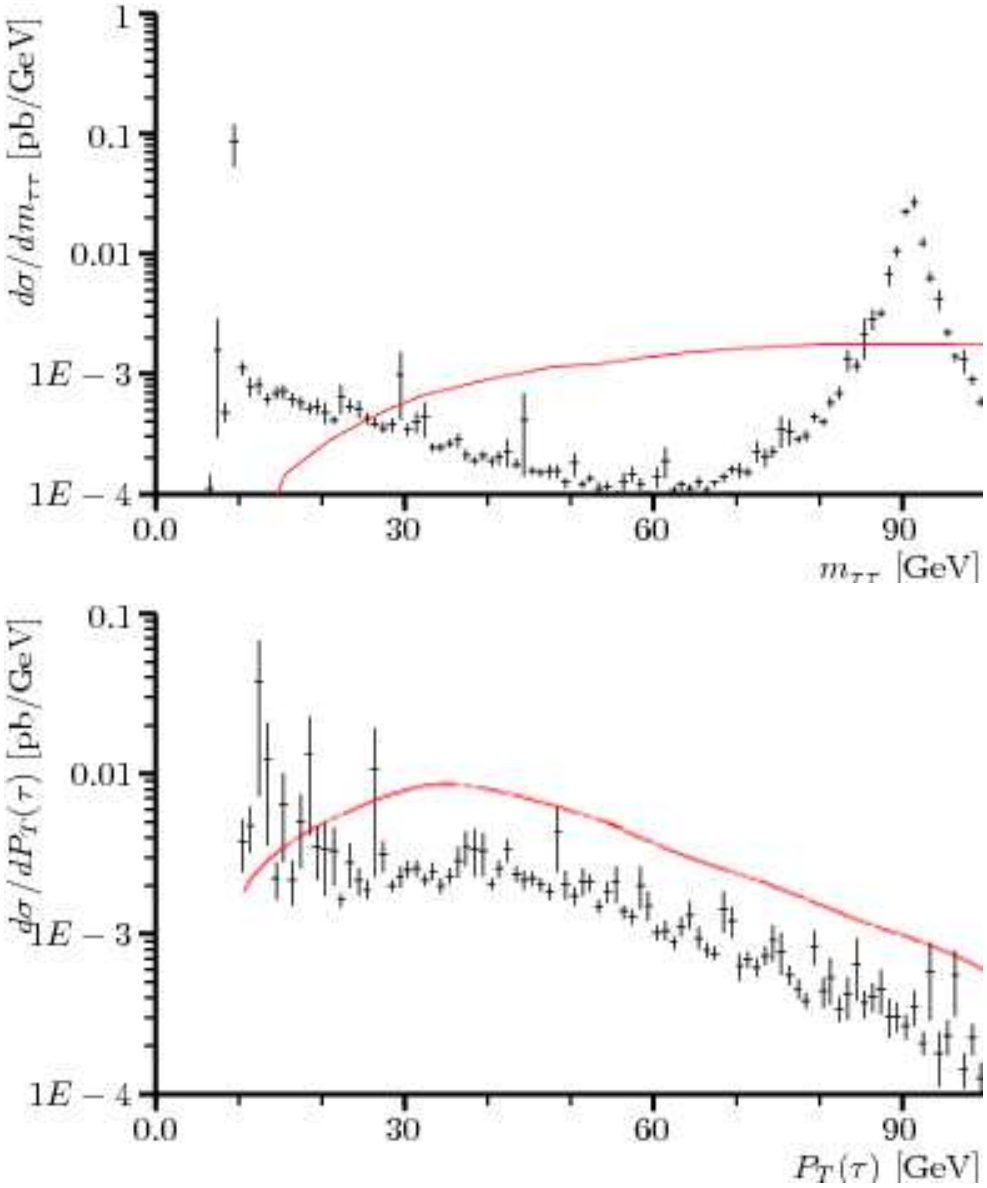

Figure 5.7: The differential cross section in the $\tau^+\tau^-$ channel for m_{a_1}=9.76 GeV as a function of $m_{\tau\tau}$ (top) and of $P_T(\tau)$ (bottom) after applying the cuts in (5.5). The histogram points represent the signal and irreducible background together while the red line is the $t\bar{t}$ background.

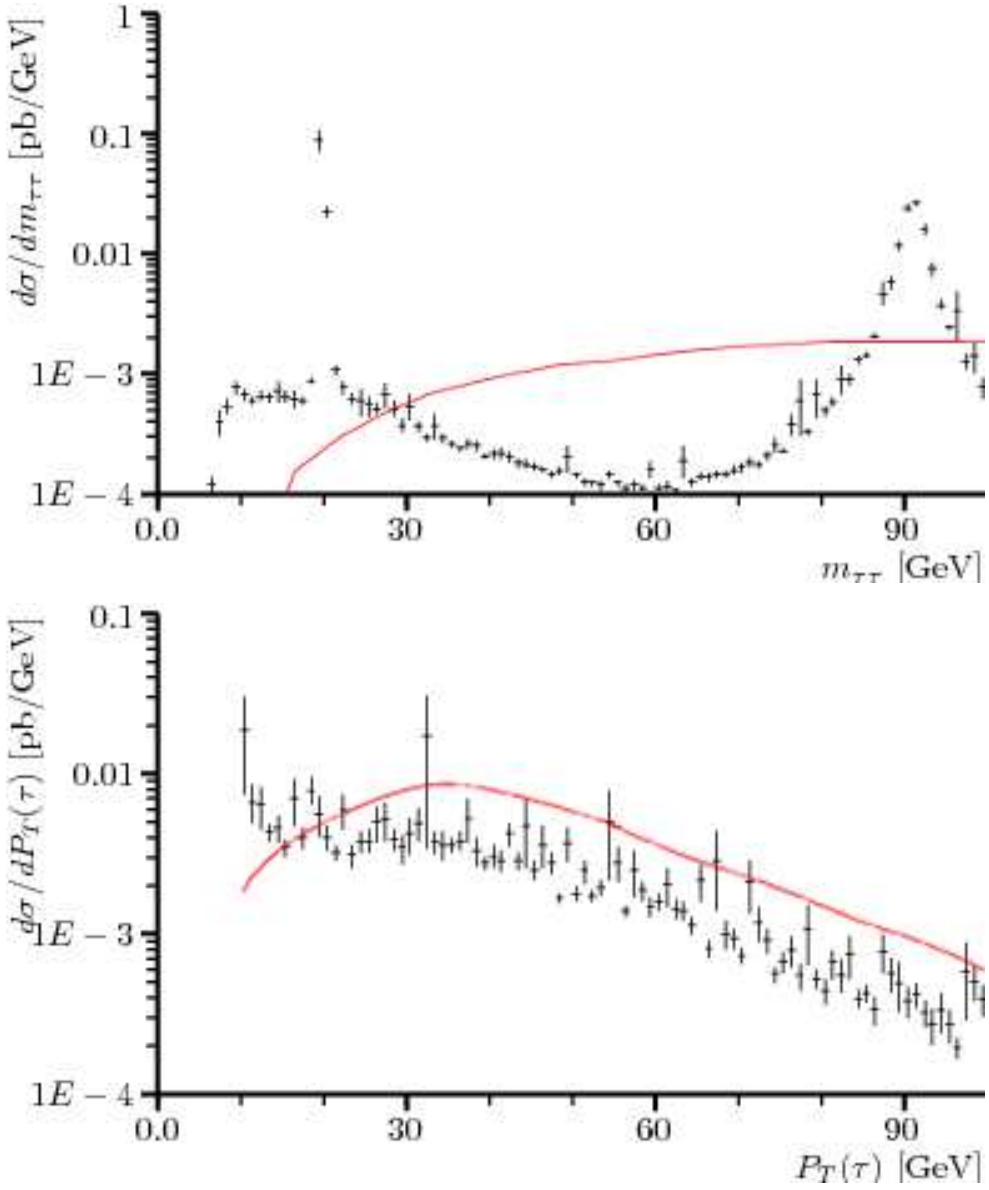

Figure 5.8: The differential cross section in the $\tau^+\tau^-$ channel for m_{a_1}=19.98 GeV as a function of $m_{\tau\tau}$ (top) and of $P_T(\tau)$ (bottom) after applying the cuts in (5.5). The histogram points represent the signal and irreducible background together while the red line is the $t\bar{t}$ background.

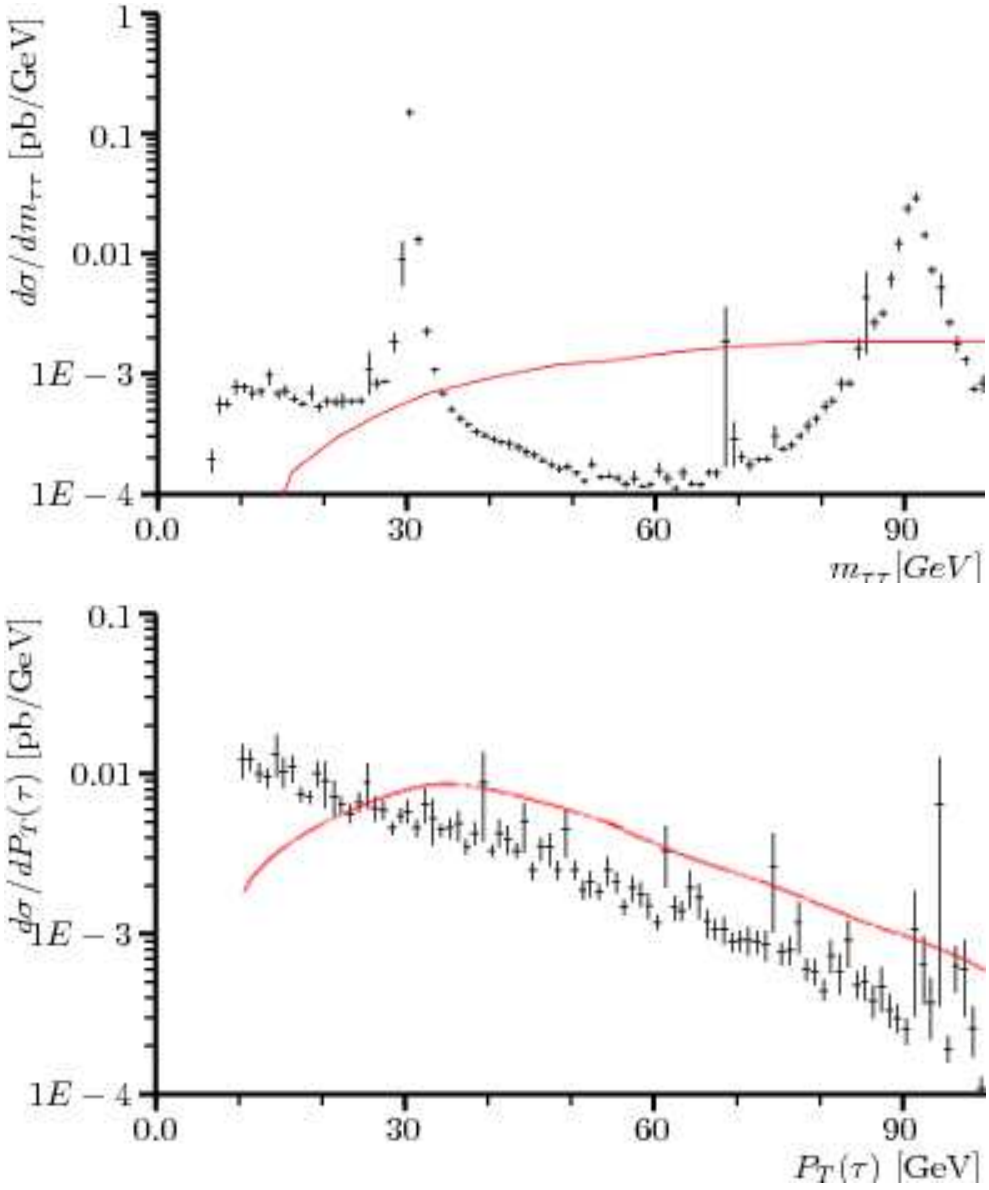

Figure 5.9: The differential cross section in the $\tau^+\tau^-$ channel for m_{a_1}=30.67 GeV as a function of $m_{\tau\tau}$ (top) and of $P_T(\tau)$ (bottom) after applying the cuts in (5.5). The histogram points represent the signal and irreducible background together while the red line is the $t\bar{t}$ background.

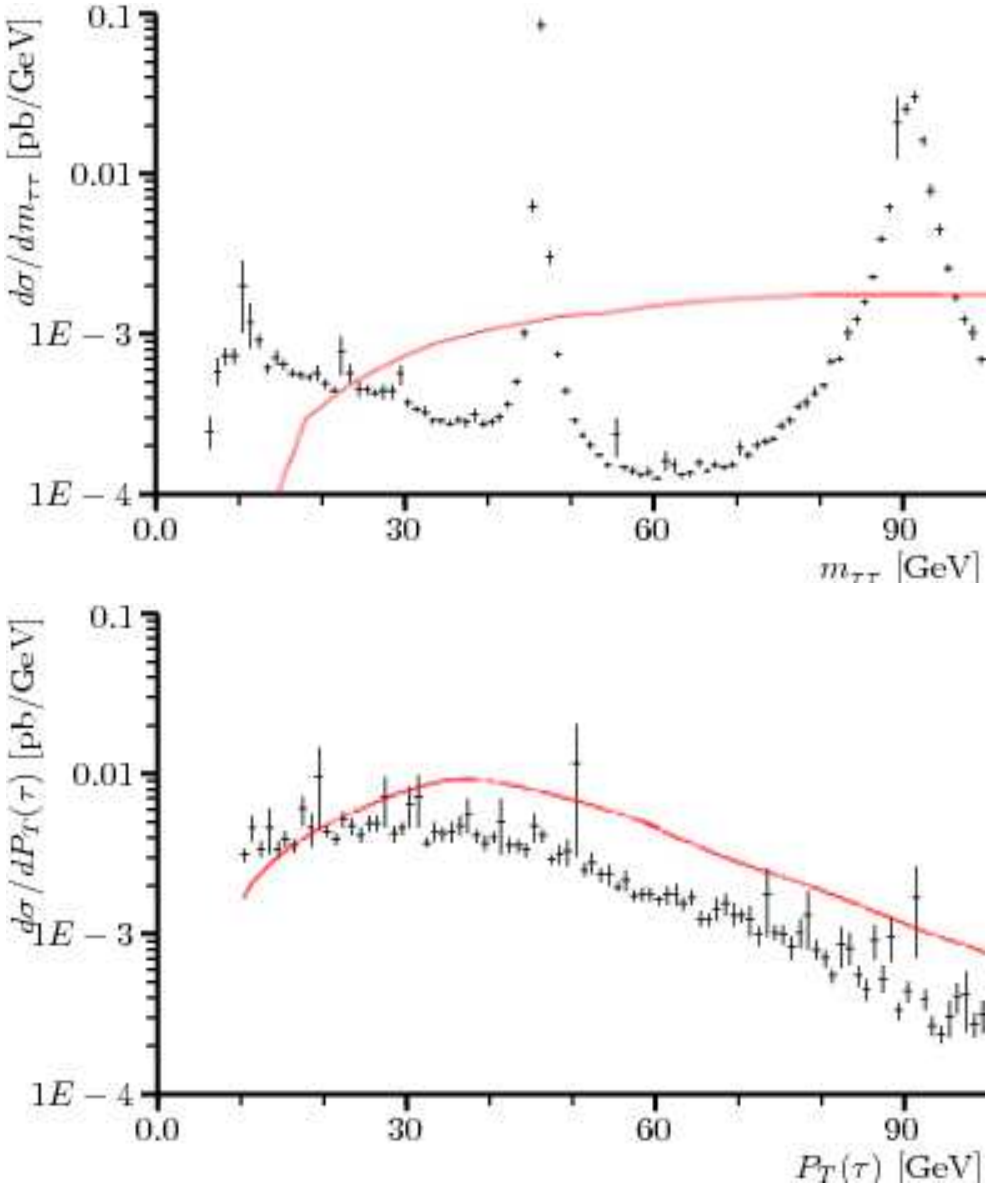

Figure 5.10: The differential cross section in the $\tau^+\tau^-$ channel for m_{a_1}=46.35 GeV as a function of $m_{\tau\tau}$ (top) and of $P_T(\tau)$ (bottom) after applying the cuts in (5.5). The histogram points represent the signal and irreducible background together while the red line is the $t\bar{t}$ background.

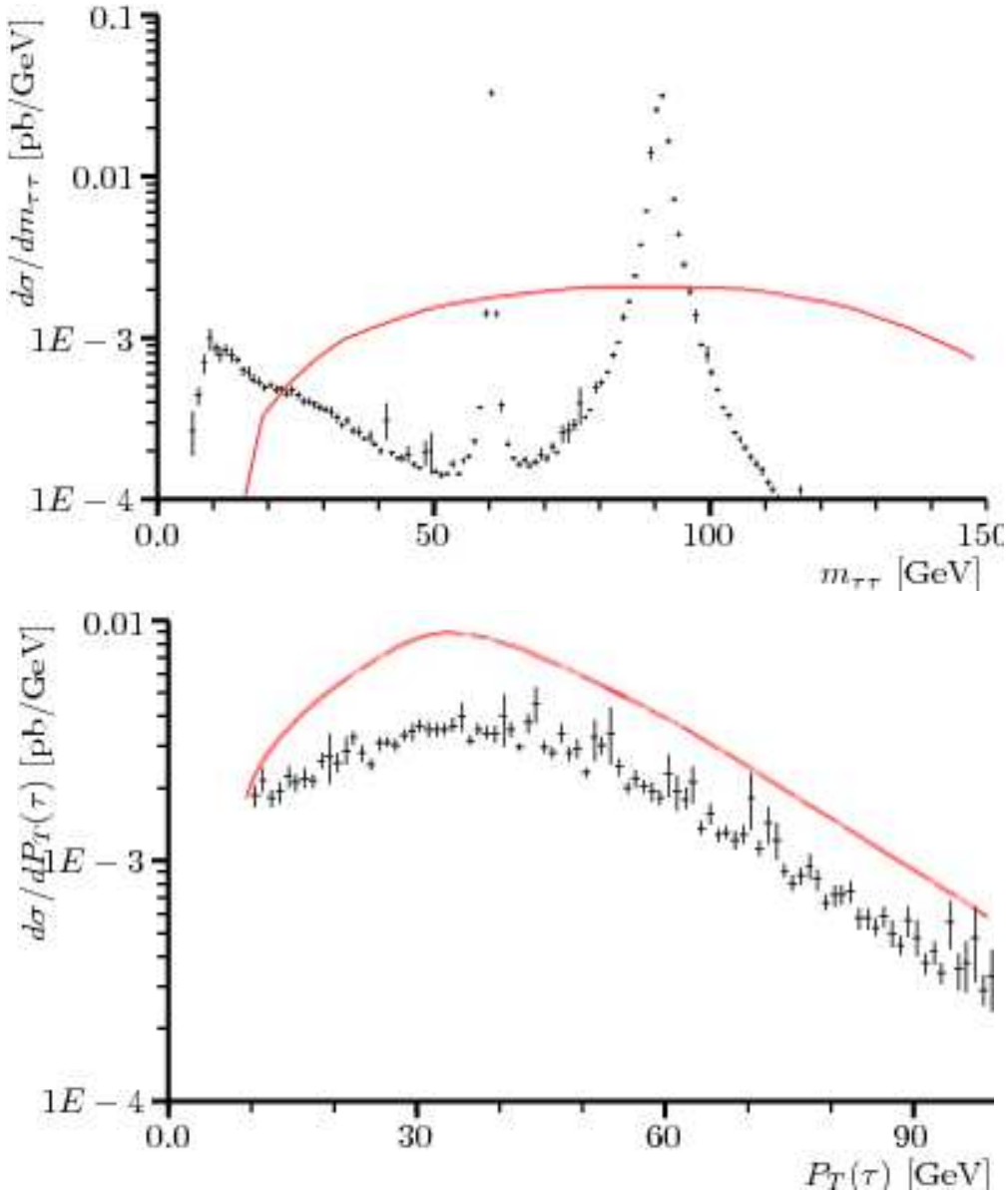

Figure 5.11: The differential cross section in the $\tau^+\tau^-$ channel for m_{a_1}=60.51 GeV as a function of $m_{\tau\tau}$ (top) and of $P_T(\tau)$ (bottom) after applying the cuts in (5.5). The histogram points represent the signal and irreducible background together while the red line is the $t\bar{t}$ background.

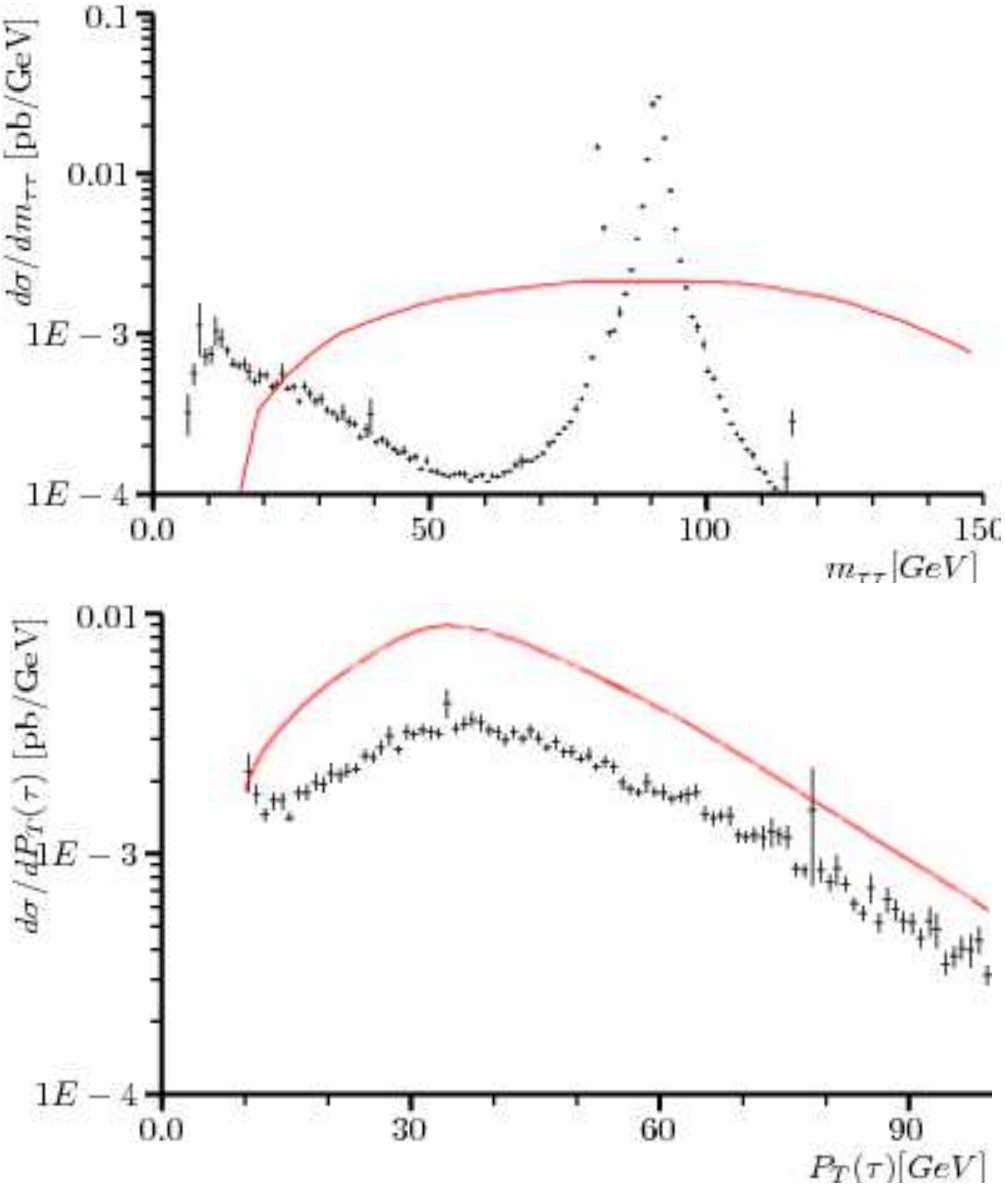

Figure 5.12: The differential cross section in the $\tau^+\tau^-$ channel for m_{a_1}=80.91 GeV as a function of $m_{\tau\tau}$ (top) and of $P_T(\tau)$ (bottom) after applying the cuts in (5.5). The histogram points represent the signal and irreducible background together while the red line is the $t\bar{t}$ background.

5.5 Summary of the chapter

In short, we have proven that there exist some regions of the NMSSM parameter space where very light CP-odd Higgs states produced in association with $b\bar{b}$ pairs can be discovered at the LHC. In our analysis, we have shown that the $\tau^+\tau^-$ decay mode is a promising channel to detect an a_1 with mass $\lesssim M_Z$. After a realistic S/B analysis at parton level, we have in fact produced results showing that the extraction of very light mass $a_1 \to \tau^+\tau$ resonances above both the irreducible and (dominant) reducible backgrounds should be feasible, at least when one of the two tau leptons decays leptonically. In practice, more refined analyses, incorporating τ-decay, parton shower, hadronisation and detector effects, are needed in order to claim the true discovery potential of the LHC over the actual NMSSM parameter space. However, we believe that our results are a step in the right direction to prove the existence of a 'More-to-gain theorem' at the CERN collider for the NMSSM with respect to the MSSM, as $\tau^+\tau^-$ signals from such light Higgs bosons are not possible in the latter scenario. In addition, some of the parameter regions where the aforementioned signal can be detected overlap with those where $h_{1,2} \to a_1 a_1$ is kinematically possible. So, the process discussed here also offers an alternative handle to establish the 'No-lose theorem' for the NMSSM at the LHC by direct production of the a_1 rather than looking for the decay $h_{1,2} \to a_1 a_1$.

Furthermore, notice that we have explored here the two regimes $2m_\tau < m_{a_1} < 2m_b$ and $2m_b < m_{a_1}$. The former is where the $a_1 \to \tau^+\tau^-$ decay rate dominates (these are the points in the 'red island' to the outermost right-hand side of the middle-right plot of figure 5.3), for which the $\mathrm{Br}(a_1 \to \tau^+\tau^-) \gtrsim 0.9$ because the $b\bar{b}$ decay channel is closed. (Our mass point $m_{a_1} = 9.76$ GeV was representative of this situation.) The latter is where the $a_1 \to b\bar{b}$ decay rate is dominant (the corresponding points are most of the remaining ones in figure 5.3), since here the $\mathrm{Br}(a_1 \to \tau^+\tau^-) \lesssim 0.1$ because the $b\bar{b}$ decay channel is open. (Our mass points m_{a_1} =19.98, 30.67, 46.35, 60.51 and 80.91 GeV were representative of this situation.)

Unfortunately, a similar analysis in the $a_1 \to \gamma\gamma$ channel has showed that the LHC discovery potential is hindered by an overwhelming irreducible background. Finally, It is worth mentioning that in the NMSSM there is a possibility that the $\mathrm{Br}(a_1 \to \gamma\gamma)$ is dominant, reaching unity when the a_1 state is a pure singlet, a peculiarity of the NMSSM with respect to the MSSM.

Chapter 6

Muon and b-quark signals of very light CP-odd Higgs states of the NMSSM at the LHC

6.1 Introduction

In this chapter we study the detectability of the lightest CP-odd Higgs boson of the NMSSM, a_1, at the LHC through its production in association with a bottom-quark pair followed by $a_1 \to \mu^+\mu^-$ and $a_1 \to b\bar{b}$ decays. It is shown that, for large tanβ and very high luminosity of the LHC, there exist regions of the NMSSM parameter space that can be exploited to detect the a_1 through $a_1 \to \mu^+\mu^-$. These signatures are characteristic features of the NMSSM in comparison to the MSSM, as the a_1 masses involved are well below those allowed in the MSSM for the corresponding CP-odd Higgs state. On the other hand, the detection of a_1 through $b\bar{b}$ remains uncertain due to the huge QCD backgrounds.

In this analysis, we explore the 'No-lose' and 'More-to-gain' theorems at once through studying direct production of a very light a_1 (with $m_{a_1} < M_Z$). This work is complementary to the one carried out in the previous chapter, in which we explored the $\tau^+\tau^-$ and $\gamma\gamma$ decay modes of such a light a_1 state. The work in this chapter has been published in [33, 34]

6.2 Di-muon decay mode

This mode has an advantage that it has a clean signature with excellent mass resolution. However, the $\mu^+\mu^-$ branching ratio is small in most regions of parameter space but this decay mode is enhanced for large tanβ.

6.2.1 Inclusive signal rates

In our exploration of the Higgs sector of the NMSSM, we have done a random scan using NMSSMTools. The features of the scan performed have been already discussed in the previous chapter.

As a first step in analysing our data, we have computed the production cross section $\sigma(gg \rightarrow b\bar{b}a_1)$ multiplied by the Br$(a_1 \rightarrow \mu^+\mu^-)$ against each of the six tree level parameters of the NMSSM. Figures 6.1 and 6.2 show the results of our random scan for the points that passed the various constraints implemented in NMSSMTools.

Figure 6.1 illustrates the distribution of the inclusive event rates over the six NMSSM parameters and the distribution as a function of the Br$(a_1 \rightarrow \mu^+\mu^-)$ and of m_{a_1}. In our choice of parameter space, it is clear that the large tanβ, small μ_{eff} and rather small λ region is the one most compatible with current theoretical and experimental constraints while the distributions in κ, A_λ and A_κ are rather uniform (top six panes in figure 6.1).

Figure 6.2 shows the correlations between the a_1 mass and the di-muon decay rate. One can see from this figure that the Br$(a_1 \rightarrow \mu^+\mu^-)$ can be of $\mathcal{O}(10\%)$, $\mathcal{O}(1\%)$ and $\mathcal{O}(0.1\%)$ or less for the mass intervals $2m_\mu < m_{a_1} < 2m_\tau$, $2m_\tau < m_{a_1} < 2m_b$ and $2m_b < m_{a_1}$, respectively. The first region of parameter space ($m_{a_1} < 2m_\tau$) is rather small, the second one ($2m_\tau < m_{a_1} < 2m_b$) more significant and the third one ($2m_b < m_{a_1}$) is by far the widest one.

Further, by looking at the two bottom panes of figure 6.1, it is remarkable to notice that the inclusive event rates are sizable in all such mass regions. These event rates reach the $10^4\ fb$ level in the two lower mass intervals and the $10^3\ fb$ level in the higher mass range and clearly decrease by increasing m_{a_1}, as expected. Finally, notice that the mass region below the $\mu^+\mu^-$ threshold is very severely constrained [85].

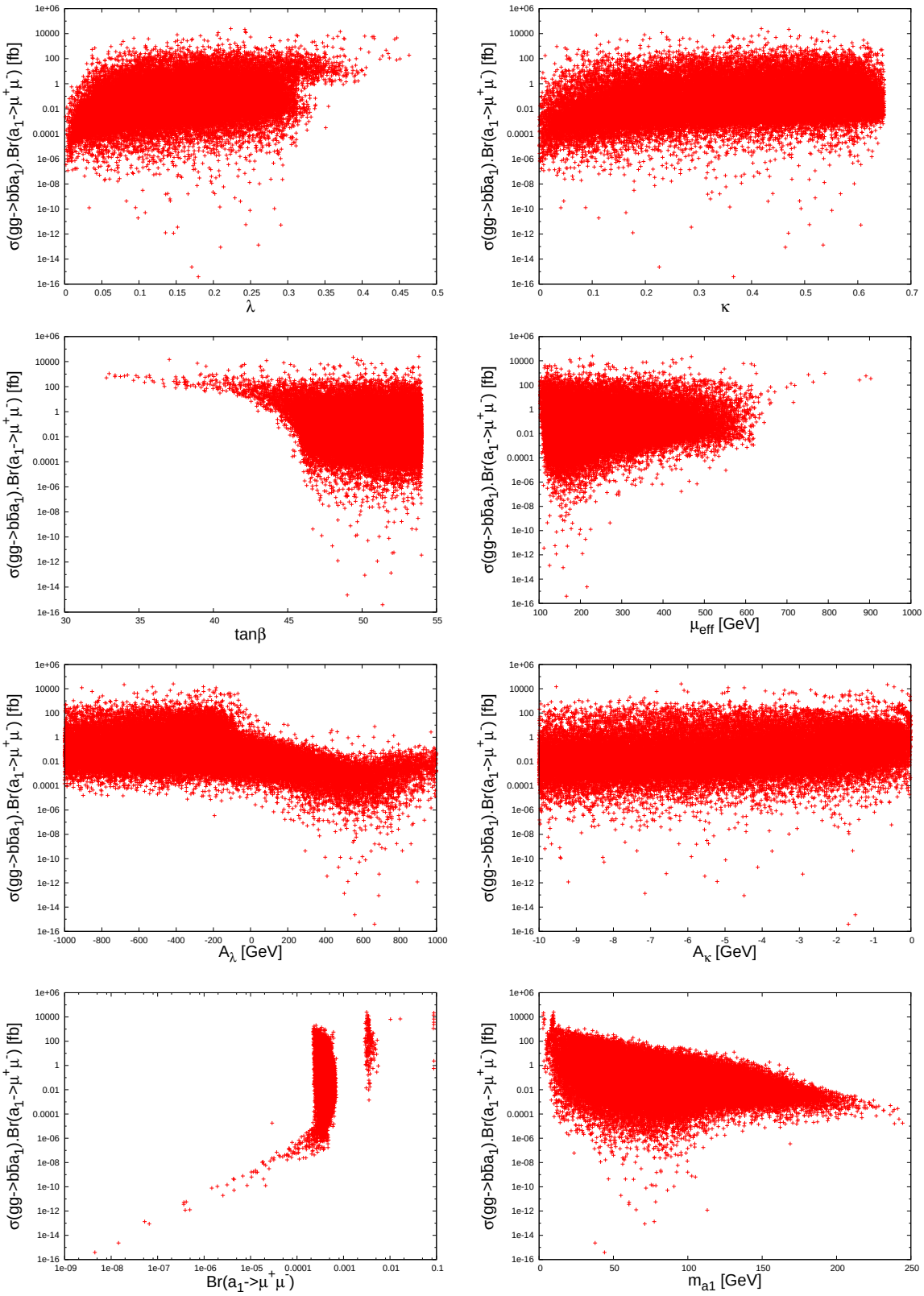

Figure 6.1: The rates for $\sigma(gg \to b\bar{b}a_1)\ \mathrm{Br}(a_1 \to \mu^+\mu^-)$ as a function of λ, κ, $\tan\beta$, μ_{eff}, A_λ, A_κ, $\mathrm{Br}(a_1 \to \mu^+\mu^-)$ and of m_{a_1}.

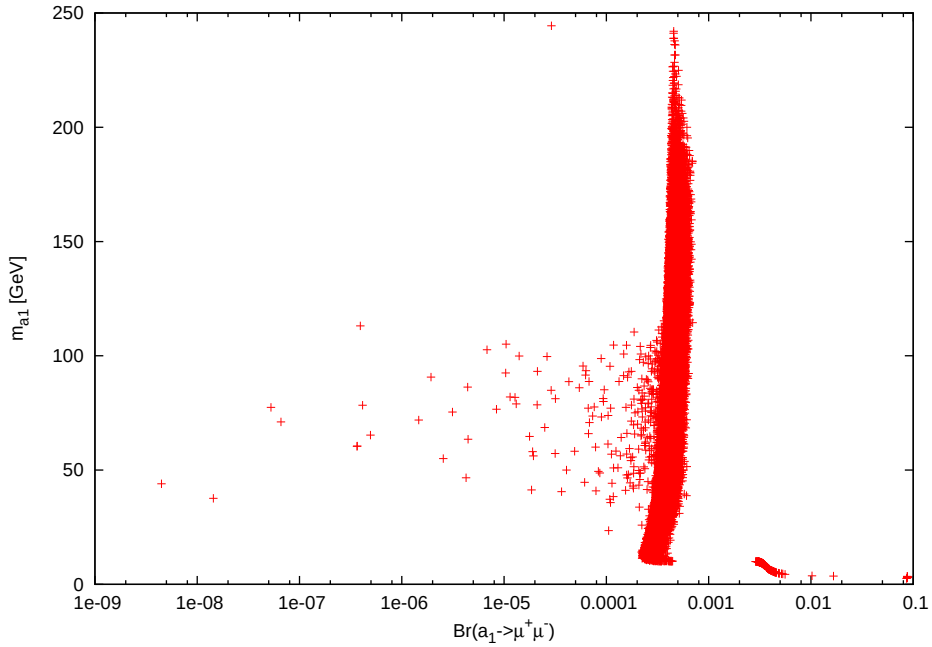

Figure 6.2: The CP-odd Higgs mass m_{a_1} as a function of the Br$(a_1 \to \mu^+\mu^-)$.

6.2.2 Signal-to-background analysis

We follow the same procedure of the work done in the previous chapter by performing a partonic signal-to-background (S/B) analysis. We assume $\sqrt{s} = 14$ TeV throughout for the LHC energy and in our numerical analyses we have taken $m_\tau^{\rm pole} = 1.777$ GeV and $m_\mu^{\rm pole} = 0.1057$ GeV for the (pole) tau- and (pole) muon-lepton mass, respectively. Furthermore, we assume the following cuts

$$\Delta R(b,\bar{b}), \Delta R(b,\mu^+), \Delta R(\bar{b},\mu^+), \Delta R(b,\mu^-), \Delta R(\bar{b},\mu^-), \Delta R(\mu^+,\mu^-) > 0.4,$$

$$0 < \eta(b), \eta(\bar{b}), \eta(\mu^+), \eta(\mu^-) < 2.5,$$

$$P_T(b), P_T(\bar{b}) > 20 \text{ GeV}, P_T(\mu^+), P_T(\mu^-) > 5 \text{ GeV}. \tag{6.1}$$

After implementing the cuts, we obtain the invariant masses of the $\mu^+\mu^-$ system depicted in figures 6.3–6.7[1]. In these figures, we show the combined yield of the signal induced by $gg \to b\bar{b}\mu^+\mu^-$ (via g and a_1 exchange) and of the irreducible background due to $pp \to b\bar{b}\mu^+\mu^-$ (via g, γ and Z exchange), including their interference. We also show in the same figures the top-antitop distribution, the dominant reducible background, i.e., $pp \to t\bar{t} \to b\bar{b}W^+W^- \to b\bar{b}\mu^+\mu^- P_T^{\rm miss}$.

We notice that the $\gamma \to \mu^+\mu^-$ tail of the irreducible background is dominant at very small invariant masses of the di-muon system. In addition, the reducible background

[1]The benchmark points used in this chapter are given in Sec. 5.4.

starts reaching its maximum at around $M_W/2$. Finally, the $Z \to \mu^+\mu^-$ peak of the irreducible background becomes overwhelming, starting at 60 GeV or so and reaching its maximum when $m_{\mu\mu} = M_Z$. Overall, the number of $\mu^+\mu^-$ signal events in such a mass region is of order 75 events for m_{a_1} reaching 60 GeV or so to 1440 events for m_{a_1} starting at 10 GeV or so over a sizably smaller background. Notice that the plots are in logarithmic scale and that we are assuming 300 fb^{-1} of integrated luminosity as an example.

In fact, the number of signal events is not so large, in particular at low luminosity. Nevertheless, there is still potential scope to extract a significant signal for the selected points, thanks to the high mass resolution that can be achieved using muon pairs. Assuming $\mu^+\mu^-$ resolutions of 1 GeV [22], we show in the top-pane of figure 6.8 the relation between the signal significance $S/\sqrt{B}$ (where S and B are the signal and background rates, respectively) and the integrated luminosity for five of the benchmark points mentioned above. The corresponding signal event rates are shown in the bottom-pane of the same figure. From these last results, it is clear that the discovery of a_1 at the LHC could occur for a_1 masses between ≈ 10 and ≈ 40 GeV with rather modest luminosity, 30 fb^{-1} or so, while $\approx 50(\approx 60)$ GeV masses require some 200(300) fb^{-1}. However, heavier states will not be resolvable for the LHC even with up to 300 fb^{-1} of integrated luminosity.

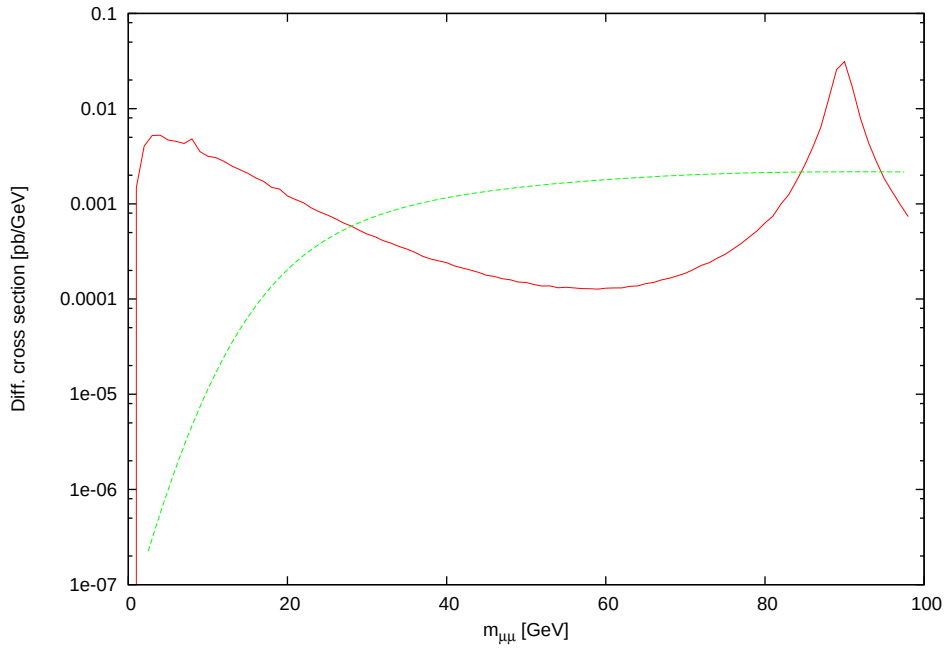

Figure 6.3: The differential cross section in the $\mu^+\mu^-$ channel for m_{a_1}=9.76 GeV as a function of $m_{\mu\mu}$ after applying the cuts in (6.1). The solid line represents the signal and irreducible background together while the dashed line is the $t\bar{t}$ background. (Notice that here $2m_b^{\text{pole}} > m_{a_1}$ and that the small bump corresponding to $m_{\mu\mu} = 9.76$ GeV is the signal.)

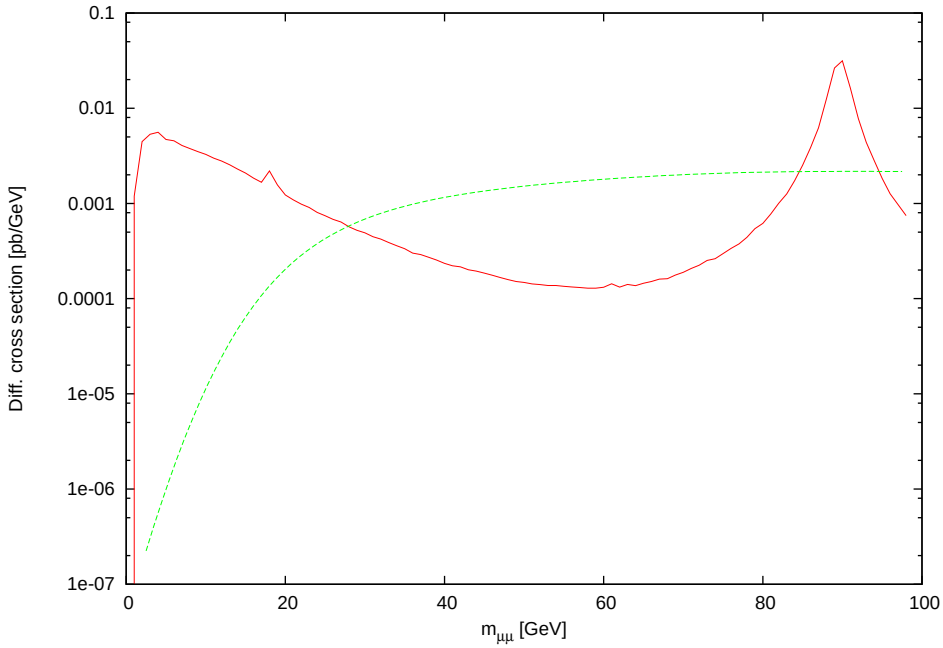

Figure 6.4: The differential cross section in the $\mu^+\mu^-$ channel for m_{a_1}=19.98 GeV as a function of $m_{\mu\mu}$ after applying the cuts in (6.1). The solid line represents the signal and irreducible background together while the dashed line is the $t\bar{t}$ background.

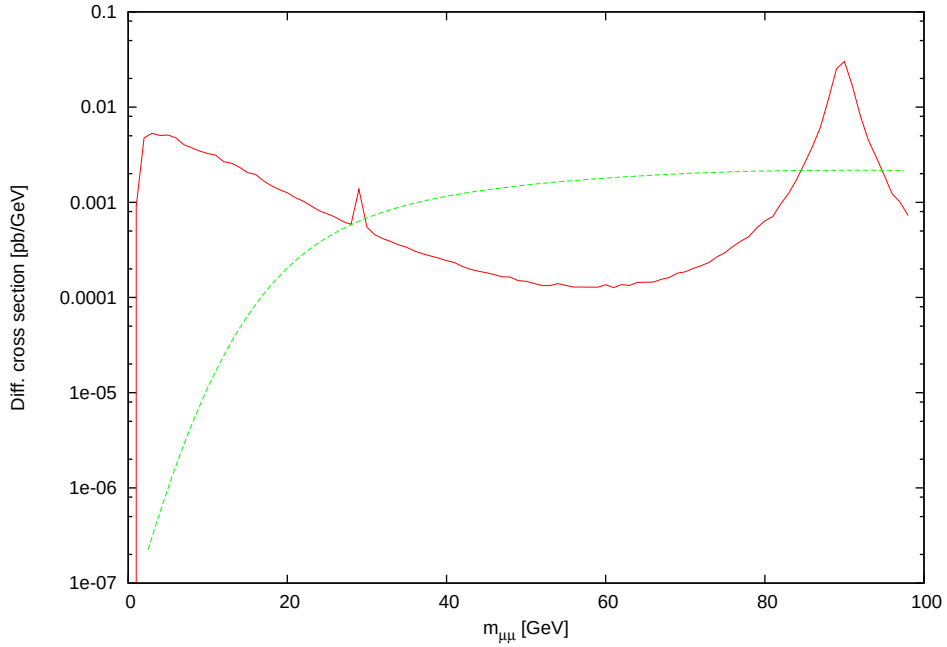

Figure 6.5: The differential cross section in the $\mu^+\mu^-$ channel for m_{a_1}=30.67 GeV as a function of $m_{\mu\mu}$ after applying the cuts in (6.1). The solid line represents the signal and irreducible background together while the dashed line is the $t\bar{t}$ background.

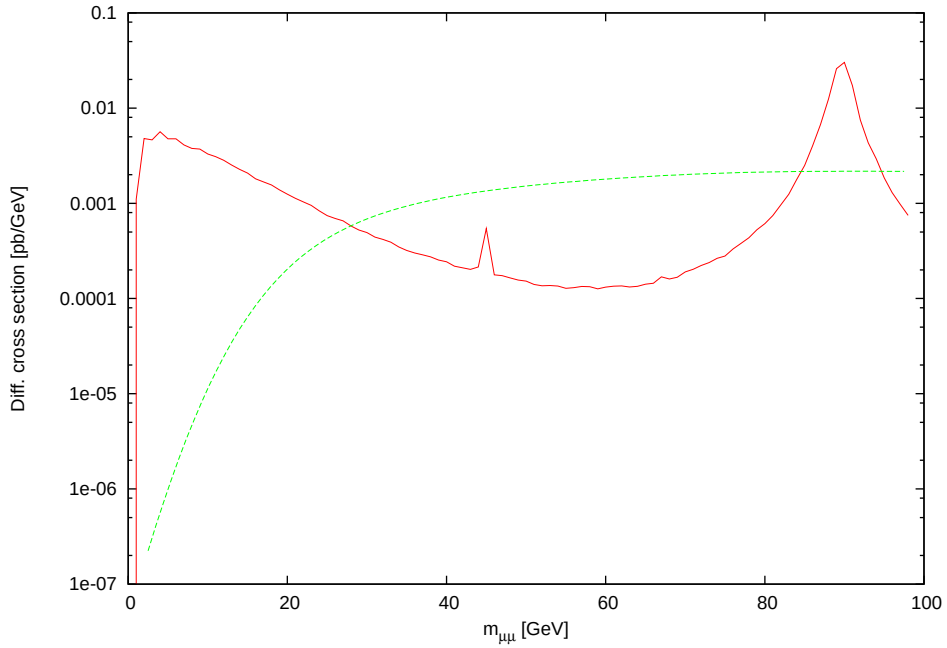

Figure 6.6: The differential cross section in the $\mu^+\mu^-$ channel for m_{a_1}=46.35 GeV as a function of $m_{\mu\mu}$ after applying the cuts in (6.1). The solid line represents the signal and irreducible background together while the dashed line is the $t\bar{t}$ background.

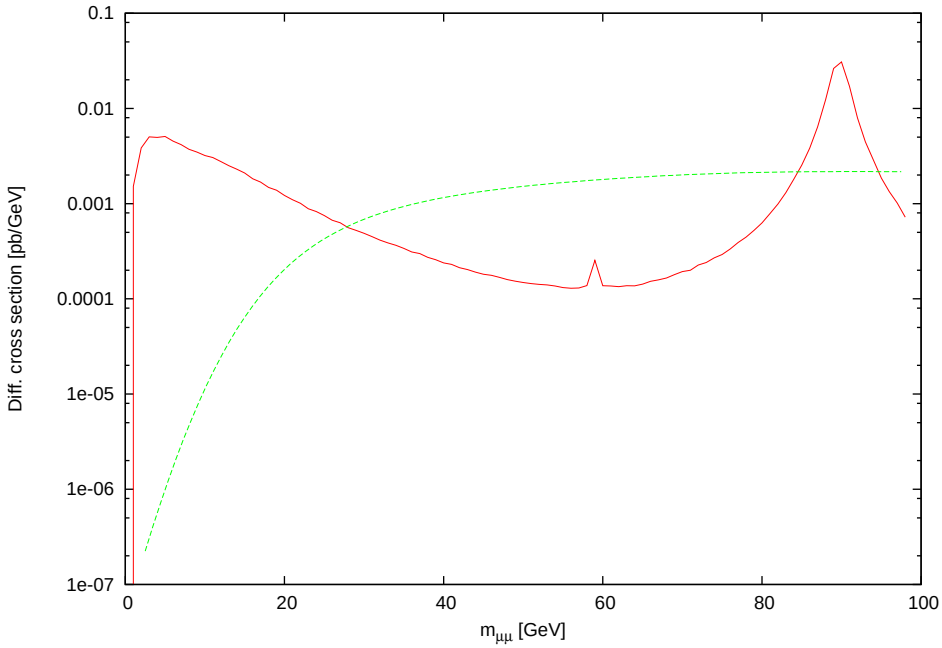

Figure 6.7: The differential cross section in the $\mu^+\mu^-$ channel for m_{a_1}=60.51 GeV as a function of $m_{\mu\mu}$ after applying the cuts in (6.1). The solid line represents the signal and irreducible background together while the dashed line is the $t\bar{t}$ background.

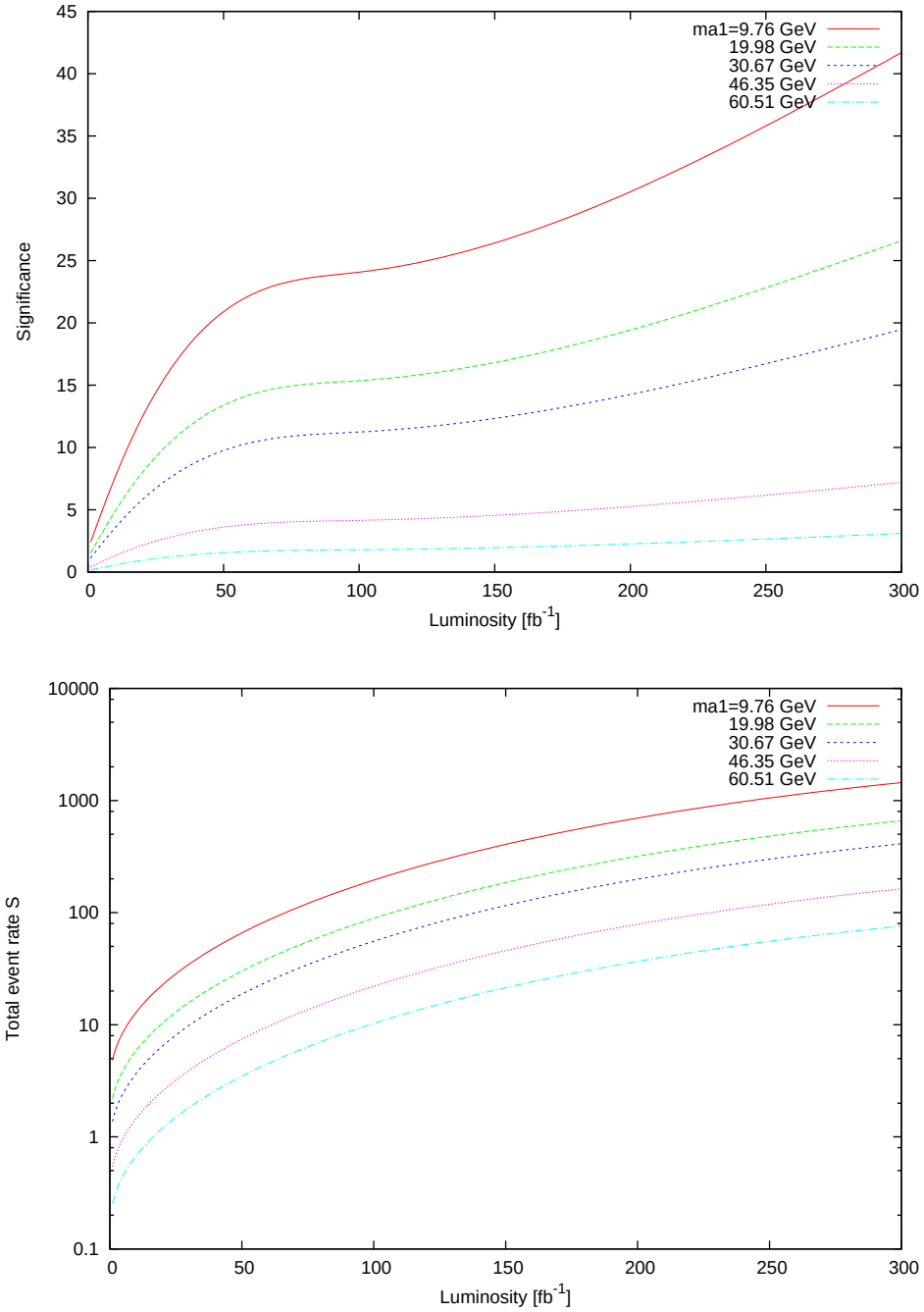

Figure 6.8: The significance $S/\sqrt{B}$ (top) and total event rate S (bottom) of the $gg \to b\bar{b}a_1 \to b\bar{b}\mu^+\mu^-$ signal as a function of the integrated luminosity.

6.3 $4b$-quark final states

At large tanβ values, the cross-section of the a_1 produced in association with a bottom-antibottom pair followed by the decay $a_1 \to b\bar{b}$ is strongly enhanced, in general. However, since the channel is a 4 quark final state, it is plagued by very large irreducible and reducible backgrounds. In this section, we examine whether or not the production mode $gg \to b\bar{b}a_1 \to b\bar{b}b\bar{b}$ can be exploited to detect the a_1 at the LHC. In fact, the existence of b-jets in the final states offers the advantage of b-tagging, which can be exploited to trigger on the signal and enable us to require four displaced vertices in order to reject light jets. The ensuing $4b$ signature has already been exploited to detect neutral Higgs bosons of the MSSM at the LHC and proved useful, provided that tanβ is large and the collider has good efficiency and purity in tagging b-quark jets, albeit for the case of rather heavy Higgs states (with masses beyond M_Z, typically) [89, 90].

6.3.1 Inclusive signal rates

As usual, in the first step of the analysis, we have computed the fully inclusive signal production cross section $\sigma(gg \to b\bar{b}a_1)$ multiplied by the branching fraction Br$(a_1 \to b\bar{b})$ against each of the six parameters of the NMSSM. Figures 6.9 and 6.10 present the results of our scan, the first series of plots (in figure 6.9) illustrate the distribution of the inclusive event rates over the six NMSSM parameters and the distribution as a function of the Br$(a_1 \to b\bar{b})$ and of m_{a_1}. The plots in figure 6.10 display instead the correlations between the $a_1 \to b\bar{b}$ decay rate and the a_1 mass (top-pane) and between the $a_1 \to b\bar{b}$ decay rate and the $a_1 \to \gamma\gamma$ decay rate. Again, it is clear from figure 6.9 that, for our parameter space, the large tanβ and small μ_{eff} (and, to some extent, also small λ) region is the one most compatible with current theoretical and experimental constraints while the distributions in κ, A_λ and A_κ are rather uniform (top six panes in figure 6.9). From a close look at the bottom-left pane of figure 6.9, it is clear that the Br$(a_1 \to b\bar{b})$ is dominant for most points in the parameter space, about 90% and above. In addition, by looking at the the bottom-right pane of the figure, it is remarkable to notice that the event rates are sizable in most regions of parameter space, topping the 10^7 fb level for small values of m_{a_1} and decreasing rapidly with increasing m_{a_1}. One can also notice that there are some points in the parameter space with m_{a_1} between 40 and 120 GeV, as shown in the top-pane of figure 6.10, in which the Br$(a_1 \to b\bar{b})$ is suppressed due to the enhancement of the Br$(a_1 \to \gamma\gamma)$ (see the bottom-pane of the

same figure), a phenomenon peculiar to the NMSSM that depends upon the amount of Higgs singlet-doublet mixing[2], see [32]. (We discussed this in a previous chapter.)

6.3.2 Signal-to-background analysis

Here, we follow the same procedure as mentioned in the previous decay modes by performing a partonic signal-to-background (S/B) analysis, based on CalcHEP results. We assume $\sqrt{s} = 14$ TeV throughout for the LHC energy. Further, we apply the following cuts in our calculations:

$$\Delta R(j,j) > 0.4, \qquad 0 < \eta(j) < 2.5, \qquad P_T(j) > 15 \text{ GeV}. \tag{6.2}$$

Here, we assume that the b-tagging probability of a b-quark is 50% while the mis-tagging probability of a gluon is 1% and the one for a light quark is 2%. Figures 6.11–6.15 show the distributions in the invariant mass of a two b-jet (di-jet) system after multiplying the production times decay rates (after cuts) by the aforementioned efficiency/rejection factors, i.e., true b-tagging and mis-tagging probability. It is clear that the largest background is the irreducible one $b\bar{b}b\bar{b}$[3], which is one order of magnitude larger than the reducible background $b\bar{b}gg$. Further, the other reducible background, involving light quarks, labelled here as $b\bar{b}c\bar{c}$, is negligible compared to the other two. Notice that all these backgrounds reach their maximum in invariant mass at around 40 GeV. Our plots have a bin width of 1 GeV and account for all combinatorial effects (as appropriate in absence of jet-charge determination).

To explore the detectability of the lightest CP-odd Higgs, a_1, at the LHC, we plotted in figures 6.16 and 6.17 both signal significances (top-panes) and corresponding signal event rates (bottom-panes) as functions of the integrated luminosity, after integrating

[2]Notice that recent constraints coming from Tevatron [91] do not affect our results since the singlet field plays a primary role in the NMSSM. But under severe conditions such as $\lambda \to 0$ and $\kappa \to 0$, the NMSSM and MSSM become similar and those constraints may be applied.

[3]Recall that our calculations are all Leading Order (LO). However, notice that the signal $pp \to b\bar{b}a_1$ has a positive (albeit small, in the mass range considered here) k-factor through Next-to-LO (NLO) QCD, of order a few percent [92]. Further, the dominant (as just seen) $b\bar{b}b\bar{b}$ background has also been computed recently through NLO QCD [93], showing roughly a +50% correction with respect to the LO result. In both cases, the theoretical uncertainty estimated by variation of the renormalisation and factorisation scales is strongly reduced by the inclusion of such NLO corrections. Therefore, these results, when implemented in the context of a full production and decay analysis like the one carried out here, would affect somewhat our significances.

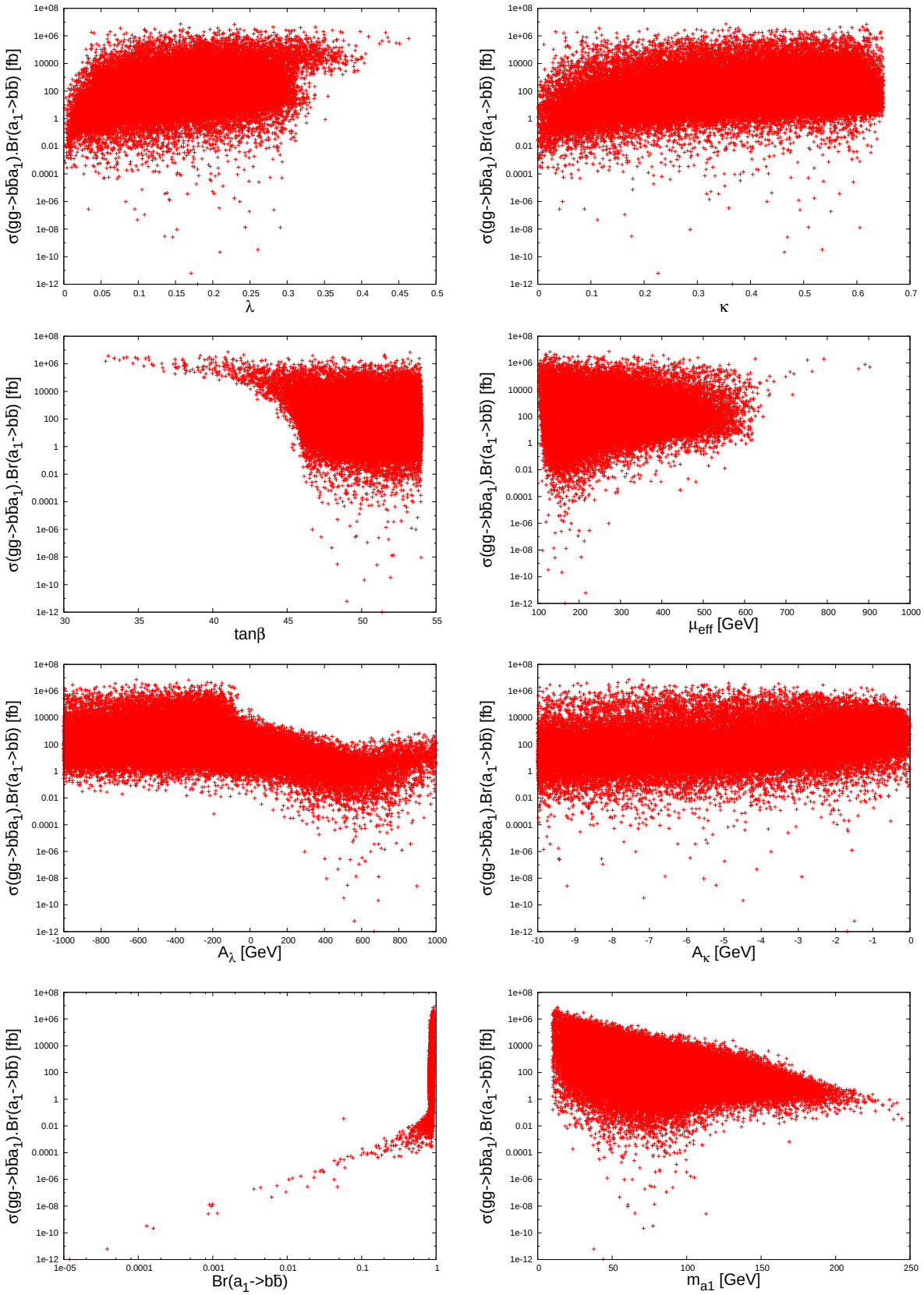

Figure 6.9: The rates for $\sigma(gg \to b\bar{b}a_1)$ Br$(a_1 \to b\bar{b})$ as a function of λ, κ, tanβ, $\mu_{\rm eff}$, A_λ, A_κ, the Br$(a_1 \to b\bar{b})$ and of m_{a_1}.

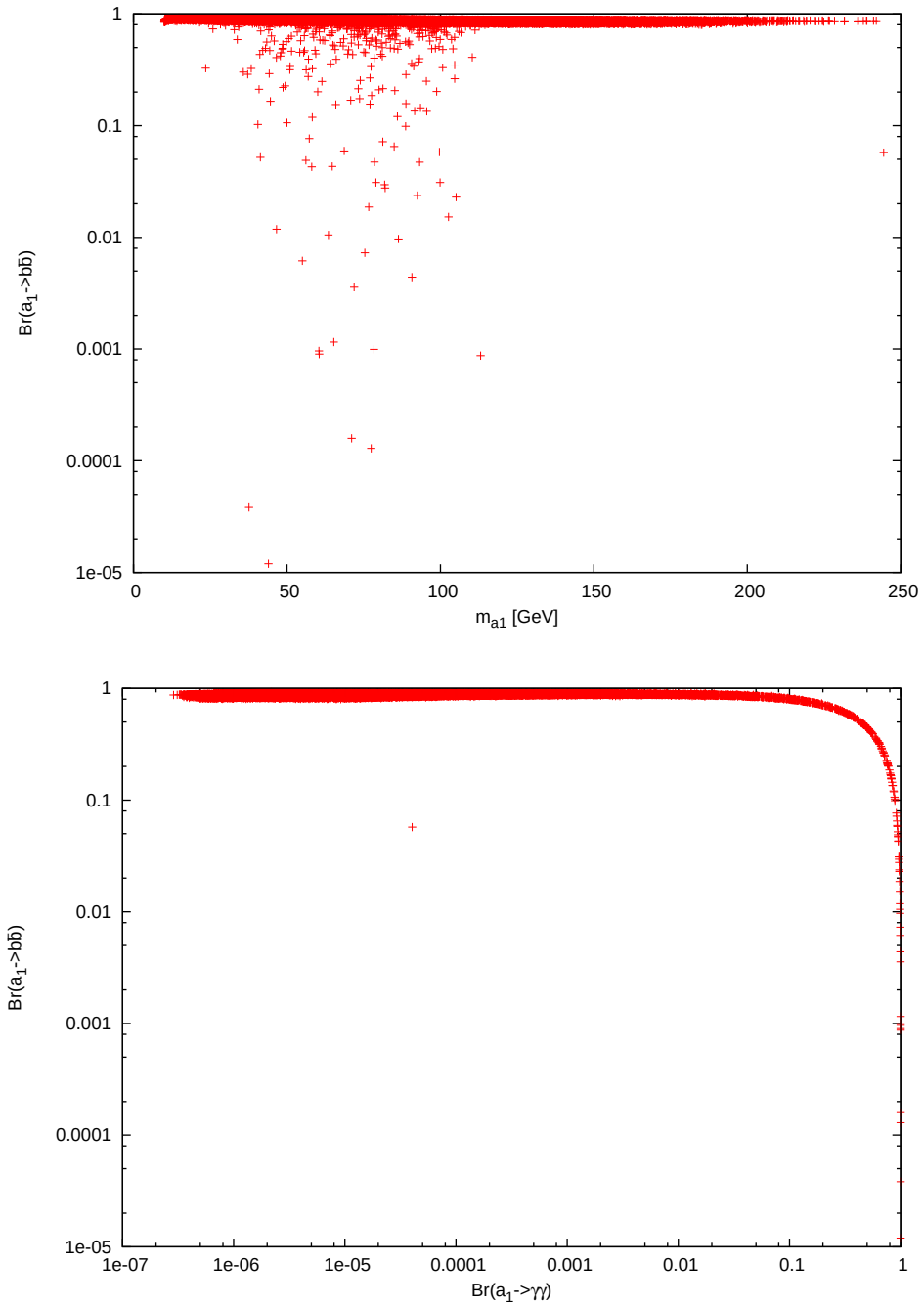

Figure 6.10: The Br($a_1 \to b\bar{b}$) as a function of the CP-odd Higgs mass m_{a_1} and of the Br($a_1 \to \gamma\gamma$) .

over 10 and 5 bins to mimic a more optimistic detector resolution in mass of a di-jet system. From these figures, it is clear that a_1 with mass between 35 and 50 GeV at a very large luminosity, $L = 300\ fb^{-1}$, has a good signal significance, $S/\sqrt{B} \gtrsim 4$, and a significant signal rate, $S \gtrsim 1000$ events. Further, for an upgraded LHC, with a tenfold increase in design luminosity, known as the Super-LHC (SLHC) [94], which could well lead to data samples with $L = 1000\ fb^{-1}$, the a_1 with mass up to 80 GeV or so can have such a good significance and with larger signal rate. However, since the signal-to-background ratio S/B is quite low, about 1.2% or less as shown in figure 6.18, the systematic errors in $4b$ final state, which is of order of several percent [21], make the $a_1 b\bar{b}$ production in the $a_1 \to b\bar{b}$ decay channel very difficult.

Finally, we show in figures 6.19 and 6.20 the differential cross section distribution over pseudorapidity-azimuth (the standard cone measure) separation of di-jet pairs and over average transverse momentum of the jets, respectively (in the latter case we also distinguish between b-jets and non-b-jets). Guided by Refs. [89, 90], this has been done to check whether further cuts (in addition to those in Eq. (6.2)) could be employed to diagnose the detectability of a_1 through the $b\bar{b}$ final state. While some combinations of cuts in these quantities are more efficient for the signal than the backgrounds, there is no overall gain in the signal significance. (Results are here shown for just one signal mass value, yet they are typical also for the other masses considered.)

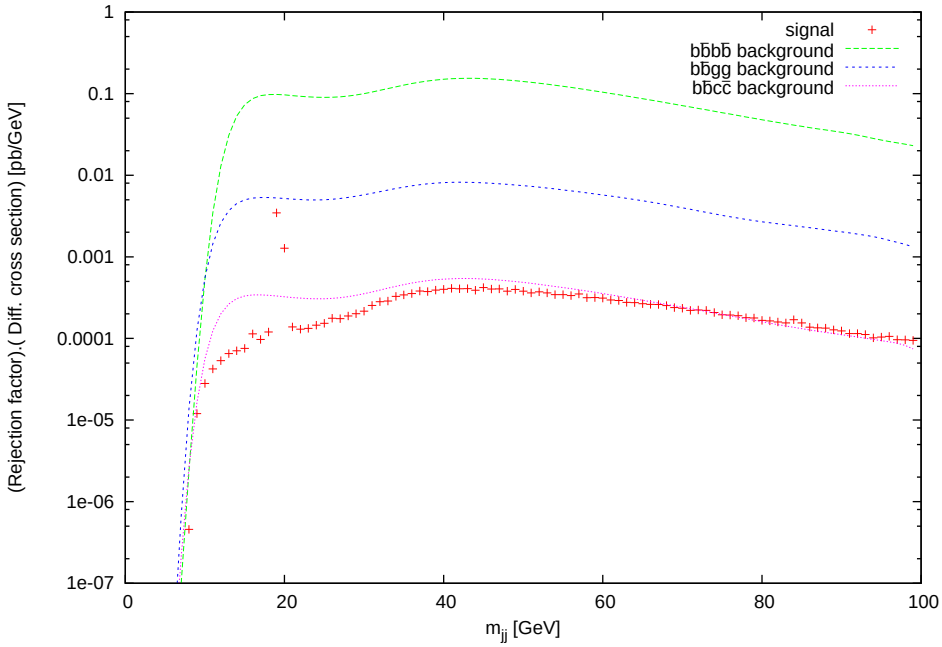

Figure 6.11: The differential cross section in di-jet invariant mass m_{jj} after applying the cuts in (6.2) for signal with m_{a_1}=19.98 GeV and for backgrounds.

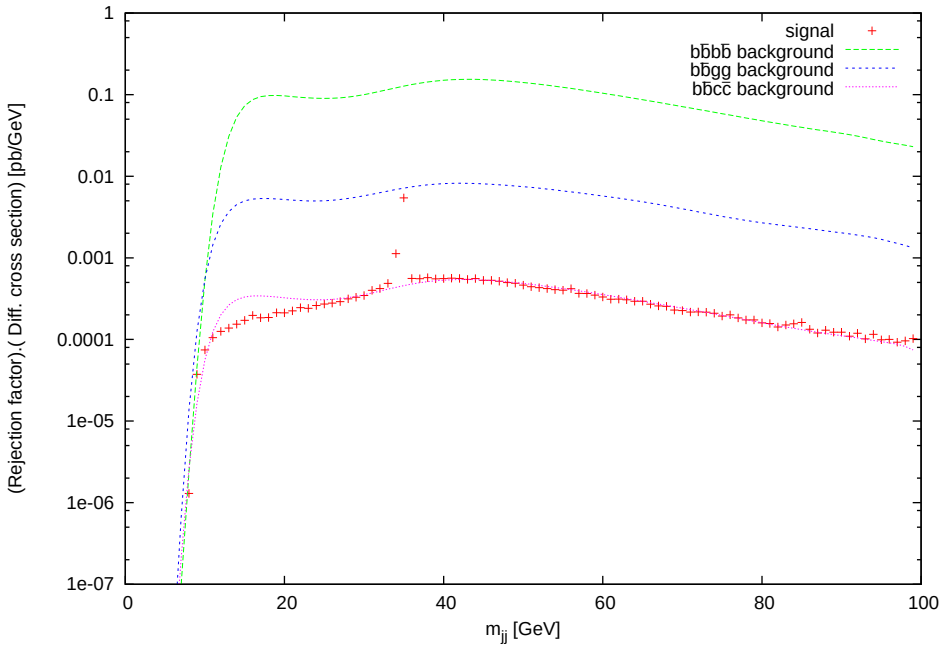

Figure 6.12: The differential cross section in di-jet invariant mass m_{jj} after applying the cuts in (6.2) for signal with m_{a_1}=35.14 GeV and for backgrounds.

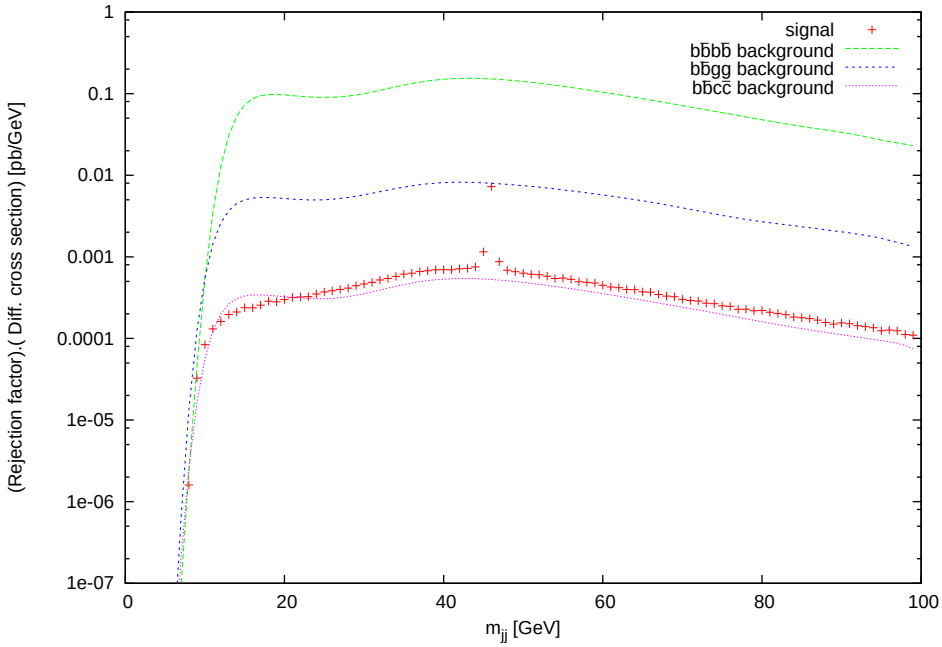

Figure 6.13: The differential cross section in di-jet invariant mass m_{jj} after applying the cuts in (6.2) for signal with m_{a_1}=46.35 GeV and for backgrounds.

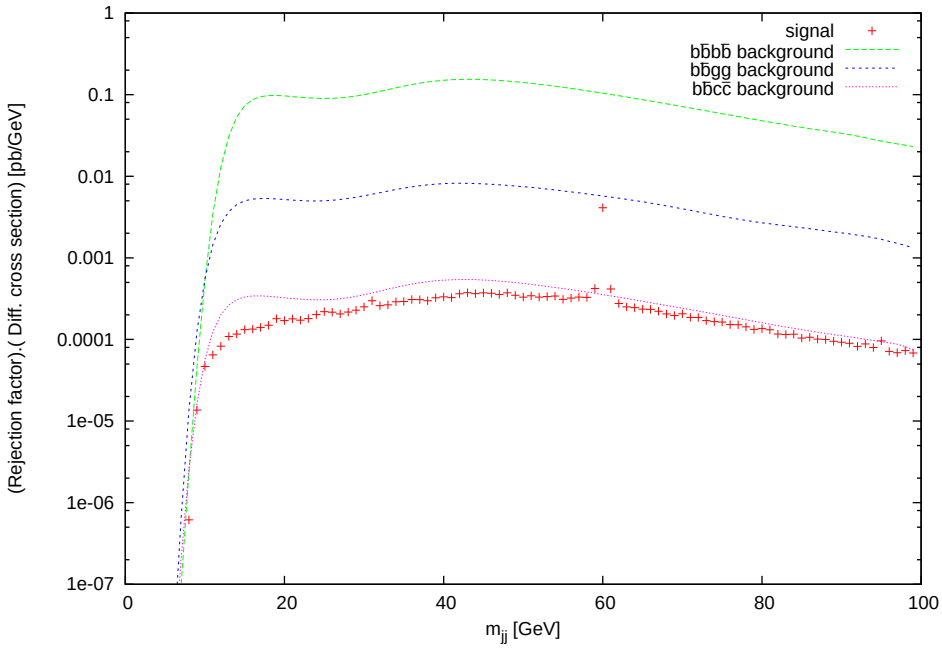

Figure 6.14: The differential cross section in di-jet invariant mass m_{jj} after applying the cuts in (6.2) for signal with m_{a_1}=60.51 GeV and for backgrounds.

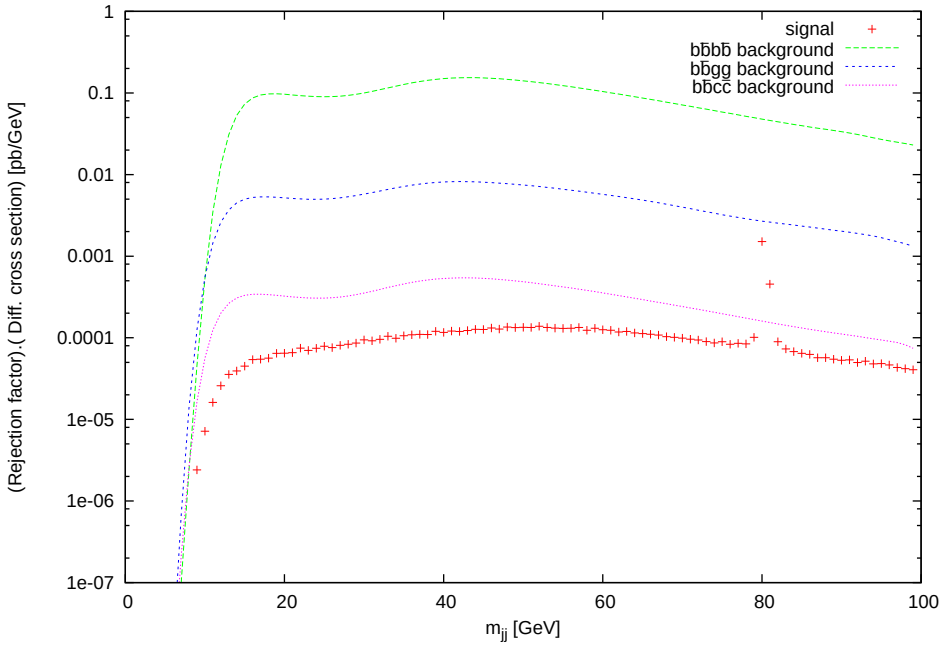

Figure 6.15: The differential cross section in di-jet invariant mass m_{jj} after applying the cuts in (6.2) for signal with m_{a_1}=80.91 GeV and for backgrounds.

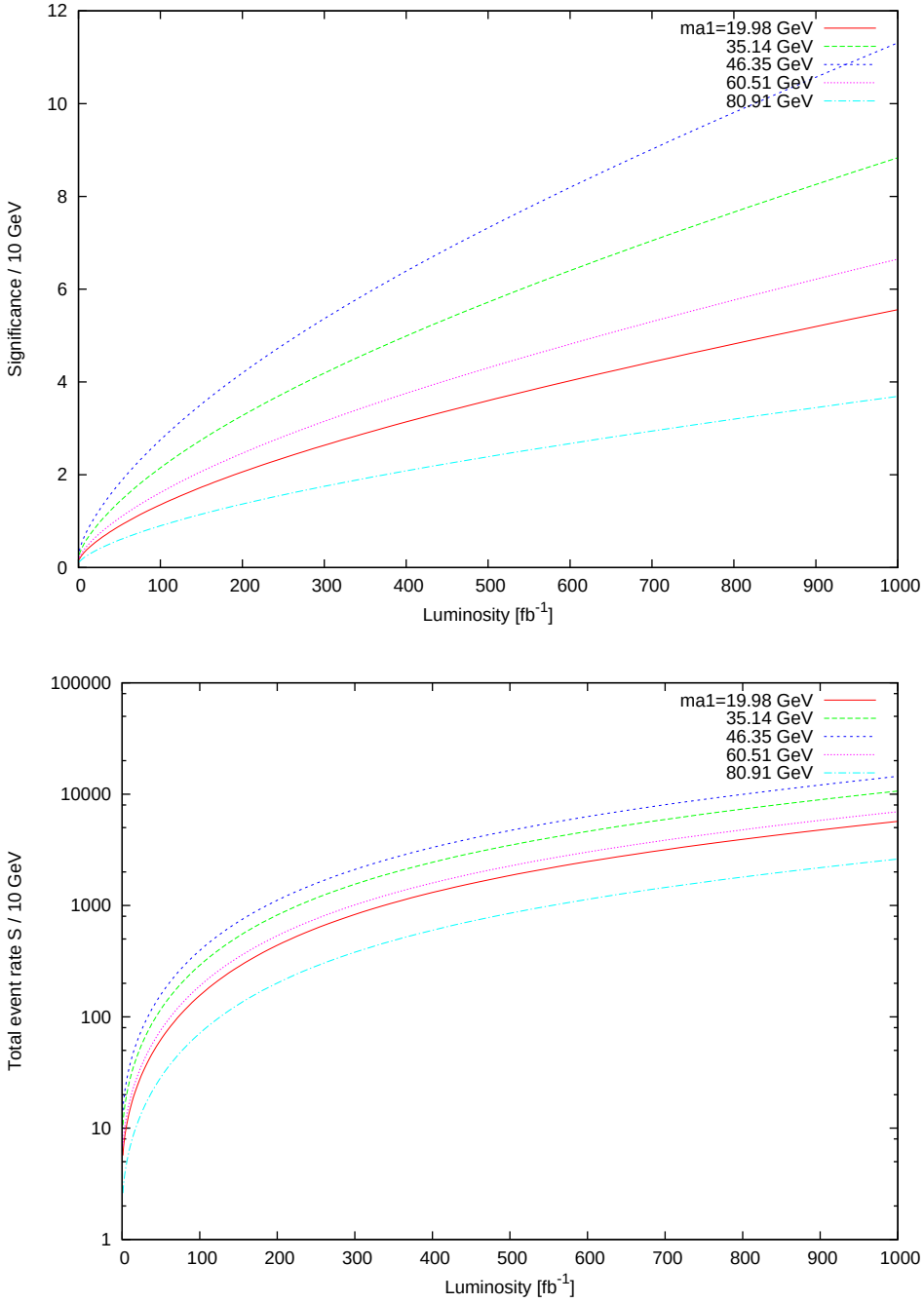

Figure 6.16: The significance $S/\sqrt{B}$ (top) and total event rate S (bottom) of the $gg \to b\bar{b}a_1 \to b\bar{b}b\bar{b}$ signal as functions of the integrated luminosity for 10 GeV di-jet mass resolutions.

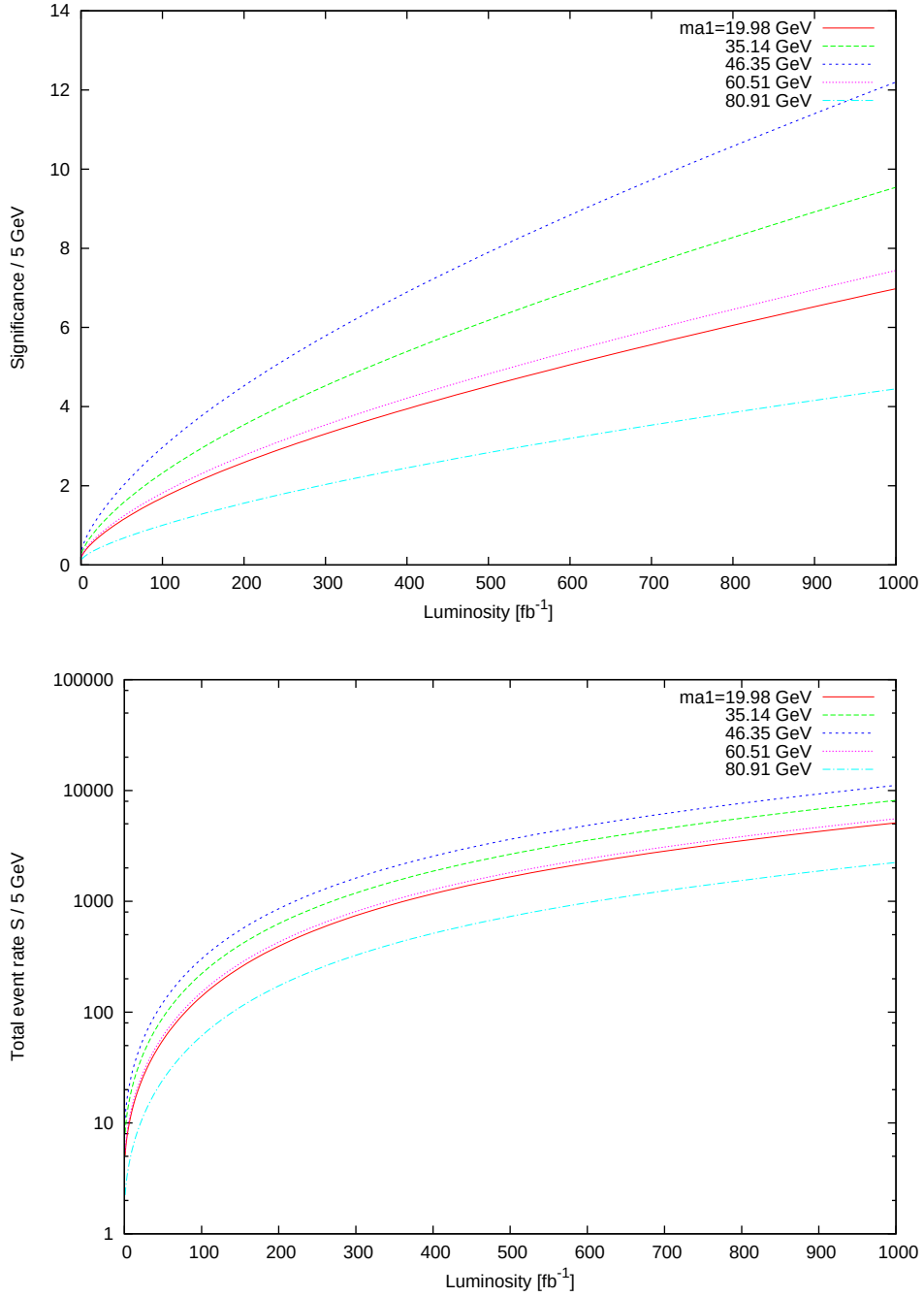

Figure 6.17: The significance $S/\sqrt{B}$ (top) and total event rate S (bottom) of the $gg \to b\bar{b}a_1 \to b\bar{b}b\bar{b}$ signal as functions of the integrated luminosity for 5 GeV di-jet mass resolutions.

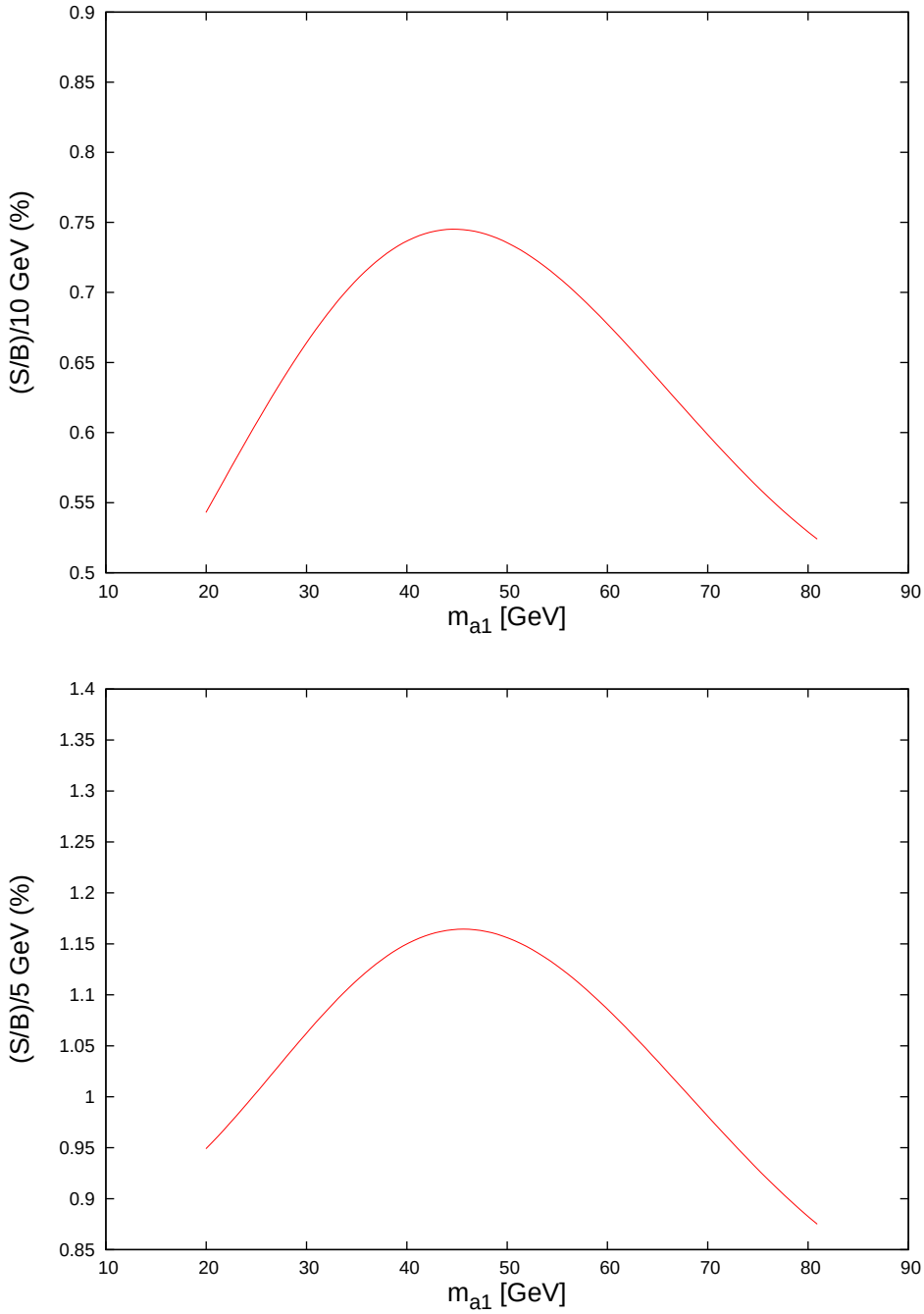

Figure 6.18: The signal-to-background ratios S/B of the $gg \to b\bar{b}a_1 \to b\bar{b}b\bar{b}$ as functions of m_{a1} for 10 GeV (top) and 5 GeV (bottom) di-jet mass resolutions.

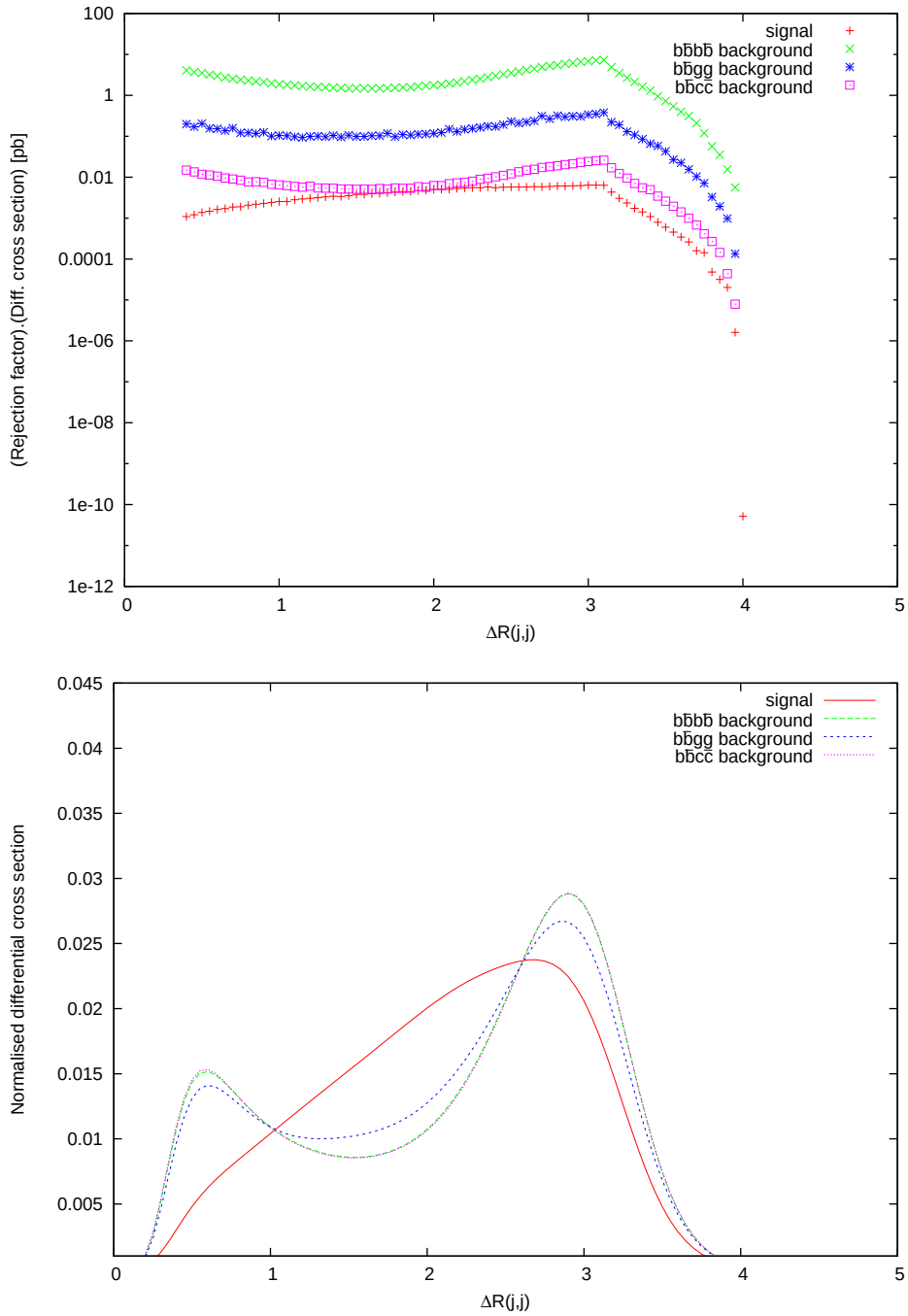

Figure 6.19: The differential cross section distribution over di-jet (pseudorapidity-azimuth) separation after applying the cuts in (6.2) for signal with m_{a_1}=46.35 GeV and for backgrounds. In the top-pane the absolute normalisations are given while below those to 1.

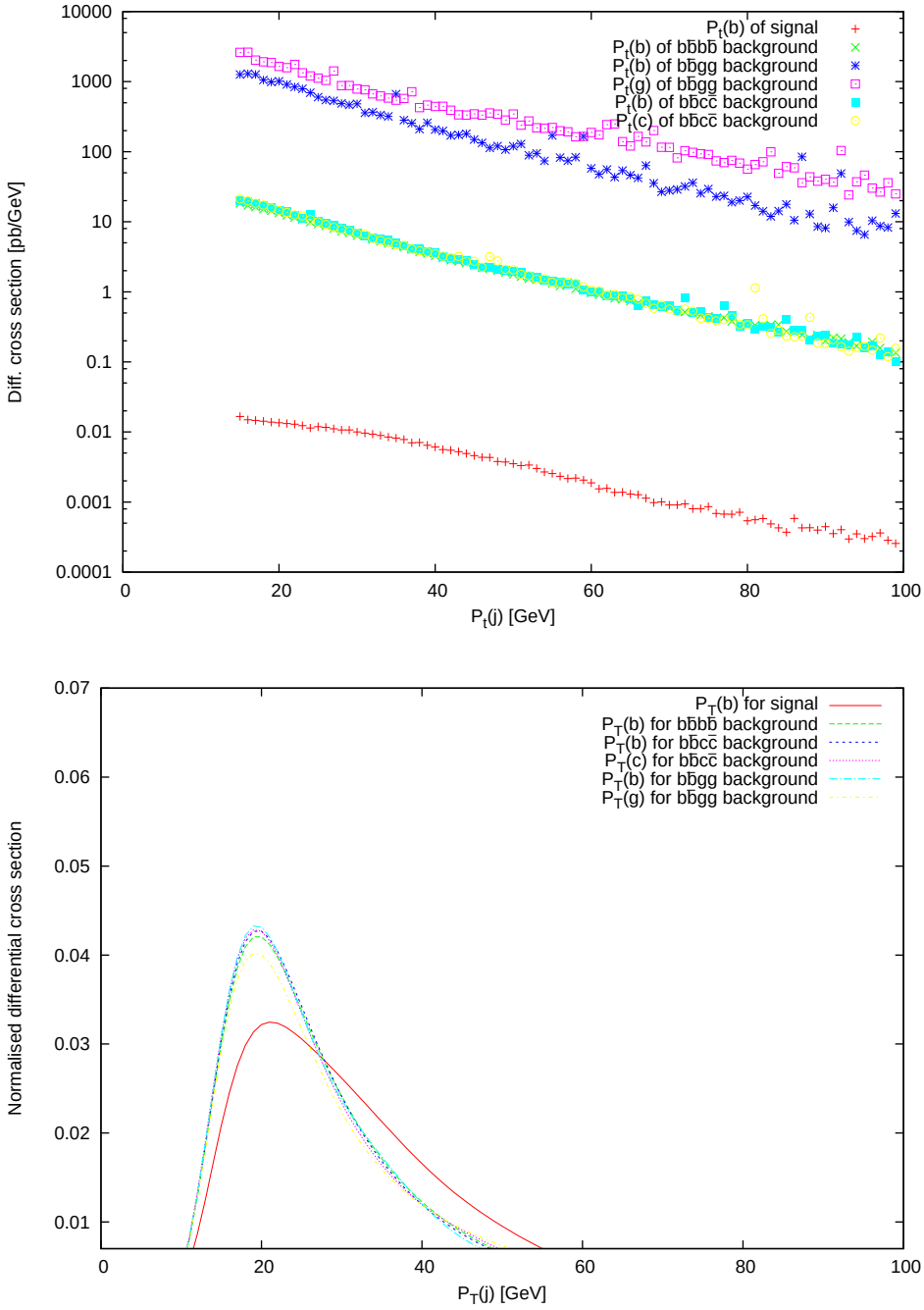

Figure 6.20: The differential cross section distribution over jet transverse momentum after applying the cuts in (6.2) for signal with m_{a_1}=46.35 GeV and for backgrounds. In the top-pane the absolute normalisations are given while below those to 1.

6.4 Summary of the chapter

The Higgs sector of the NMSSM is phenomenologically richer than that of the MSSM as it has two more (neutral) Higgs states. Because of introducing a complex singlet Superfield in the NMSSM, one can have a CP-odd Higgs boson with very low mass. We have proven that there exist sizable regions of the NMSSM parameter space where this kind of Higgs state, with a mixed singlet and doublet nature, can be discovered at the LHC through its production in association with $b\bar{b}$. In this chapter, we explored the detectability of the lightest CP-odd Higgs state of the NMSSM, a_1, through its decays into $\mu^+\mu^-$ and $b\bar{b}$. We have shown that large tanβ, typically above 30, and very large integrated luminosity are required for this detection in $\mu^+\mu^-$ decay mode. As for $b\bar{b}$ decay mode, although the signal rates and significances are good enough, it is unlikely to discover the a_1 through this mode due to the huge QCD background and the smallness of the signal-to-background ratio.

Firstly, these results in the $\mu^+\mu^-$ decay mode (together with those of the previous chapter) support the 'No-lose theorem' by looking for the (quite possibly resolvable) direct production of a light a_1 rather than looking for its production through the decay $h_{1,2} \to a_1 a_1$, whose detectability remains uncertain. Secondly, they enable distinguishing the NMSSM Higgs sector from the MSSM one (thus contributing to enforcing the 'More-to-gain theorem') since such light CP-odd Higgs states, below M_Z in mass (which have a large singlet component), are not at all possible in the context of the MSSM.

In brief, the potential discovery of an a_1 produced in association with a pair of b-quarks at the LHC can be through the following decay modes: (i) $\tau^+\tau^-$ if $m_{a_1} \lesssim M_Z$; (ii) $\mu^+\mu^-$ if 10 GeV $< m_{a_1} \lesssim 60$ GeV. On the other hand, despite the fact that the $b\bar{b}$ decay mode has the largest branching ratio except when a_1 is highly singlet so that $\gamma\gamma$ is dominant (albeit unresolvable), this channel is unfeasible to detect a_1 at the LHC. Finally, notice that this collection of channels, i.e., associated production of a_1 with a $b\bar{b}$ pair, with the a_1 decaying in such a variety of channels, when a_1 discovery is possible, can be exploited to measure the bottom Yukawa coupling $b\bar{b}a_1$ at the LHC.

Chapter 7

The No-lose theorem for NMSSM Higgs discovery at the LHC in difficult scenarios

7.1 Introduction

In this chapter, we investigate whether or not the 'No-lose theorem' of the NMSSM at the LHC can be proven by considering a Higgs production channel so far neglected, i.e., Higgs boson production in association with a b-quark pair (aka Higgs-strahlung off b-quark pair). We do so based on the interesting results obtained in the previous two chapters. Further, notice that the counterpart process in which a bottom-antibottom pair is replaced by a top-antitop pair was discussed in [61], where it was found to be very subleading over the NMSSM parameter space.

We will be looking at inclusive event rates in presence of various Higgs-to-Higgs decays, $h_{1,2} \to a_1 a_1$, $h_2 \to h_1 h_1$ and $h_{1,2} \to Z a_1$, for h_1 and h_2 produced in association with b-quark pairs. Recall that this production mode is in general the largest one at large values of tanβ. We will also be studying the decay patterns of the lightest Higgs boson pairs, $a_1 a_1$ or $h_1 h_1$, and of the gauge boson and a light CP-odd Higgs boson, $Z a_1$, into different types of processes. Most parts of this chapter can be found in our papers [35] and [36].

7.2 Parameter space scan and inclusive signal rates

We have used NMSSMTools to perform a random scan over 20 million points in the specified parameter space, mentioned in Chapter 5, and required that $m_{h_2} \leq 300$ GeV. We used CalcHEP [82] to determine the cross sections for NMSSM $h_{1,2}$ productions for the following processes:

$$gg \to b\bar{b}\, h_1 \quad \text{and} \quad gg \to b\bar{b}\, h_2, \tag{7.1}$$

The lightest two CP-even neutral Higgs boson masses are given by Eq.(4.25). Recall that the equation is at tree level, mainly for guidance in interpreting the upcoming figures, in fact notice that NMSSMTools includes radiative corrections as well.

To probe the NMSSM parameter space, we have computed m_{h_1} and m_{h_2} against each of the six parameters of the NMSSM (figures 7.1 and 7.2). As it is clear from the two figures, in our chosen parameter space, small values of λ, κ and μ_{eff} are preferred while large values of $\tan\beta$ and positive values of A_λ are the most compatible with theoretical and experimental data. The distribution over A_κ is uniform primarily because only small negative values of A_κ are scanned over.

Figure 7.3 shows the correlations between all three Higgs masses m_{a_1}, m_{h_1} and m_{h_2}. Since the successful points emerging from the scan have small values of λ, κ and also A_κ, only rather small values of m_{a_1} are allowed. It is remarkable that the smaller the m_{a_1}, the smaller the m_{h_1} and the m_{h_2} (two top-panes). In the bottom-pane of the same figure, for m_{h_2} around 120 GeV, m_{h_1} can have values from just above 0 up to slightly less than 120 GeV, showing the possibility that the two Higgs states can have the same mass, i.e., $m_{h_1} \sim m_{h_2}$. Notice also that the majority of points have m_{h_1} between 115 and 120 GeV, i.e., just above the LEP limit on a SM-like Higgs mass.

7.3 Production of h_1 and h_2 decaying into two lighter Higgs bosons

The production times decay rates of h_1 and h_2, in which h_1 decays into two lighter a_1's and h_2 decays into either a pair of a_1's or a pair of h_1's, as functions of the Higgs masses m_{h_1} and m_{h_2} (the left-panes of figure 7.4) and of the corresponding branching ratio of Higgs-to-Higgs decay (the right-panes of figure 7.4) have been computed. In our choice of parameter space, which has large $\tan\beta$, we have noticed that the production

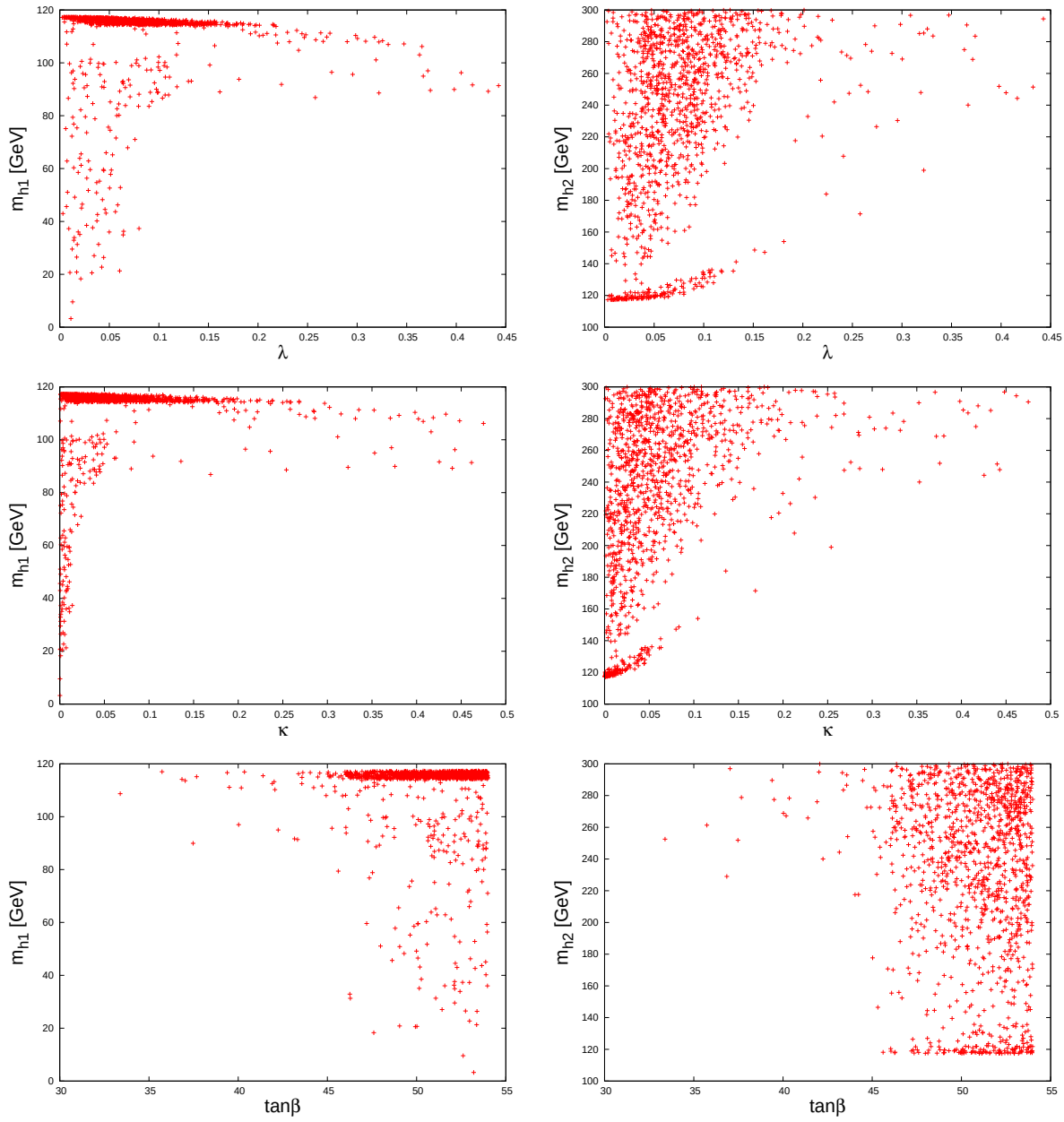

Figure 7.1: The lightest two scalar Higgs masses m_{h_1} and m_{h_2} as functions of λ, κ and of $\tan\beta$.

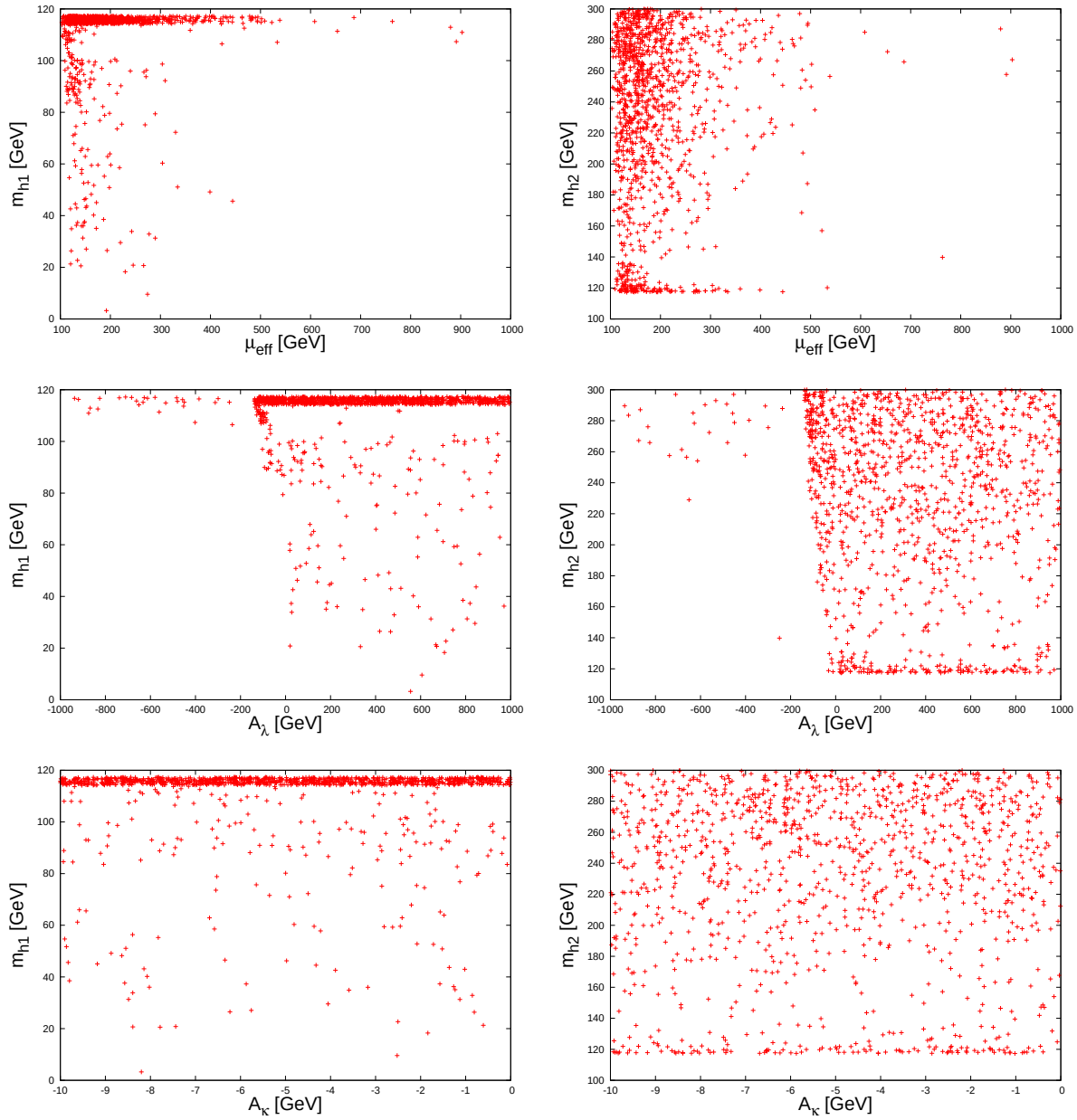

Figure 7.2: The lightest two scalar Higgs masses m_{h_1} and m_{h_2} as functions of μ_{eff}, A_λ and of A_κ.

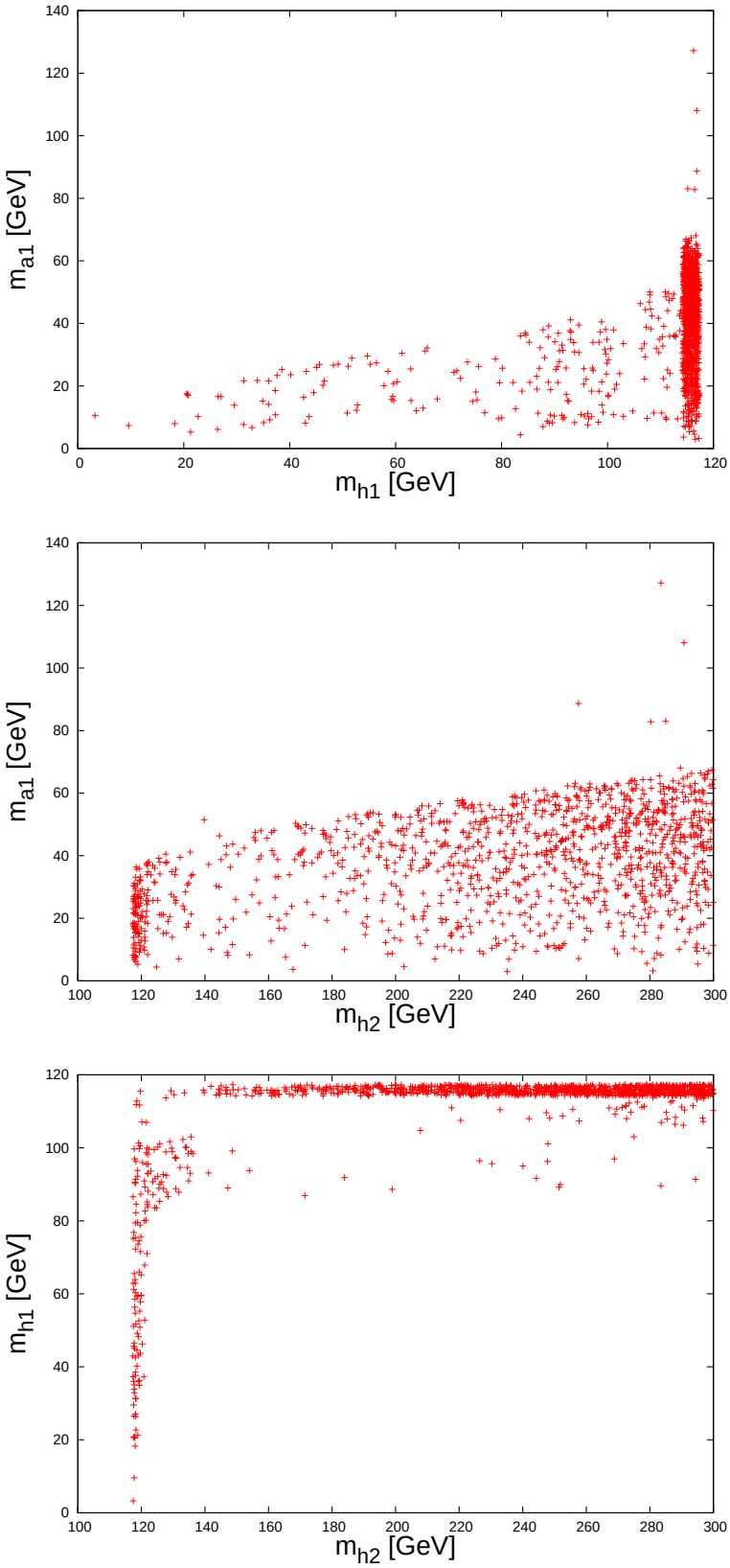

Figure 7.3: The correlations between the lightest CP-odd Higgs mass m_{a_1} and the lightest two CP-even Higgs masses m_{h_1} and m_{h_2} and between the latter two.

rate of h_1 in association with a bottom-antibottom $\sigma(gg \to b\bar{b}h_1)$ is nearly constant, i.e., it only depends slightly on the tree level parameters while the production rate of h_2 $\sigma(gg \to b\bar{b}h_2)$ is strongly dependent on $\tan\beta$ and on the other tree level parameters. Notice that in the figure we multiply the production rates by the decay rates of Higgs-to-Higgs particles, which play crucial roles in the changes of the inclusive cross section.

It is clear that Higgs-to-Higgs decays are dominant over a large area of the NMSSM parameter space if Higgs-to-Higgs decays are kinematically allowed and so these decays should be taken seriously before claiming any validity (or otherwise) of the 'No-lose theorem' for the NMSSM, see the right-panes of figure 7.4. Fortunately, for considerable regions of the NMSSM parameter space, with different masses of h_1 and h_2, these production rates are sizable (topping 1000 fb or so) except in the case of the decay $h_2 \to h_1 h_1$ where only few points have large production rates due to the smallness of the $\mathrm{Br}(h_2 \to h_1 h_1)$ compared to the $\mathrm{Br}(h_{1,2} \to a_1 a_1)$ in general.

Figure 7.5 displays the correlations between the three discussed production and decay processes. It is quite remarkable that the overall trend, despite an obvious spread also in the horizontal and vertical directions, is such that when one channel grows in event yield there is also another one which also does, hence opening up the possibility of the simultaneous discovery of several Higgs states of the NMSSM (three neutral Higgses at the same time: h_1, h_2 and a_1), an exciting prospect in order to distinguish the NMSSM Higgs sector from the MSSM one.

In figure 7.6 we have calculated the inclusive signal rates of h_1 and h_2 through their cascade decays that finish with $a_1 a_1 \to b\bar{b}b\bar{b}$, $a_1 a_1 \to b\bar{b}\tau^+\tau^-$ and $a_1 a_1 \to \tau^+\tau^-\tau^+\tau^-$. It is shown that the signal rates are quite large, topping 1000 fb for h_1 and 100 fb for h_2, respectively, in the case of both $4b$ and 4τ final states due to the fact that the $\mathrm{Br}(a_1 \to b\bar{b})$ is dominant for $m_{a_1} \gtrsim 10$ GeV and the $\mathrm{Br}(a_1 \to \tau^+\tau^-)$ is dominant for m_{a_1} < 10 GeV. The $2b$ plus 2τ rates are in fact one order of magnitude less than the former two due to the fact that only the parameter space points with $m_{a_1} \gtrsim 10$ GeV have these final states in which the $\mathrm{Br}(a_1 \to \tau^+\tau^-)$ is only about 10% of the $\mathrm{Br}(a_1 \to b\bar{b})$. Overall, there are some regions of the NMSSM parameter space that have considerable signal rates and that could be sufficient to discover the h_1 and h_2 through their $a_1 a_1$ cascade decays at the LHC.

The h_2 cascade decays ending up with $h_1 h_1 \to b\bar{b}b\bar{b}$, $h_1 h_1 \to b\bar{b}\tau^+\tau^-$ and $h_1 h_1 \to \tau^+\tau^-\tau^+\tau^-$ have less cross section (see figure 7.7). Only for m_{h_2} around 120 GeV, the rates are quite sizable, topping 50 fb, 5 fb and 0.5 fb level for $4b$, $2b$ plus 2τ and 4τ

final states, respectively.

We also looked at the scope of $a_1a_1 \to \gamma\gamma\gamma\gamma$ decays. The corresponding inclusive production rates are found in figure 7.8 as functions of m_{h_1} and m_{h_2} (the top-panes) for both $h_1 \to a_1a_1 \to 4\gamma$ and $h_2 \to a_1a_1 \to 4\gamma$. Despite inclusive rates are never very large, it should be noticed a consistent population of points in the former case at $m_{h_1} \approx 115$ GeV yielding up to $\mathcal{O}(1\ fb)$ rates, with also a possibility of rates reaching up to 100 fb for smaller m_{h_1}. In the latter case, the points well spread out in m_{h_2} between 115 and 300 GeV, yielding signal rates between 0.1 fb and 1 fb for some points. Moreover, we have shown in the bottom-panes of the same figure the inclusive production rates for the channels $h_1 \to a_1a_1 \to \tau^+\tau^-\mu^+\mu^-$ and $h_2 \to a_1a_1 \to \tau^+\tau^-\mu^+\mu^-$. The maximum rates for h_1 are 1 fb while for h_2 are roughly 0.5 fb.

Finally, notice that the cases $h_1 \to a_1a_1 \to \mu^+\mu^-\mu^+\mu^-$ and $h_2 \to a_1a_1 \to \mu^+\mu^-\mu^+\mu^-$ contribute below the 0.01 fb level over the entire NMSSM parameter space, so we do not show the corresponding plots.

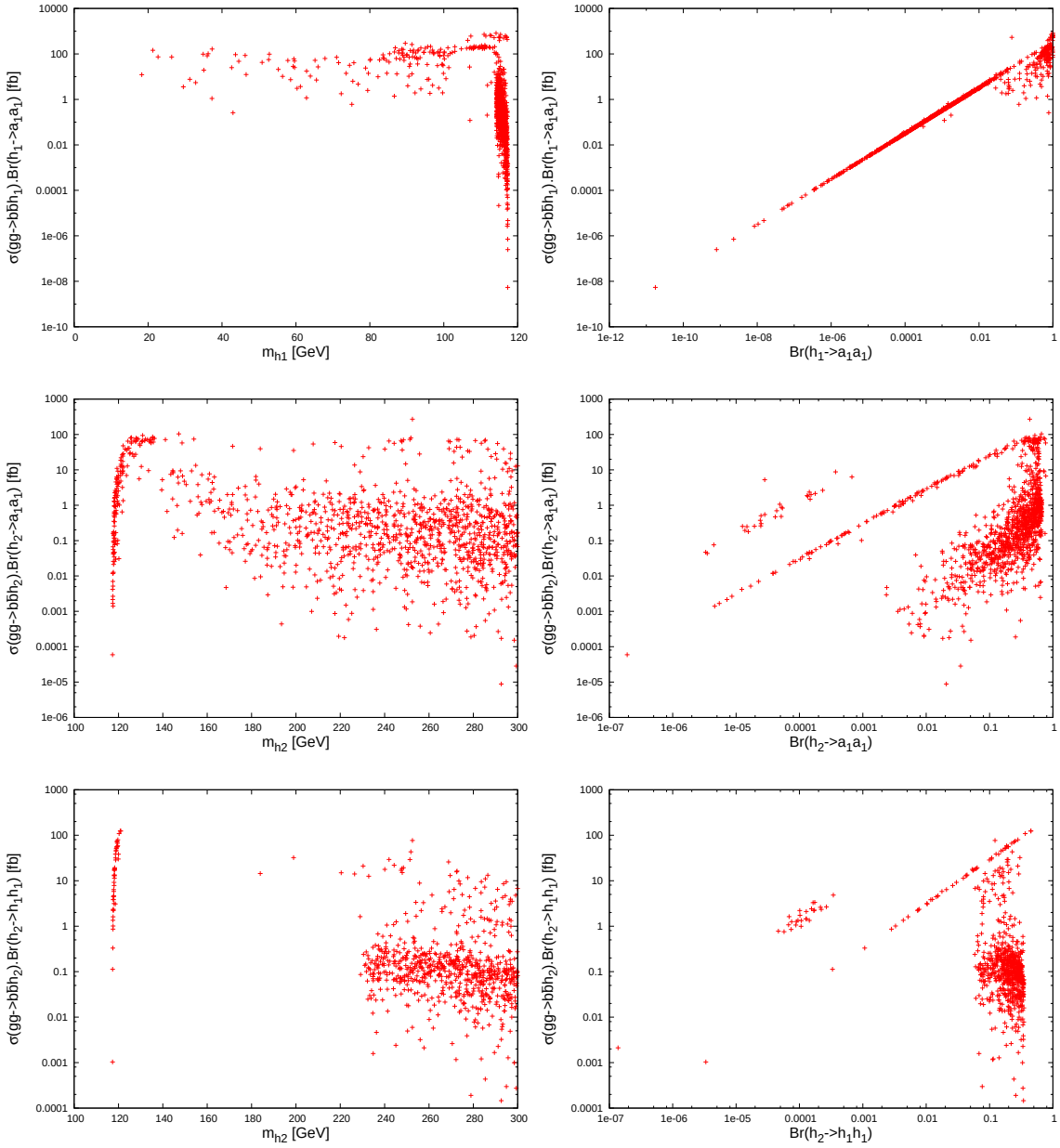

Figure 7.4: The rates for $\sigma(gg \to b\bar{b}h_1)$ Br$(h_1 \to a_1a_1)$, $\sigma(gg \to b\bar{b}h_2)$ Br$(h_2 \to a_1a_1)$ and for $\sigma(gg \to b\bar{b}h_2)$ Br$(h_2 \to h_1h_1)$ as functions of the corresponding Higgs masses and of the corresponding Br's.

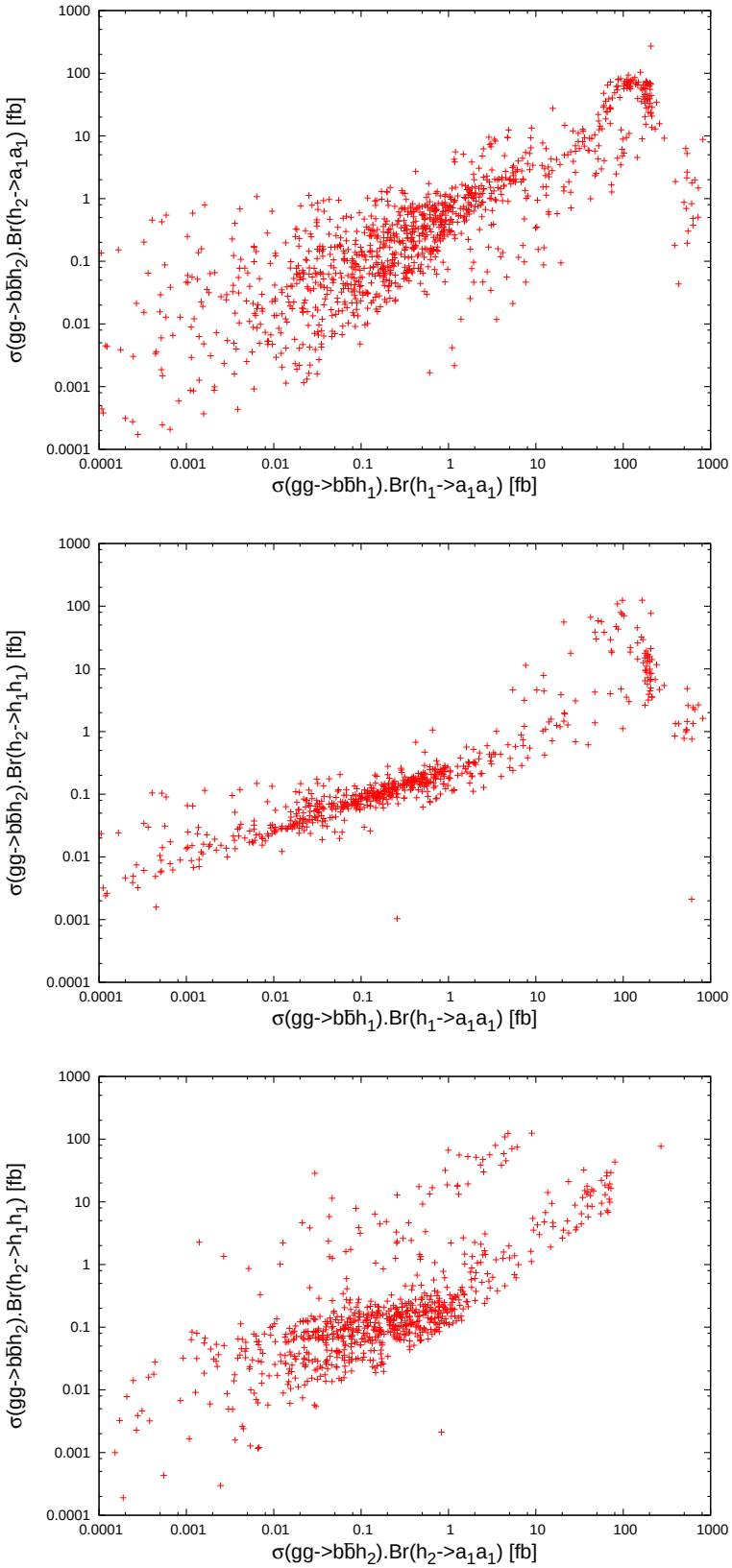

Figure 7.5: The rates for $\sigma(gg \to b\bar{b}h_1)$ Br$(h_1 \to a_1a_1)$ versus $\sigma(gg \to b\bar{b}h_2)$ Br$(h_2 \to a_1a_1)$, $\sigma(gg \to b\bar{b}h_1)$ Br$(h_1 \to a_1a_1)$ versus $\sigma(gg \to b\bar{b}h_2)$ Br$(h_2 \to h_1h_1)$ and for $\sigma(gg \to b\bar{b}h_2)$ Br$(h_2 \to a_1a_1)$ versus $\sigma(gg \to b\bar{b}h_2)$ Br$(h_2 \to h_1h_1)$.

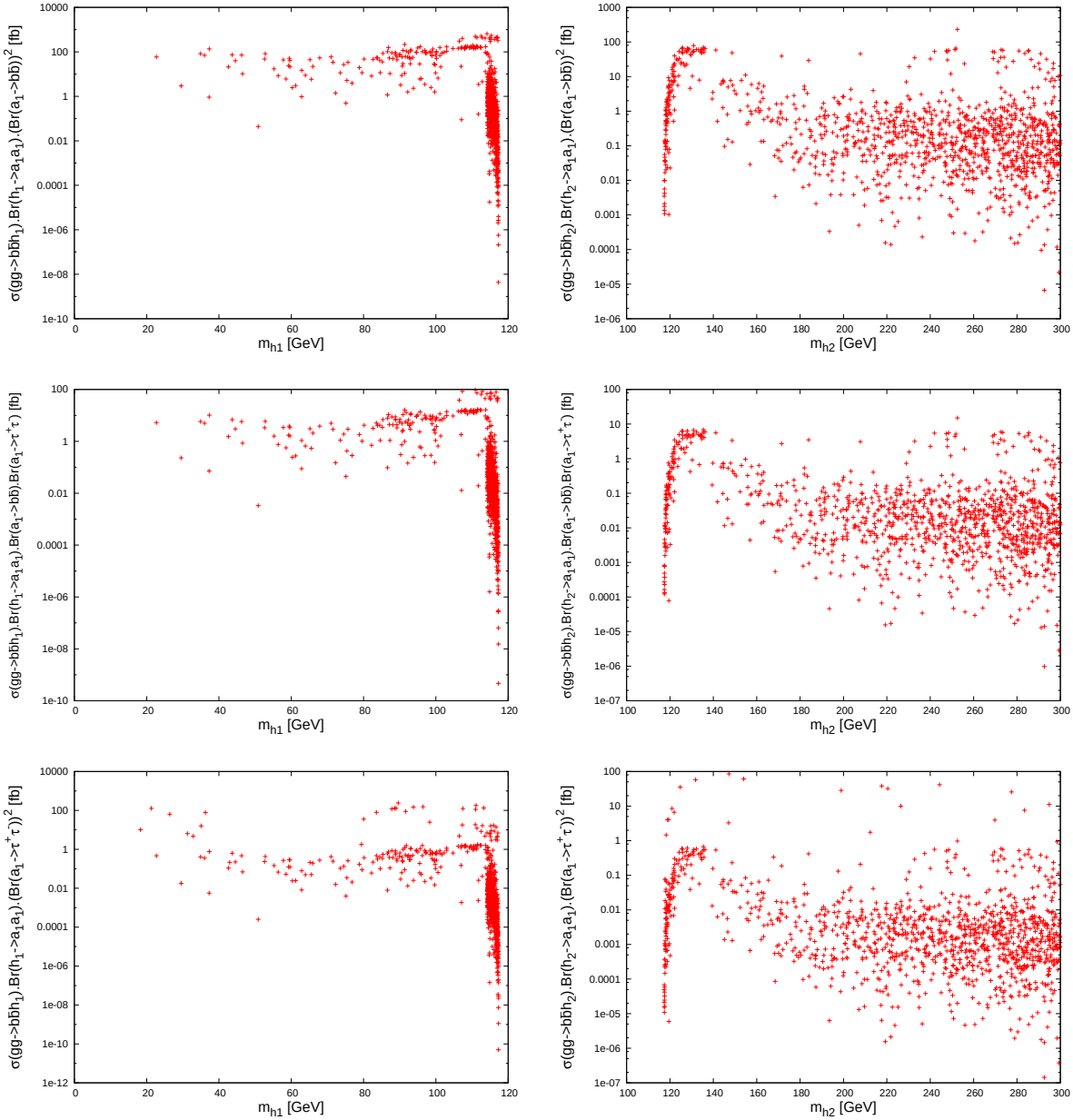

Figure 7.6: The signal rates for both $\sigma(gg \to b\bar{b}h_1)$ Br$(h_1 \to a_1a_1)$ and $\sigma(gg \to b\bar{b}h_2)$ Br$(h_2 \to a_1a_1)$ times Br$(a_1a_1 \to b\bar{b}b\bar{b})$, times Br$(a_1a_1 \to b\bar{b}\tau^+\tau^-)$ and times Br$(a_1a_1 \to \tau^+\tau^-\tau^+\tau^-)$ as functions of m_{h_1} and of m_{h_2}.

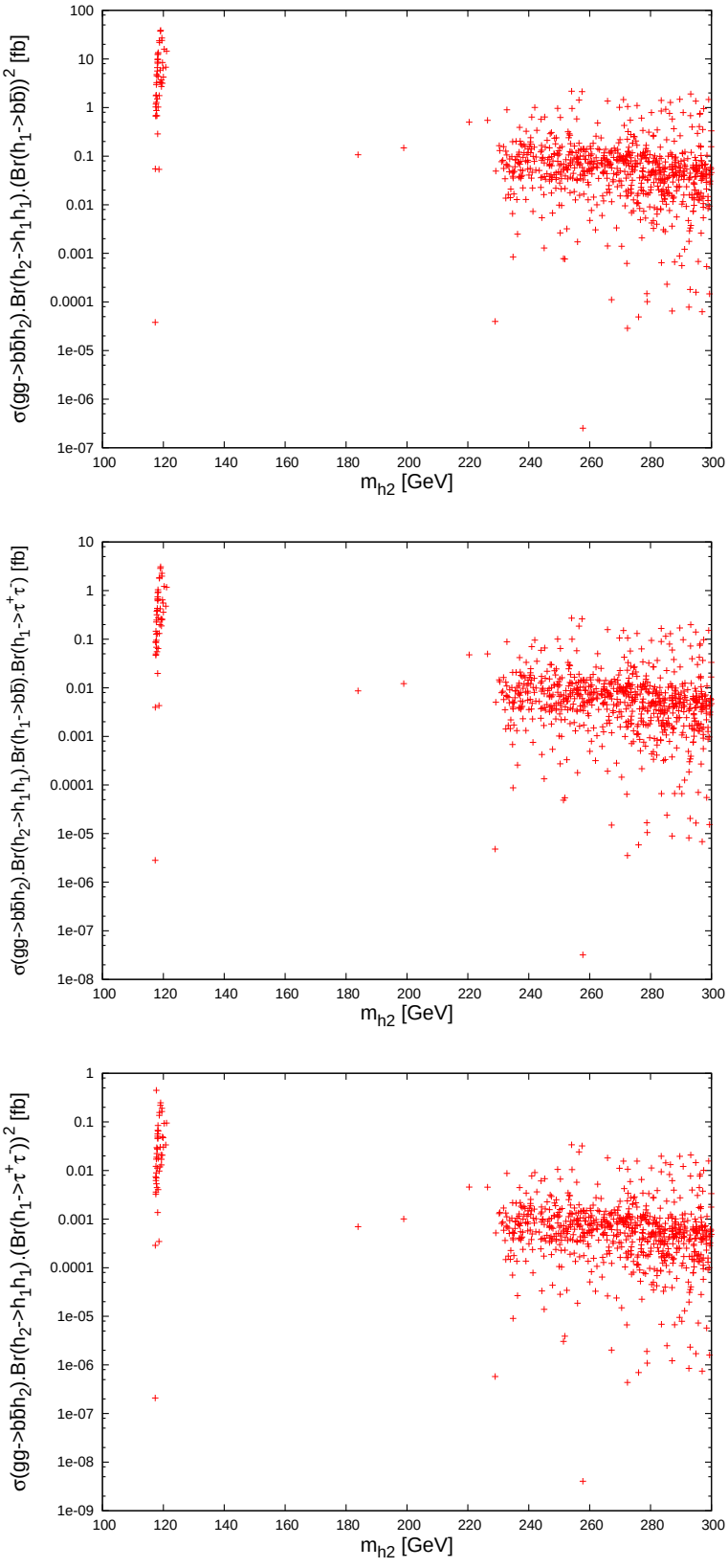

Figure 7.7: The signal rates for $\sigma(gg \to b\bar{b}h_2)$ Br$(h_2 \to h_1h_1)$ times Br$(h_1h_1 \to b\bar{b}b\bar{b})$, times Br$(h_1h_1 \to b\bar{b}\tau^+\tau^-)$ and times Br$(h_1h_1 \to \tau^+\tau^-\tau^+\tau^-)$ as functions of m_{h_2}.

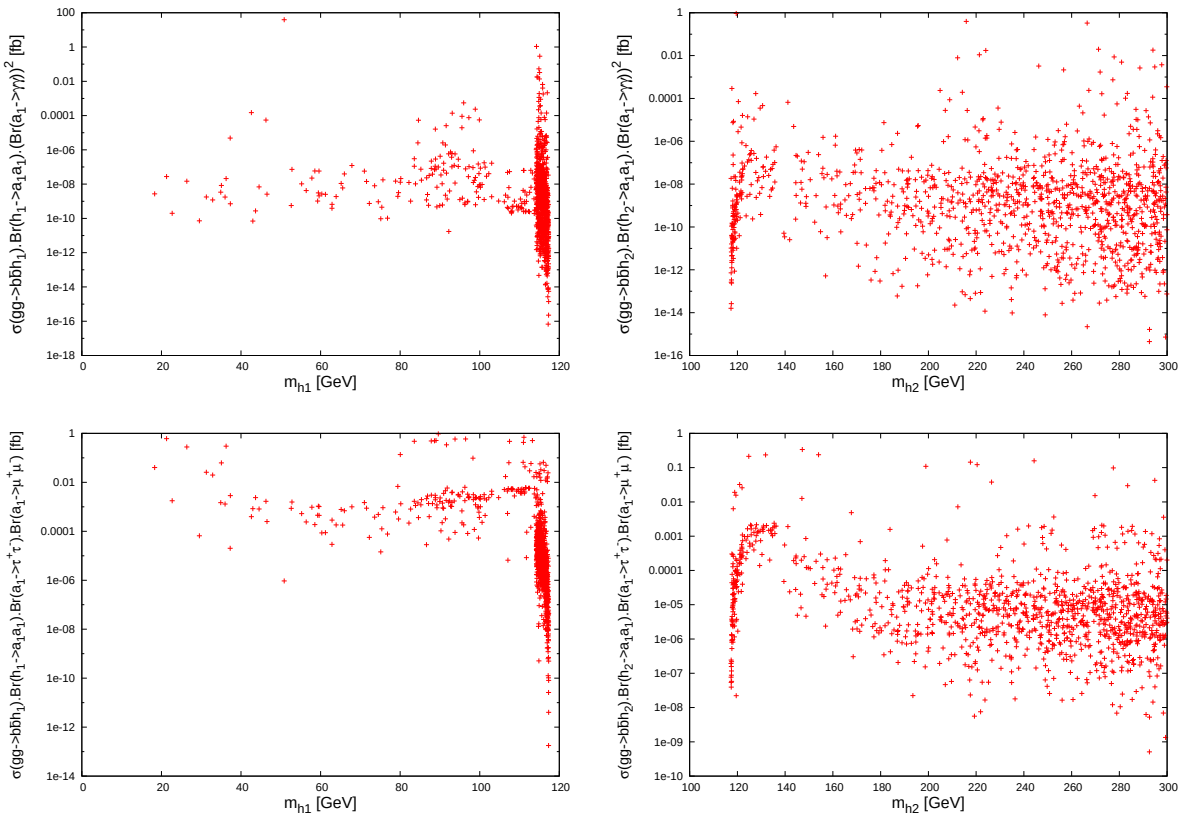

Figure 7.8: The signal rates for both $\sigma(gg \to b\bar{b}h_1)$ Br$(h_1 \to a_1a_1)$ and $\sigma(gg \to b\bar{b}h_2)$ Br$(h_2 \to a_1a_1)$ times $(\text{Br}(a_1 \to \gamma\gamma))^2$ and times Br$(a_1 \to \tau^+\tau^-)$ Br$(a_1 \to \mu^+\mu^-)$ as functions of m_{h_1} and of m_{h_2}.

7.4 Production of h_1 and h_2 decaying into a gauge boson and a light CP-odd Higgs

In this section, we examine the LHC discovery potential of the lightest two CP-even Higgs states $h_{1,2}$, followed by the decay $h_{1,2} \to Za_1$. Figure 7.9 shows that the production rate for the h_1, produced in association with a $b\bar{b}$ pair, is small, topping the 0.001 fb level. Such a production rate is not enough to discover the h_1 at the LHC. The top-pane of the figure shows that there is a linear relation between the h_1 production rate and the Br($h_1 \to Za_1$) because the production rate $\sigma(gg \to b\bar{b}h_1)$ is nearly constant in our parameter space, which has large tanβ. The bottom-pane of the figure shows that the points passing the constraints have $m_{h_1} > 100$ GeV.

Figure 7.10 illustrates the inclusive production rates ending up with $Za_1 \to \mu^+\mu^- b\bar{b}$, $Za_1 \to \mu^+\mu^-\tau^+\tau^-$ and $Za_1 \to jj\tau^+\tau^-$ (where j = jet). It is clear that the production rates are small, topping 10^{-4} fb for the first and last channels and 10^{-5} fb for the second one. Such rates are not enough to discover the h_1 neither at the LHC nor at the SLHC with 1000 fb^{-1} of luminosity.

In contrast, the situation for h_2 is promising as one can notice that the $\sigma(gg \to b\bar{b}h_2)$Br($h_2 \to Za_1$) is sizable, topping the 10000 fb level (figure 7.11). The highest values of the cross section are accompanied by an intriguingly large Br($h_2 \to Za_1$), reaching up to 10%. It is clear from the top-pane of the figure that the distribution over the branching fraction for h_2 is not as uniform as that for the h_1 because the production rate $\sigma(gg \to b\bar{b}h_2)$ depends strongly on the tree level parameters unlike that for h_1. The bottom-pane of the figure shows that the highest cross section occurs for $m_{h_2} > 220$ GeV.

In order to study the detectability of h_2 decaying into a gauge boson and a light CP-odd Higgs at the LHC, we have calculated the inclusive production rates ending up with $\mu^+\mu^- b\bar{b}$, $\mu^+\mu^-\tau^+\tau^-$ and $jj\tau^+\tau^-$ (figure 7.12). The event rates for these processes are at the $\mathcal{O}(100)$ fb level at the most. While clearly this number is not very large, signal events may still be detectable at planned LHC luminosities, especially if the background can be successfully reduced to manageable levels[1]. In short, there is a small but well defined region of the NMSSM parameter space where the h_2 and a_1 states, both with a mixed singlet and doublet nature, could potentially be detected at the LHC if 220

[1]A partonic signal-to-background (S/B) analysis for $jj\tau^+\tau^-$ final state has been done in [36].

GeV $\lesssim m_{h2} \lesssim$ 300 GeV and 15 GeV $\lesssim m_{a1} \lesssim$ 60 GeV, in the $h_2 \to Za_1 \to \mu^+\mu^- b\bar{b}$, $h_2 \to Za_1 \to \mu^+\mu^-\tau^+\tau^-$ and $h_2 \to Za_1 \to jj\tau^+\tau^-$ modes, when the CP-even Higgs state is produced in association with a $b\bar{b}$ pair for rather large tanβ.

Here, we give some illustrative examples for 4 benchmark points that could enable the discovery of the h_2 at the LHC.

• point 1

λ=0.11784333, κ=0.099759129, tanβ=45.413385,

$\mu_{\rm eff}$=653.63068 GeV, A_λ=-561.08302 GeV, A_κ=-9.7511471 GeV,

m_{a_1}= 44.1 GeV, m_{h_2}=272.4 GeV,

Br($a_1 \to b\bar{b}$)=0.848, Br($a_1 \to \tau^+\tau^-$)=0.141, Br($a_1 \to \mu^+\mu^-$)=0.0005,

$\sigma(gg \to b\bar{b}h_2)$.Br($h_2 \to Za_1$)=1286.35 fb.

• point 2

λ=0.036954734, κ=0.074106016, tanβ=35.731787,

$\mu_{\rm eff}$=338.52788 GeV, A_λ=-683.64824 GeV, A_κ=-1.3135077 GeV,

m_{a_1}=15.9 GeV, m_{h_2}=261.4 GeV,

Br($a_1 \to b\bar{b}$)=0.91, Br($a_1 \to \tau^+\tau^-$)=0.074, Br($a_1 \to \mu^+\mu^-$)=0.0003,

$\sigma(gg \to b\bar{b}h_2)$.Br($h_2 \to Za_1$)=377.3 fb.

• Point 3

λ=0.055822718, κ=0.041921611, tanβ=47.269331,

$\mu_{\rm eff}$=389.90121 GeV, A_λ=-299.09449 GeV, A_κ=-5.3814631 GeV,

m_{a_1}=61.5 GeV, m_{h2}=275.6 GeV,

Br($a_1 \to b\bar{b}$)=0.868, Br($a_1 \to \tau^+\tau^-$)=0.126, Br($a_1 \to \mu^+\mu^-$)=0.00044,

$\sigma(gg \to b\bar{b}h_2)$.Br($h_2 \to Za_1$)=109 fb.

• Point 4

λ=0.15630654, κ=0.084945744, tanβ=48.122165,

$\mu_{\rm eff}$=422.93377 GeV, A_λ=-236.27361 GeV, A_κ=-7.4575765 GeV,

m_{a_1}=31.9 GeV, m_{h_2}=287.9 GeV,

Br($a_1 \to b\bar{b}$)=0.878, Br($a_1 \to \tau^+\tau^-$)=0.111, Br($a_1 \to \mu^+\mu^-$)=0.0004,

$\sigma(gg \to b\bar{b}h_2)$.Br($h_2 \to Za_1$)=447 fb.

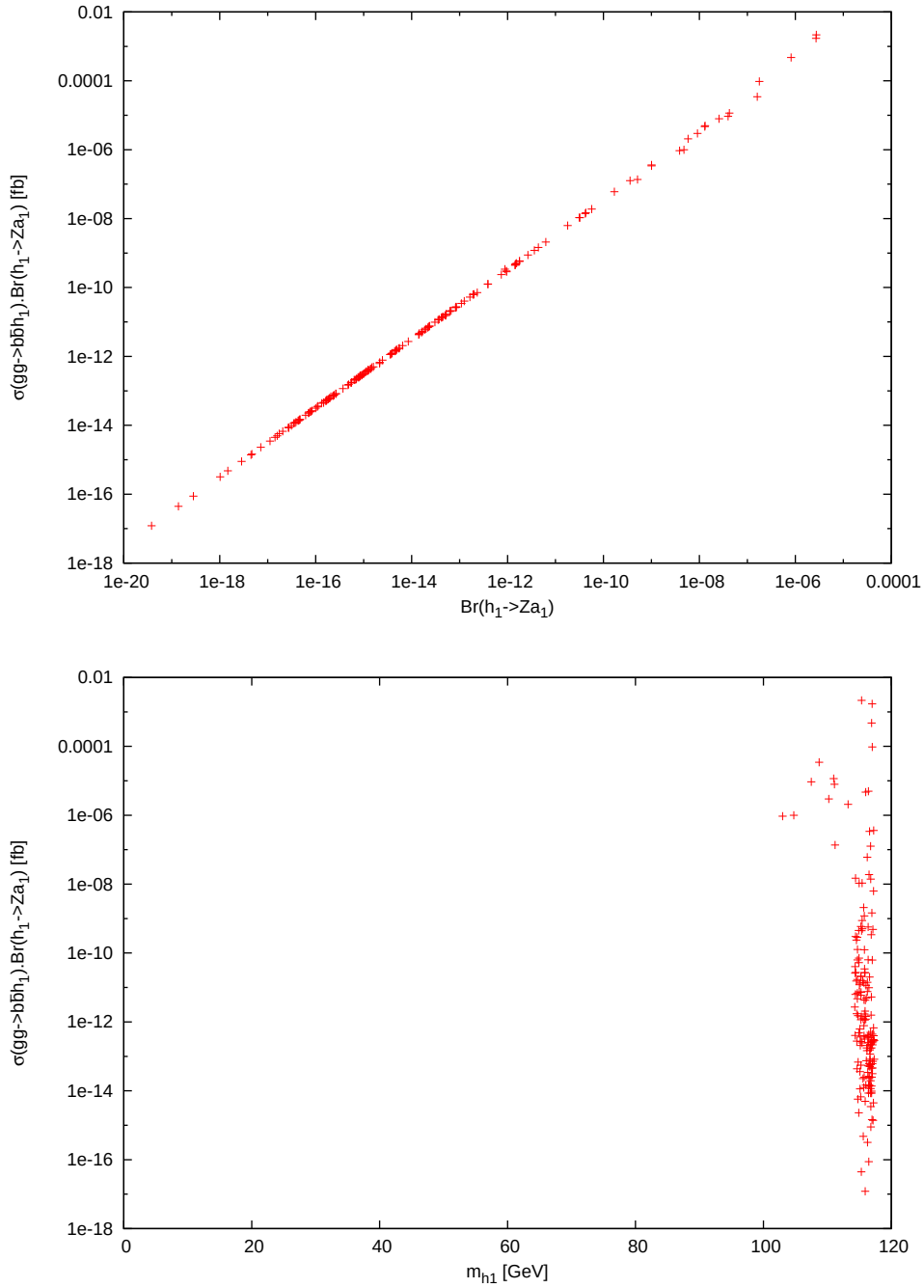

Figure 7.9: The signal rate for $\sigma(gg \to b\bar{b}h_1)$ Br$(h_1 \to Za_1)$ as a function of the Br$(h_1 \to Za_1)$ and of m_{h_1}.

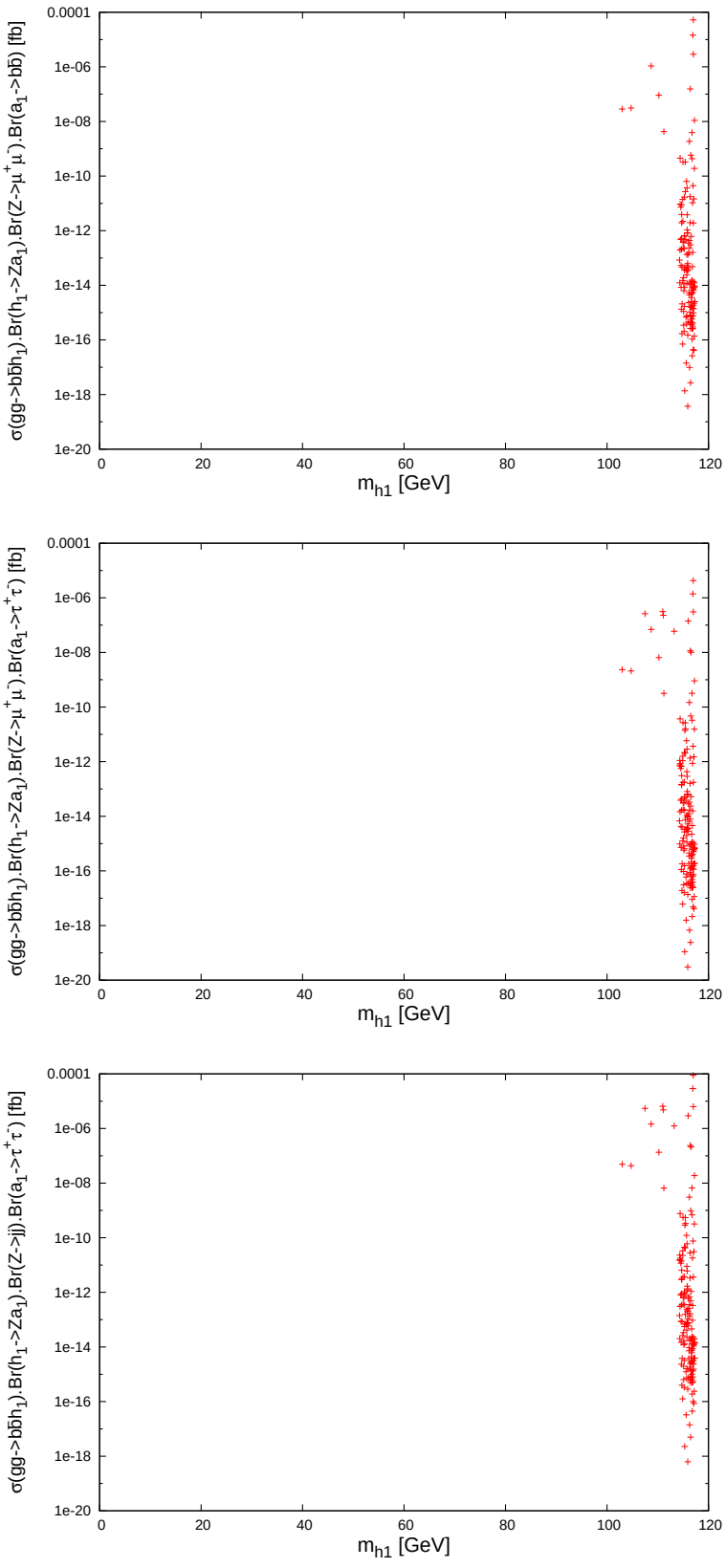

Figure 7.10: The signal rate for $\sigma(gg \to b\bar{b}h_1)$ Br$(h_1 \to Za_1)$ times Br$(Za_1 \to \mu^+\mu^- b\bar{b})$, times Br$(Za_1 \to \mu^+\mu^-\tau^+\tau^-)$ and times Br$(Za_1 \to jj\tau^+\tau^-)$ as functions of m_{h_1}.

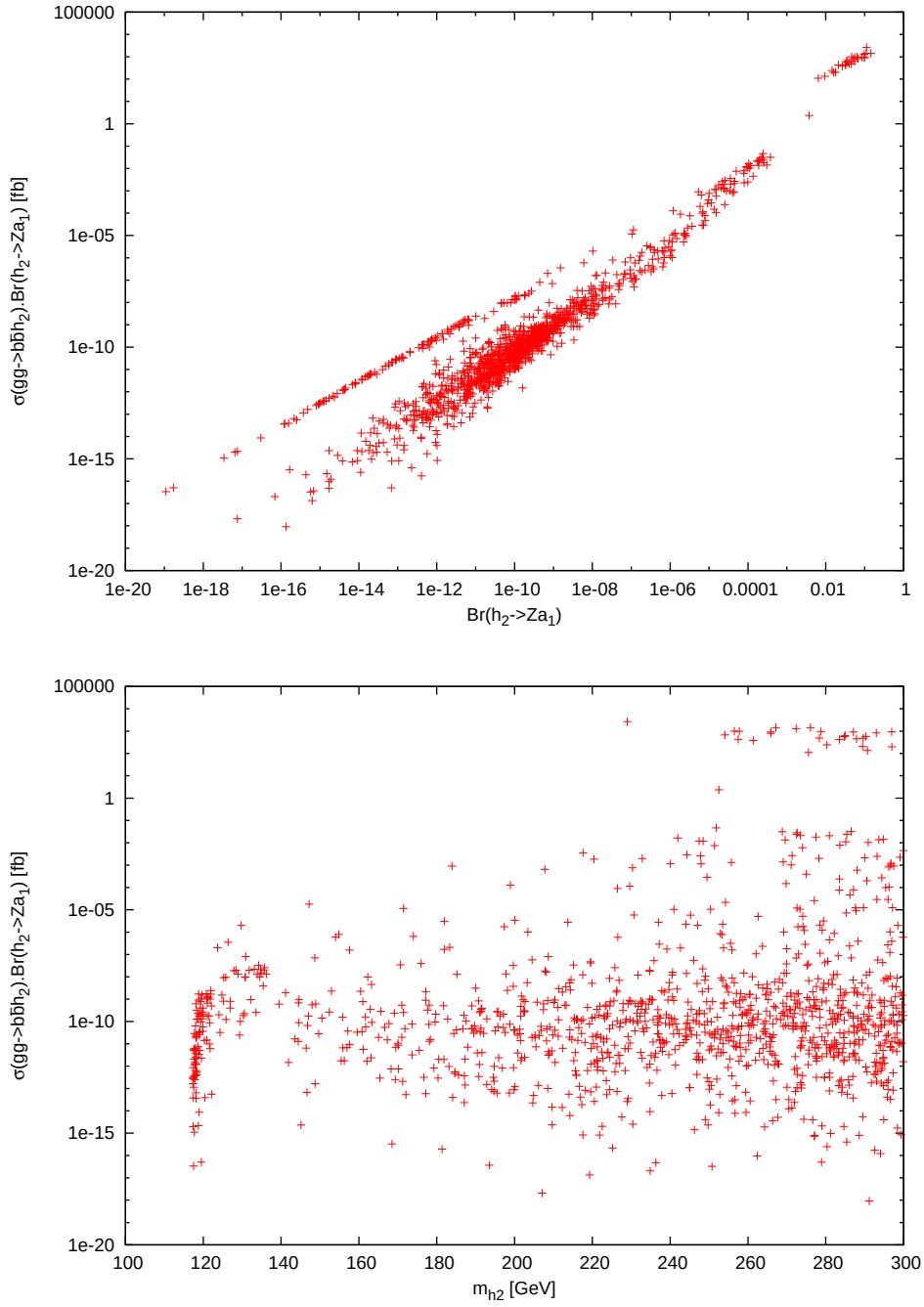

Figure 7.11: The signal rate for $\sigma(gg \to b\bar{b}h_2)$ Br$(h_2 \to Za_1)$ as a function of the Br$(h_2 \to Za_1)$ and of m_{h_2}.

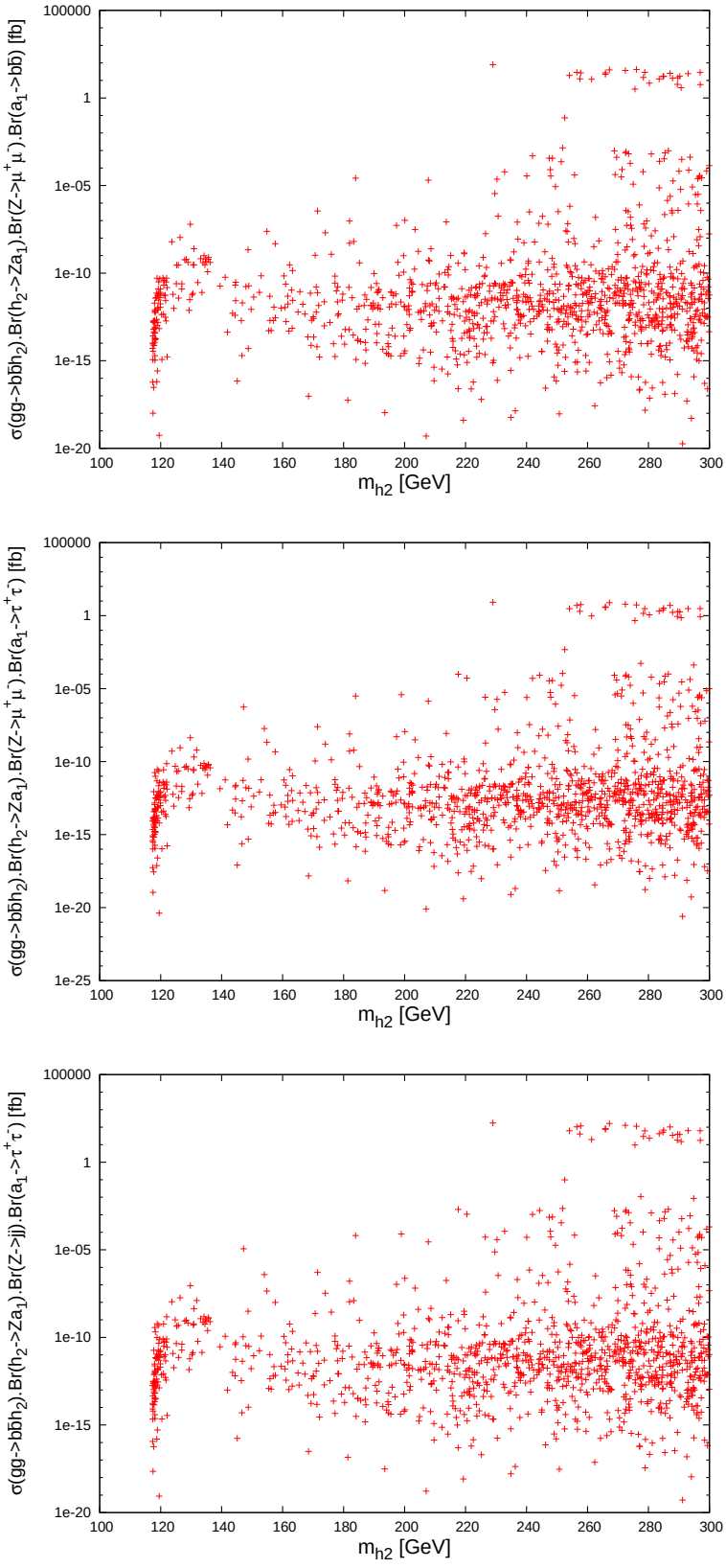

Figure 7.12: The signal rate for $\sigma(gg \to b\bar{b}h_2)$ $\mathrm{Br}(h_2 \to Za_1)$ times $\mathrm{Br}(Za_1 \to \mu^+\mu^- b\bar{b})$, times $\mathrm{Br}(Za_1 \to \mu^+\mu^-\tau^+\tau^-)$ and times $\mathrm{Br}(Za_1 \to jj\tau^+\tau^-)$ as functions of m_{h_2}.

7.5 Possible signatures

In the last two sections, we have calculated the inclusive signal rates, the production times decay rates. In fact, we have not applied any cuts on the final state particles but, practically, in order to detect these particles at the LHC, a finite volume of an LHC detector has to be chosen. In addition, in order to claim the discovery of a Higgs state h_1 or h_2 decaying into such particles, a background simulation (within the same detector region) has to be taken into account.

In this section, we would like to discuss the possible scope of detecting h_1 or h_2 through its decay into various decay modes without resorting to such a complicated simulation. The key issue to be handled is whether one or more of the b-quarks, say 'prompt' b-quarks, produced in association with h_1 or h_2 in the process (7.1) ought to be tagged. Figure 7.13 shows the efficiency to tag one or two 'prompt' b-quarks in the final states, done by S. Moretti. In fact, these b-quarks have generally very low transverse momentum (denoted here by p_{T_b}) as they often emerge from the splitting of a gluon inside the proton. In order to tag b-quarks with good efficiency, say $\varepsilon_b = 60\%$, a minimum p_{T_b} value is always required. The lowest reasonable value of p_{T_b} is 15 GeV or so. For the case of a single b-tag the overall efficiency is some 2–3% for very small values of Higgs masses and growing to 14–15% for large values of Higgs masses (of $\mathcal{O}(300)$ GeV) irrespectively of considering either h_1 or h_2 being produced. For the case of a double b-tag, we are instead speaking of the efficiency at the 1% to 8% level, respectively. In short, the scope of detecting Higgs state produced in association with b-quarks largely depends on both the mass and decay mode of the Higgs state.

We think that for the 4γ and 4μ final states it is not necessary to tag any of the 'prompt' b-quarks at all. The reason behind this is that these final states, typically have high transverse momentum and are isolated, so they could act as trigger and the SM backgrounds are not prohibitively large. This is in fact important as the production rate for the Higgs states decaying into 4γ and 4μ are quite small compared to the other decay modes. Regarding final states containing $\tau's$, 4τ and $2\tau 2b$, one could certainly exploit a τ trigger (both leptonic and hadronic) [21, 22]. However, it may be necessary to tag at least one 'prompt' b-quark to suppress QCD backgrounds, especially in case of hadronic τ decays. The case of $2\tau 2\mu$ would clearly exploit a muon trigger instead. Finally, the case of a $4b$ signature of $h_{1,2} \to a_1 a_1$, $h_2 \to h_1 h_1$ and $h_2 \to Z a_1$ decays is totally unfeasible, especially considering the fact that the entire final state is made up

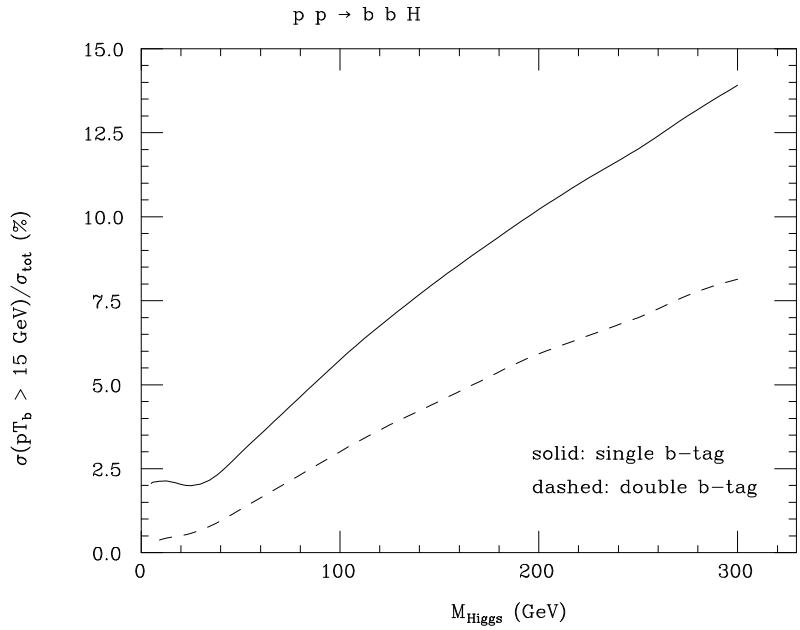

Figure 7.13: The efficiency to tag one or two 'prompt' b-quarks in the final state, given as percent ratio of the production cross section for $pp \to b\bar{b}$ Higgs (where Higgs can equally refer to an h_1 or h_2 state) after the cut $p_{T_b} > 15$ GeV over the total one (also including the b-tagging performances, ε_b and ε_b^2, respectively), as a function of the Higgs boson mass. The distributions have been produced at parton level by using CalcHEP. Herein we use $\varepsilon_b = 60\%$.

of six quarks, i.e., with unavoidable huge combinatorics and burdened by an extremely large pure QCD background.

In essence, only a dedicated kinematical analysis of the decay products could in the end ascertain the true selection efficiency of a signature and its scope. What we can responsibly do here is to highlight three possible scenarios. Firstly, one whereby the signal rates in the preceding sections will not be reduced substantially after enforcing acceptance cuts: this is certainly applicable to 4γ, 4μ and 4τ events (with $\tau's$ decaying leptonically to electrons and muons). Secondly, one whereby all decay signatures involving (one or more) hadronic $\tau's$ and b's are reduced by a factor between 7 and 50, depending on the produced Higgs mass, assuming a single tag only of 'prompt' b's. Thirdly, one whereby most possibly the $6b$ final state requires a double tag of 'prompt' b-quarks, reducing the signal yield by a factor between 12.5 and 100, depending on the $h_{1,2}$ mass[2].

[2]Notice that for a_1 masses comparable to typical transverse momentum thresholds of the decay products further severe reductions could occur, however, there is plenty of NMSSM parameter space giving sizable signals for heavier a_1 states for all signatures considered here.

7.6 Summary of the chapter

Searching for NMSSM Higgs states at the LHC is very complicated compared to the MSSM ones due to the dominance of Higgs-to-Higgs decays in large regions of parameter space of the next-to-minimal SUSY model. This is the main reason why the 'No-lose theorem' has not been confirmed in the context of the NMSSM yet. We have found here that, at large values of $\tan\beta$, the h_1 and h_2 productions in association with bottom-antibottom pairs and decaying into lighter Higgses can have sizable signal rates in some regions of the NMSSM parameter space, in a variety of decay patterns including photons, muons, tauons and b-quarks themselves. We have verified this by calculating the inclusive signal rates.

In addition, we have examined the LHC discovery potential for $h_{1,2}$ decaying into a light CP-odd Higgs and Z gauge boson. While the inclusive production rate for h_1 is not enough to discover the h_1 at the LHC, the production rate for h_2 is promising and large enough to discover the boson at the LHC though the channels $\mu^+\mu^-\tau^+\tau^-$, $\mu^+\mu^- b\bar{b}$ and $jj\tau^+\tau^-$. We have proven that there exists a small but well defined region of the NMSSM parameter space where the h_2 and a_1 states can be simultaneously discovered at the LHC.

Clearly, in the end, more experimental analysis are needed, in particular in calculating backgrounds, and will determine whether signal extraction is possible and through which signatures. However, our present study should eventually direct the NMSSM parameter space exploration for $h_{1,2}$ production in association with $b\bar{b}$ pair where discovery significances can be found. In all circumstances, just like with other previous attempts at extracting NMSSM Higgs-to-Higgs signatures, evidence of those investigated here will require a rather large LHC luminosity sample, of $\mathcal{O}(300\ fb^{-1})$ or more.

Chapter 8

Conclusions

The NMSSM has a singlet Superfield in addition to the usual Higgs doublets of the MSSM. This singlet gives rise to a more varied phenomenology of the NMSSM, compared to that of the MSSM. For instance, this singlet Superfield mixes with the neutral components of the doublets, giving rise to one CP-even Higgs, one CP-odd Higgs and one extra neutralino in addition to the usual spectrum of the MSSM. Therefore, in the NMSSM, by assuming CP-conservation, there are seven Higgses: three CP-even, two CP-odd and a pair of charged Higgses. We have investigated whether or not at least one Higgs boson of the NMSSM can be discovered at the LHC ('No-lose theorem') and/or is possible to find some regions in the parameter space where more and/or different Higgs states of the NMSSM are detectable at the LHC, compared to those available within the MSSM ('More-to-gain theorem').

Because of the mixing between the Higgs singlet and doublets, Higgs-to-Higgs decays are kinematically possible for large regions of the NMSSM parameter space even for small masses of the Higgs states, which is impossible in the MSSM. For instance, a SM-like Higgs can decay into a pair of the lightest NMSSM CP-odd Higgses. This decay can be dominant in sizable areas of the NMSSM parameter space. Such a decay has a significant meaning if one notices that it can explain a 2.3σ event excess occurred at LEP for the process $e^+e^- \to Zb\bar{b}$ for $M_{b\bar{b}} \sim$ 98 GeV. Moreover, a SM-like Higgs with mass of order 100 GeV, which has no-fine tunning, can naturally occur in the NMSSM and this scenario is preferred by precision EW data. In addition, the NMSSM can solve both the μ-problem and the little hierarchy problem of the MSSM.

In the context of the NMSSM, we have proven that a very light CP-odd Higgs state with mass $m_{a_1} \lesssim M_Z$, which has large singlet component and a small doublet one, can be

discovered at the LHC via Higgs production in association with a bottom-antibottom pair. This mode is dominant at large tanβ. After making some analyses for signals and dominant backgrounds, we have proven that this mode is the ideal one to discover the a_1 through the following signatures: (i) $\tau^+\tau^-$ decay mode, in which a_1 can be discovered with mass up to M_Z; (ii) $\mu^+\mu^-$ decay mode, if $10 \lesssim m_{a_1} \lesssim 60$ GeV. On the other hand, despite the fact that the $b\bar{b}$ decay mode is dominant in most regions of parameter space that have light a_1, this channel is unfeasible to detect a_1 due to the huge QCD background and the smallness of the signal-to-background ratio. Further, we also looked at the detectability of a_1 through the $\gamma\gamma$ decay mode but this proved unuseful despite the fact that this decay mode can be dominant in some areas of the NMSSM parameter space. We have also shown that the dominance of the $\gamma\gamma$ decay mode causes a suppression of the $b\bar{b}$ decay mode and thus this also helps to explain the 2.3σ event excess observed at LEP for a Higgs mass ~ 98 GeV, when Higgs $\to a_1a_1$ decays are kinematically allowed and dominant even with $m_{a_1} > 10$ GeV.

We believe that our results presented in chapters 5 and 6 have a twofold relevance. Firstly, they support the 'No-lose theorem' by looking for direct a_1 production rather than looking for its production through the decays $h_{1,2} \to a_1a_1$, which may not give a sufficient signal significance. Secondly, they corroborate the 'More-to-gain theorem' as such very light a_1's (with $m_{a_1} \lesssim M_Z$) are not at all possible in the MSSM. Altogether, the existence of such a light neutral Higgs state is a direct evidence for the non-minimal nature of the SUSY Higgs sector.

Finally, we have mentioned in chapter 7 the importance of Higgs-to-Higgs decays in the NMSSM and have shown that such decays should be taken seriously before proving, or otherwise, the 'No-lose theorem'. We also have shown that such decays are dominant in sizable regions of the NMSSM parameter space. We have studied the LHC discovery potential of a CP-even Higgs boson h_1 or h_2, decaying into a pair of light CP-odd Higgses a_1's, and also h_2 decaying into a pair of h_1's, through its production in association with a $b\bar{b}$ pair. We have found that these channels can give sizable signal rates, which could allow one to detect simultaneously two Higg bosons: h_1 and a_1, h_2 and a_1 or h_2 and h_1. In addition, we have shown that the LHC has the potential to discover the three neutral Higgs bosons at the same time. Furthermore, we have studied the LHC discovery potential for h_1 and h_2 decaying into Za_1 and have shown that, while the discovery of the h_1 through this channel is impossible, there is a small but well defined region of the NMSSM parameter space where the h_2 and a_1 states could potentially be discovered.

Bibliography

[1] S. Glashow, Nucl. Phys. **22** (1961) 579;
S. Weinberg, Phys. Rev. Lett. **19** (1967) 1264;
A. Salam, in Elementary Particle Theory, ed. N. Svartholm, Almqvist and Wiksells, Stockholm (1969), p. 367.

[2] P. Ramond, Phys. Rev. D **3** (1971) 2415;
A. Neveu and J. H. Schwarz, Nucl. Phys. B **31** (1971) 86;
Yu. A. Golfand and E. P. Likhtman, JETP Lett. **13** (1971) 323;
J. L. Gervais and B. Sakita, Nucl. Phys. B **34** (1971) 632;
D. V. Volkov and V. P. Akulov, Phys. Lett. B **46** (1973) 109;
J. Wess and B. Zumino, Nucl. Phys. B **70** (1974) 39;
A. Salam and J. A. Strathdee, Nucl. Phys. B **76** (1974) 477.

[3] S. P. Martin, arXiv:hep-ph/9709356.

[4] A. Djouadi, Phys. Rept. **459** (2008) 1.

[5] H. P. Nilles, M. Srednicki and D. Wyler, Phys. Lett. B **120** (1983) 346;
J. M. Frere, D. R. T. Jones and S. Raby, Nucl. Phys. B **222** (1983) 11;
J. R. Ellis, J. F. Gunion, H. E. Haber, L. Roszkowski and F. Zwirner, Phys. Rev. D **39** (1989) 844;
M. Drees, Int. J. Mod. Phys. A **4** (1989) 3635;
U. Ellwanger, M. Rausch de Traubenberg and C. A. Savoy, Phys. Lett. B **315** (1993) 331;
S. F. King and P. L. White, Phys. Rev. D **52** (1995) 4183;
F. Franke and H. Fraas, Int. J. Mod. Phys. A **12** (1997) 479;
U. Ellwanger, M. Rausch de Traubenberg and C. A. Savoy, Nucl. Phys. B **492** (1997) 21.

[6] H. P. Nilles, Phys. Rept. **110** (1984) 1.

[7] H. E. Haber and G. L. Kane, Phys. Rept. **117** (1985) 75.

[8] S. Weinberg, Phys. Lett. B **82** (1979) 387;
M. J. G. Veltman, Acta Phys. Polon. B **12** (1981) 437;
C. H. Llewellyn Smith and G. G. Ross, Phys. Lett. B **105** (1981) 38.

[9] G. R. Farrar and P. Fayet, Phys. Lett. B **76** (1978) 575.

[10] A. Crivellin and M. Davidkov, Phys. Rev. D **81** (2010) 095004.

[11] H. P. Nilles, Phys. Lett. B **115** (1982) 193;
A. H. Chamseddine, R. L. Arnowitt and P. Nath, Phys. Rev. Lett. **49** (1982) 970;
R. Barbieri, S. Ferrara and C. A. Savoy, Phys. Lett. B **119** (1982) 343.

[12] M. Dine and A. E. Nelson, Phys. Rev. D **48** (1993) 1277;
M. Dine, A. E. Nelson and Y. Shirman, Phys. Rev. D **51** (1995) 1362.

[13] L. Randall and R. Sundrum, Nucl. Phys. B **557** (1999) 79;
G. F. Giudice, M. A. Luty, H. Murayama and R. Rattazzi, JHEP **9812** (1998) 027.

[14] L. O'Raifeartaigh, Nucl. Phys. B **96** (1975) 331.

[15] P. Fayet and J. Iliopoulos, Phys. Lett. B **51** (1974) 461.

[16] The LEP working group for Higgs boson searches, arXiv:hep-ex/0107030; arXiv:hep-ex/0107031.

[17] R. Barate *et al.*, Phys. Lett. B **565** (2003) 61.

[18] P. Draper, T. Liu and C. E. M. Wagner, Phys. Rev. D **80** (2009) 035025.

[19] European Organization for Nuclear Research, http://public.web.cern.ch/public/.

[20] ALICE Collaboration, http://aliweb.cern.ch.

[21] ATLAS Collaboration, arXiv:0901.0512 [hep-ex].

[22] CMS Collaboration, J. Phys. G **34** (2007) 995.

[23] LHCb Collaboration, CERN-LHCC-98-04, CERN-LHCC-P-4.

[24] A. De Roeck, Acta Phys. Polon. B **39** (2008) 2455.

[25] ATLAS Collaboration, *Detector and Physics Performance Technical Design Report*, Vols. 2, CERNLHCC9915.

[26] T. S. Virdee, Talk given at 'Hadron Collider Physics Symposium 2011', Paris, France, November 14–18, 2011, http://hcp2011.lpnhe.in2p3.fr.

[27] For reviews, see: e.g., J. F. Gunion, H. E. Haber, G. Kane and S. Dawson, *The Higgs Hunter's Guide* (Perseus Publishing, Cambridge, MA, 1990).

[28] D. Denegri *et al.*, arXiv:hep-ph/0112045.

[29] M. Schumacher, arXiv:hep-ph/0410112.

[30] J. E. Kim and H. P. Nilles, Phys. Lett. B **138** (1984) 150.

[31] G. F. Giudice and A. Masiero, Phys. Lett. B **206** (1988) 480.

[32] M. M. Almarashi and S. Moretti, Eur. Phys. J. C **71** (2011) 1618.

[33] M. M. Almarashi and S. Moretti, Phys. Rev. D **83** (2011) 035023.

[34] M. M. Almarashi and S. Moretti, Phys. Rev. D **84** (2011) 015014.

[35] M. M. Almarashi and S. Moretti, Phys. Rev. D **84** (2011) 035009.

[36] M. M. Almarashi and S. Moretti, arXiv:1109.1735 [hep-ph].

[37] M. Maniatis, Int. J. Mod. Phys. A **25** (2010) 3505.

[38] U. Ellwanger, C. Hugonie and A. M. Teixeira, Phys. Rept. **496** (2010) 1.

[39] J. R. Ellis, J. F. Gunion, H. E. Haber, L. Roszkowski and F. Zwirner, in Ref. [5].

[40] M. Bastero-Gil, C. Hugonie, S. F. King, D. P. Roy and S. Vempati, Phys. Lett. B **489** (2000) 359.

[41] R. Dermisek and J. F. Gunion, Phys. Rev. Lett. **95** (2005) 041801.

[42] R. D. Peccei and H. R. Quinn, Phys. Rev. Lett. **38** (1977) 1440.

[43] R. D. Peccei and H. R. Quinn, Phys. Rev. D **16** (1977) 1791.

[44] K. Hagiwara *et al.* [Particle Data Group], Phys. Rev. D **66** (2002) 010001.

[45] Y. B. Zeldovich, I. Y. Kobzarev and L. B. Okun, Zh. Eksp. Teor. Fiz. **67** (1974) 3.

[46] D. J. Miller, R. Nevzorov and P. M. Zerwas, Nucl. Phys. B **681** (2004) 3.

[47] M. Masip, R. Muñoz-Tapia and A. Pomarol, Phys. Rev. D **57** (1998) 5340.

[48] U. Ellwanger and C. Hugonie, Eur. Phys. J. C **25** (2002) 297.

[49] U. Ellwanger, Phys. Lett. B **303** (1993) 271.

[50] T. Elliott, S. F. King and P. L. White, Phys. Rev. D **49** (1994) 2435.

[51] P. N. Pandita, Phys. Lett. B **318** (1993) 338.

[52] R. Dermisek and J. F. Gunion, Phys. Rev. D **73** (2006) 111701.

[53] R. Dermisek and J. F. Gunion, Phys. Rev. D **75** (2007) 075019.

[54] R. Dermisek and J. F. Gunion, Phys. Rev. D **76** (2007) 095006.

[55] S. Schael *et al.* [ALEPH Collaboration], JHEP **1005** (2010) 049.

[56] B. Aubert *et al.* [BABAR Collaboration], Phys. Rev. Lett. **103** (2009) 181801.

[57] R. Dermisek and J. F. Gunion, Phys. Rev. D **77** (2008) 015013.

[58] J. Dai, J. F. Gunion and R. Vega, Phys. Lett. B **315** (1993) 355 and Phys. Lett. B **345** (1995) 29; J. R. Espinosa and J. F. Gunion, Phys. Rev. Lett. **82** (1999) 1084.

[59] U. Ellwanger, J. F. Gunion and C. Hugonie, JHEP **0507** (2005) 041.

[60] U. Ellwanger, J. F. Gunion and C. Hugonie, hep-ph/0111179; C. Hugonie and S. Moretti, hep-ph/0110241; D. J. Miller and S. Moretti, hep-ph/0403137; U. Ellwanger, J. F. Gunion, C. Hugonie and S. Moretti, hep-ph/0305109 and hep-ph/0401228; A. Belyaev, S. Hesselbach, S. Lehti, S. Moretti, A. Nikitenko and C. H. Shepherd-Themistocleous, arXiv:0805.3505 [hep-ph]; J. R. Forshaw, J. F. Gunion, L. Hodgkinson, A. Papaefstathiou and A. D. Pilkington, JHEP **0804** (2008) 090; A. Belyaev, J. Pivarski, A. Safonov, S. Senkin and A. Tatarinov, Phys. Rev. D **81** (2010) 075021.

[61] S. Moretti, S. Munir and P. Poulose, Phys. Lett. B **644** (2007) 241.

[62] A. Djouadi *et al.*, JHEP **0807** (2008) 002.

[63] A. Arhrib, K. Cheung, T. J. Hou and K. W. Song, JHEP **0703** (2007) 073.

[64] K. Cheung and T. J. Hou, Phys. Lett. B **674** (2009) 54.

[65] J. F. Gunion, H. E. Haber and T. Moroi, *In the Proceedings of 1996 DPF / DPB Summer Study on New Directions for High-Energy Physics (Snowmass 96), Snowmass, Colorado, 25 Jun - 12 Jul 1996, pp LTH095* [arXiv:hep-ph/9610337].

[66] B. A. Dobrescu, G. L. Landsberg and K. T. Matchev, Phys. Rev. D **63** (2001) 075003.

[67] B. A. Dobrescu and K. T. Matchev, JHEP **0009** (2000) 031.

[68] U. Ellwanger, J. F. Gunion, C. Hugonie and S. Moretti, in Ref. [60].

[69] A. Belyaev, S. Hesselbach, S. Lehti, S. Moretti, A. Nikitenko and C. H. Shepherd-Themistocleous, in Ref. [60].

[70] A. Belyaev, J. Pivarski, A. Safonov, S. Senkin and A. Tatarinov, in Ref. [60].

[71] M. Lisanti and J. G. Wacker, Phys. Rev. D **79** (2009) 115006.

[72] U. Ellwanger, arXiv:1108.0157 [hep-ph].

[73] S. Moretti and S. Munir, Eur. Phys. J. C **47** (2006) 791.

[74] S. Munir, talk given at the 'International School of Subnuclear Physics, 43rd Course', Erice, Italy, August 29 – Sept. 7, 2005, to be published in the proceedings, preprint SHEP-05-37, October 2005.

[75] F. Mahmoudi, J. Rathsman, O. Stal and L. Zeune, Eur. Phys. J. C **71** (2011) 1608.

[76] U. Ellwanger and C. Hugonie, Private communication.

[77] U. Ellwanger, J. F. Gunion and C. Hugonie, JHEP **0502** (2005) 066; U. Ellwanger and C. Hugonie, Comput. Phys. Commun. **175** (2006) 290.

[78] See the Web site "NMSSMTools: Tools for the Calculation of the Higgs and Sparticle Spectrum in the NMSSM: NMHDECAY, NMSPEC and NMGMSB", http://www.th.u-psud.fr/NMHDECAY/nmssmtools.html.

[79] S. Schael et al., Eur. Phys. J. C **47** (2006) 547.

[80] F. Domingo and U. Ellwanger, JHEP **0807** (2008) 079.

[81] A. Czarnecki and W. J. Marciano, Phys. Rev. D **64** (2001) 013014.

[82] A. Pukhov, arXiv:hep-ph/0412191.

[83] See the Web site "CTEQ6 Parton Distribution Functions", http://hep.pa.msu.edu/cteq/public/cteq6.html.

[84] M. M. Almarashi, Talk given at 'NExT meeting at RAL', Didcot, United Kingdom, January 26, 2011, http://conference.ippp.dur.ac.uk/conferenceDisplay.py?confId=304.

[85] S. Andreas, O. Lebedev, S. R. Sanchez and A. Ringwald, JHEP **1008** (2010) 003.

[86] X. G. He, J. Tandean and G. Valencia, Phys. Lett. B **631** (2005) 100; Phys. Rev. D **74** (2006) 115015; Phys. Rev. Lett. **98** (2007) 081802; JHEP **0806** (2008) 002.

[87] T. Stelzer and W. F. Long, Comput. Phys. Commun. **81** (1994) 357.

[88] See, e.g., F. Sarri, preprint ATL-PHYS-PROC-2008-076 (and references therein); S. Horvat, preprint ATL-PHYS-PROC-2009-063 (and references therein).

[89] J. Dai, J. F. Gunion and R. Vega, Phys. Lett. B **345** (1995) 29 in Ref. [58].

[90] J. Dai, J. F. Gunion and R. Vega, Phys. Lett. B **387** (1996) 801.

[91] V. M. Abazov *et al.*, arXiv:1106.4555 [hep-ex].

[92] S. Dittmaier, M. Kramer and M. Spira, Phys. Rev. D **70** (2004) 074010; S. Dawson, C. B. Jackson, L. Reina and D. Wackeroth, Mod. Phys. Lett. A **21** (2006) 89.

[93] N. Greiner, A. Guffanti, T. Reiter and J. Reuter, Phys. Rev. Lett. **107** (2011) 102002.

[94] F. Gianotti *et al.*, Eur. Phys. J. C **39** (2005) 293.